MONTAN UNIVERSITÄT
WWW.UNILEOBEN.AC.AT

Master Thesis

Influence of Injection Molding Parameters and Aging on Geometry and Functionality of Plastic Targets for Mass Spectrometry

by

Alexander Pöhl

submitted at

KUNSTSTOFF TECHNIK LEOBEN
KUNSTSTOFFVERARBEITUNG

Institut für Kunststoffverarbeitung

Head: Univ.-Prof. Dr. Clemens Holzer

Montanuniversität Leoben

Leoben, 30.08.2010

Affidavit

I declare in lieu of oath, that I wrote this thesis and performed the associated research myself, using only literature cited in this volume.

_____ _____

Date Signature

Acknowledgment

This thesis was written in the course of a research project about matrix-assisted laser desorption/ionization mass-spectrometry (MALDI-MS) targets at Sony DADC Austria AG. Under the guidance of project leader Werner Balika, Sony DADC Austria AG in cooperation with the Vienna University of Technology managed to develop polymer-based targets for MALDI-MS, thereby winning the 3rd place of the “Dr. Wolfgang Houska Prize” in 2009.

Werner Balika brought me to the team to investigate shrinkage behavior and aging of the MALDI MS-Targets. I want to thank him for overseeing my work at Sony DADC. His advice, profound knowledge and attention to detail encouraged me to intensify my research.

Special thanks to the whole Microstructured-Polymer-Devices (MPD) department at Sony DADC Austria AG. I would like to give special mention to Georg Bauer, director of MPD-Engineering, Christian Mayrhofer, for explaining the testing equipment to me, Manuela Wagner, for her extensive knowledge on coatings, her humor and instructions regarding the sputtering equipment and Kazuhiro Shiratori, for conducting the experimental part of the shrinkage tests summarized in this thesis.

Furthermore, I want to express my gratitude to the team at the Institute of Plastics Processing at the University of Leoben. In particular Nina Krempl and Thomas Lucyshyn for carrying out the shrinkage simulation presented in this thesis. Special thanks to Clemens Holzer and Thomas Lucyshyn for supervising and assessing this thesis.

Thanks to Stefan Bugovsky and the Research Group Bio and Polymer Analysis of the Institute of Chemical Technology and Analytics at the Vienna University of Technology for conducting the MALDI-MS application tests and overseeing the targets stored in the -80 °C freezer.

Last, but not least, I want to thank my family and friends for all the support I received during my studies at the University of Leoben.

Abstract

Stability of the geometric dimensions and constant surface properties are crucial for targets used in matrix-assisted laser desorption/ionization mass-spectrometry (MALDI-MS). In this thesis research had to be done to examine how geometric and surface properties of polymeric MALDI-MS targets are influenced by parameters during injection molding as well as ambient conditions over time.

First, the ability of simulation to accurately predict shrinkage was investigated. For this purpose, the absolute difference in predicted and actual shrinkage, as well as shrinkage trends during a parameter study were evaluated. These investigations were performed for a carbon-black filled polypropylene and an unfilled cyclo-olefin-polymer. Overall, the simulation results were not precise enough to satisfy the need for high geometric accuracy.

Second, the two grades used for shrinkage evaluation, as well as steel- and gold-coated versions of the conductive polypropylene, were subjected to extensive aging tests. The goal was to investigate three different aspects during these tests. First, it was investigated whether the steel-coated design can be conditioned at higher temperatures to reach a contact angle level necessary for functionality faster than at room-temperature. Second, the life time of the target was evaluated and possible storage and transport conditions defined. Finally, the possibility of archiving at very low temperatures (-80 °C) was examined. For all these examinations, samples were exposed to temperatures ranging from -80 °C to 120 °C and up to 90 % rh humidity. Consequently, shrinkage, flatness, roughness, surface integrity, wetting behavior and adhesion of the coating were examined. The targets did not sustain any damage after long-term aging up to 80 °C. Additionally to the standard method at room temperature, three accelerated conditioning methods are recommended and no arguments against archiving at temperatures up to -80 °C were found.

Kurzfassung

Höchste geometrische Präzision und konstante Oberflächeneigenschaften sind eine Voraussetzung für Probenhalter in der Matrix-unterstützten Laser-Desorption/Ionisation Massenspektroskopie (MALDI-MS). In dieser Arbeit sollte untersucht werden, wie Dimensionen und Oberflächeneigenschaften kunststoffbasierter MALDI-MS Probenträger von den Einstellungen im Spritzguss sowie von Umgebungsbedingungen auf Dauer beeinflusst werden.

Im ersten Teil wurde die Fähigkeit von Simulationsprogrammen, Schwindung vorherzusagen, untersucht. Dazu wurden sowohl die Differenz zwischen der vorhergesagten und der tatsächlichen Schwindung als auch die verschiedenen Tendenzen in einer Parameterstudie untersucht. Diese Untersuchungen wurden für ein rußgefülltes Polypropylen und ein Cyclo-olefin-Polymer durchgeführt. Alles in allem waren die Schwindungsergebnisse nicht genau genug, um den hohen Anforderungen durch enge geometrische Toleranzen zu entsprechen.

Im zweiten Teil wurden die beiden Polymere, die für die Schwindungsuntersuchungen herangezogen wurden, sowie stahl- und goldbeschichtete Varianten ausführlichen Alterungstests unterzogen. Es wurden drei verschiedene Aspekte untersucht. Zuerst wurde geprüft, ob das Stahldesign bei höheren Temperaturen konditioniert werden kann, um schneller als bei Raumtemperatur ein für die Funktionalität notwendiges Kontaktwinkelniveau zu erreichen. Dann wurde die Lebensdauer der Probenträger abgeschätzt und Lager- und Transportbedingungen empfohlen. Zuletzt wurde die Möglichkeit, die Probenträger bei sehr niedrigen Temperaturen (-80 °C) zu archivieren, ausgelotet. Für all diese Untersuchungen wurden die Probenhalter Temperaturen von -80 bis 120 °C und einer Luftfeuchtigkeit bis zu 90 % rF ausgesetzt. Danach wurden Schwindung, Ebenheit, Rauigkeit, Oberflächengüte, Benetzungsverhalten und Haftung der Beschichtung untersucht. Es wurde keine Schädigung bei Langzeitalterungsversuchen bis 80 °C entdeckt. Zusätzlich zur bereits angewandten Konditionierungsmethode bei Raumtemperatur konnten drei beschleunigende Konditionierungsmethoden empfohlen werden. Es wurden keine Argumente gefunden, die gegen eine Archivierung bei Temperaturen bis zu -80 °C sprechen würden.

Content

1 INTRODUCTION AND OBJECTIVES

Matrix-assisted laser desorption/ionization (MALDI) mass-spectrometry (MS) was introduced in the late 1980s and is used for the analysis of biomolecules and large organic molecules [51, 21]. Sample preparation is crucial to the successes of any MALDI-MS measurement [53]. For this reason, there has been extensive research to improve sensitivity and reproducibility by optimizing sample supports or targets [25]. Until now primarily metal plates are used as reusable targets. Since test results can be influenced through inadequate cleaning procedures, demand for cheap disposable targets rises. Therefore polymer based targets for mass spectrometry were introduced to the market recently by Shimadzu Biotech – Kratos Analytical, UK (see Figure 1).

Figure 1: Polymeric MALDI-MS targets.

For MALDI-MS tests the analyte is mixed with the matrix solution and spotted manually or automatically on a MALDI plate. Reproducability of the geometric dimensions is necessary for accurate automatic sample positioning. Constant surface properties (e.g., contact angle) are crucial for homogeneous crystal formation and therefore important for accurate test results [58]. To ensure that neither geometric dimensions, nor surface properties are affected by aging or ambient conditions, an investigation into this topic was initiated by Sony DADC, Austria.

After injection molding, all parts must shrink. This phenomenon is well known and has been investigated thoroughly [18, 45, 14, 12]. Shrinkage is influenced by many factors including material, process parameters, mold design and environmental conditions. This makes accurate shrinkage predictions difficult. Still, due to the great importance of this topic for any plastic processer, considerable effort has been put into simulation of shrinkage [23, 31, 4]. Since life-science industry requires very precise dimensions, one goal of this research was to investigate the accuracy of shrinkage simulation and whether it can be applied for the purposes of Sony DADC Austria AG.

There has been much research investigating aging behavior of polymers [11, 44], [20, 1]. Most studies focus on mechanical properties, creep, optical properties or aging due to exposure to aggressive media. One good summary can be found in the book of Ehrenstein and Pongratz [11]. On the other hand, hardly any research focuses on aging behavior of surfaces. Since experience shows significant changes in surface properties (e.g., contact angle) of metal-coated polymer based MALDI-MS targets, this thesis looked into the effect of time, temperature and ambient conditions on the surface of coated and uncoated plastics.

The other goal of this thesis was to look into three different aspects during the aging tests. First, it had to be investigated whether the steel-coated design can be conditioned at higher temperatures to reach a contact angle level necessary for functionality faster than at room-temperature. Second, the life time of the target had to be evaluated and possible storage and transport conditions had to be defined. Finally, the possibility of archiving at very low temperatures (-80 °C) had to be examined.

Besides investigating the influence of aging on shrinkage, flatness, roughness, surface integrity, wetting behavior and adhesion of the coating during this research, the functionality of the plastic targets had to be investigated at the Vienna University of Technology. These mass spectrometry tests performed on the plastic targets and a reusable steel target as reference showed the same results [6].

2 BASIC CONSIDERATIONS

2.1 Shrinkage

An accurate prediction of shrinkage is crucial for injection molding. While some mold makers rely on the experience of their mold designers, others use modern simulation programs to estimate the final dimensions of the molded part [12]. For a better understanding of the processes which cause shrinkage, a detailed introduction to this topic will be given in the following chapters.

2.1.1 Definition

When describing shrinkage one has to differentiate between mold shrinkage, warpage and post-mold shrinkage. Mold shrinkage, although it actually is a volume phenomenon, is defined as the difference between the linear mold and part dimensions at room temperature and is measured within 24 hours after molding. Differential shrinkage causes out-of-plane deformation of the molded item which is referred to as warpage. Any additional shrinkage after the initial 24-hour period and after post-mold treatment (e.g., annealing) is described as post-mold shrinkage [12].

The European Standard ISO 294-4 (equivalent American document ASTM D 955) specifies the methods that are to be used to determine mold and post-mold shrinkage. The standard distinguishes between mold shrinkage parallel and normal to the flow direction, which are given in percent and defined by following equations [34]:

$$S_{Mp} = 100 \times \frac{l_c - l_1}{l_c} \qquad (1)$$

$$S_{Mn} = 100 \times \frac{l_c - l_1}{l_c} \qquad (2)$$

with S_{Mp} and S_{Mn} as the molding shrinkage parallel and normal to the flow direction, l_c is the length across the center of the cavity and l_1 is the corresponding length of the specimen.

Consequently the post-mold shrinkage S_{Pp} and S_{Pp} (parallel and normal) is defined as follows:

$$S_{Pp} = 100 \times \frac{l_1 - l_2}{l_1} \qquad (3)$$

$$S_{Pn} = 100 \times \frac{l_1 - l_2}{l_1} \quad (4)$$

with l_2 as the length of the specimen after post mold treatment.

Hence the total shrinkage S_{Tp} and S_{Tp} (parallel and normal) is:

$$S_{Tp} = 100 \times \frac{l_c - l_2}{l_c} \quad (5)$$

$$S_{Tn} = 100 \times \frac{l_c - l_2}{l_c} \quad (6)$$

with the symbols defined as above.

The test parts should be molded with a constant holding pressure between 20 and 100 MPa. The change-over point is to be selected carefully to avoid both a depression (if chosen too early) and a peak (if chosen too late) in the time against pressure curve. All dimensions have to be measured at 23 ± 2 °C. If the warpage of a specimen exceeds 2 mm in height, this specimen should be discarded. At least 5 specimens should be used for each set of molding parameters. The dimensions are to be measured to the nearest 0.02 mm between appropriate reference points on opposite sides or optically with reference marks engraved in the mold which should be positioned at least 4 ± 1 mm from the edges [34].

2.1.2 Influencing factors

Besides material, mold design and ambient conditions shrinkage is influenced to a great amount by processing parameters. Figure 2 demonstrates the possible effect of six important factors on shrinkage which will be discussed in the following paragraphs:

- Holding pressure time
- Holding pressure
- Melt temperature
- Mold temperature
- Injection rate
- Wall thickness

It has to be pointed out that Figure 2 illustrates general trends. The extent of shrinkage due to these influences will depend on the specific material and part geometry. Especially materials with high filler contents can show trend differing from those depicted in Figure 2 [12].

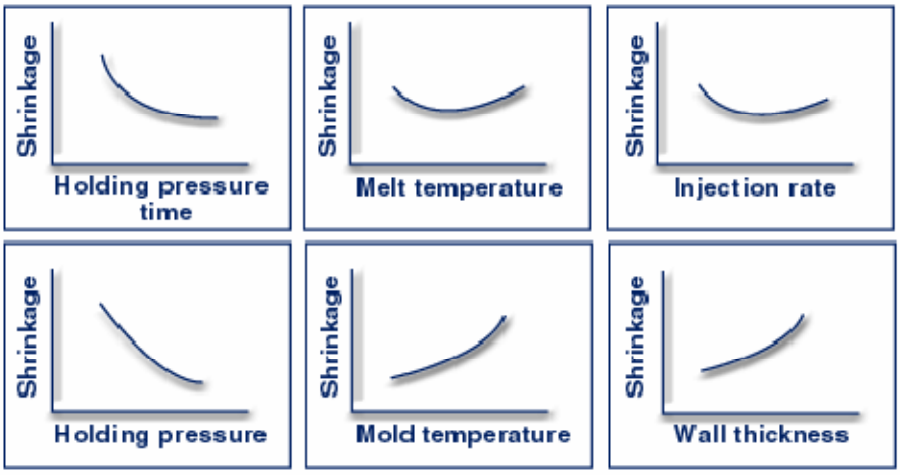

Figure 2: Factors influencing shrinkage [41].

2.1.2.1 Holding pressure time

It is important that the holding pressure is applied until the gate is frozen. If the holding pressure is removed too early, the material will expand out of the cavity into the runner system, thus increasing shrinkage. After the gate is solid and no material can pass in either direction, holding pressure no longer has an effect on the part and additional holding pressure time would be a waste of energy [12].

2.1.2.2 Holding pressure

Holding pressure is considered the processing variable having most effect on shrinkage. Since plastic is compressible, the greater the holding pressure, the less the shrinkage. If the holding pressure is too large when the gate freezes, the compression can exceed the shrinkage and after demolding the part will become larger than the cavity, leading to problems [12, 31].

2.1.2.3 Melt temperature

The curve in Figure 2 shows that shrinkage is high at both high and low melt temperatures. This can be explained due to two different phenomena. At low melt temperature the pressure gradient from the gate to the end of the flow is high and there is hardly any time to pack out the cavity, resulting in high shrinkage.

High melt temperatures lead to higher core temperatures when the gate freezes, thus leading to greater temperature difference during cooling. This effect leads to greater shrinkage [12, 31].

2.1.2.4 Mold temperature

Mold temperature determines the cooling rate of plastic parts. Higher mold temperatures will lead to a lower cooling rate.

The formation of the crystalline structure in semi-crystalline grades is a time-consuming process. The lower the cooling rate, the more numerous the structures and the greater the shrinkage.

The shrinkage of amorphous grades will be increased too, since lower cooling rates allow a relaxation of the internal molecular stresses. It has been observed that rapidly cooled parts are prone to greater post-mold shrinkage and warpage [12, 31].

2.1.2.5 Injection rate

Similar to melt temperature, the curve illustrating the effect of the injection rate on shrinkage in Figure 2 shows a U-shape. A slow injection rate means that the material will cool more before the cavity is filled, inhibiting packing since the gate will freeze shortly after the mold cavity is filled.

If the cavity is filled fast, the temperature of the plastic in the cavity will increase due to greater amounts of frictional heat generated at the gate restriction. Both extreme states lead to higher shrinkage, thus the optimum fill rate has to be found for each part and will depend on geometry, size and location of the gate, mold temperature and melt temperature. Furthermore, injection speed will influence orientation effects [12, 31].

2.1.2.6 Wall thickness

An increase in wall thickness has the same effect on shrinkage as an increase in mold temperature does. At a given mold temperature, the average temperature of thicker walls decreases more slowly, thus reducing the cooling rate. This has the same effects on crystallization and stress relaxation as mentioned above. Special attention has to be brought to parts with non-uniform wall thickness, since strong anisotropic shrinkage and therefore significant warpage will occur [12, 31].

2.1.3 Post-mold shrinkage

Although the major amount of shrinkage takes place within 48 hours after demolding, some shrinkage can occur after this time period, referred to as post-mold shrinkage. The main influencing factors for post-mold shrinkage are temperature and moisture conditions during molding and in-service exposure after production [12].

Over time, molded in stress relaxation and slight additional crystallization can occur. Both phenomena lead to increased shrinkage.

Since higher mold temperatures allow for extensive crystallization and stress relaxation in the mold, such parts show hardly any post-mold shrinkage. Figure 3 shows how post-mold shrinkage is affected by mold temperature. One can see that post-mold shrinkage can be reduced to a minimum, if the parts are annealed after production. After annealing, one can no longer differentiate between different processing settings [12].

Another explanation for post mold size change can be absorption or loss of fluids. Especially hygroscopic materials such as polyamide (PA) tend to absorb moisture from the environment. This usually leads to dimensional change [12].

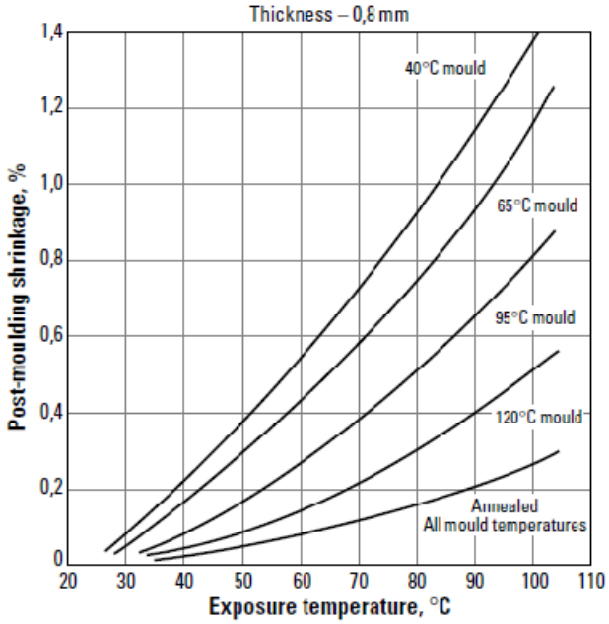

Figure 3: Post molding shrinkage of Delrin® acetal resins [32].

2.1.4 Simulation

Since injection molding tools are very expensive and faults discovered during production most likely lead to costly retooling and loss of time, molding simulation can be of high value especially to the injection molding industry. For accurate molding simulation, data in correlation to shear rate, pressure and temperature for viscosity, specific heat, thermal conductivity and density is required. A common problem is that this data is often measured at laboratory conditions which must not necessarily correspond with conditions during injection molding. The choice of the correct simulation model is crucial to the accuracy of the calculation. Possible calculation models are 2.5D and 3D [23, 31].

2.1.4.1 Comparison of 2.5D and 3D computational fluid dynamics

If one regards the possible flow conditions (Figure 4) in a simple plastic part, one can see different possible situations.

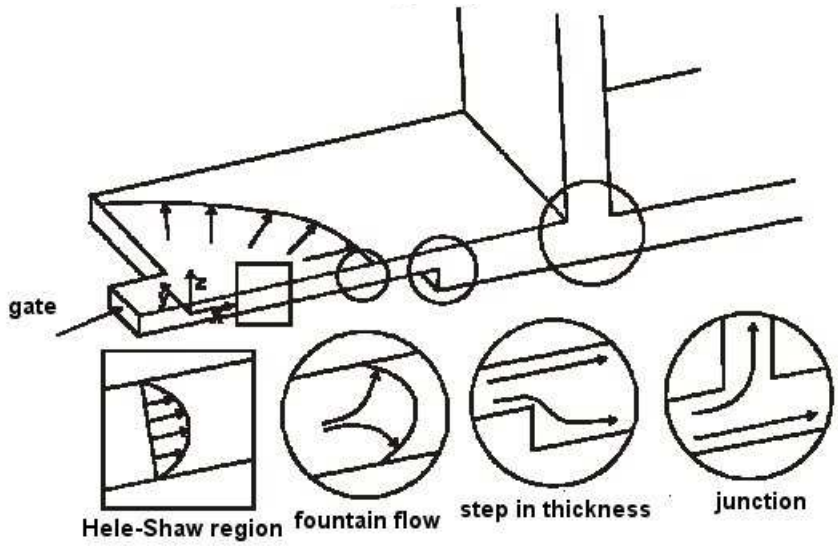

Figure 4: Fluid dynamics in an injection molded part [42].

In flat areas behind the flow front, there is no flow in z-direction (in through-thickness direction) and the pressure is a function of x and y only. This is referred to as Hele-Shaw flow. Since the z-direction is neglected in calculation, the computing time decreases drastically without causing a significant accuracy loss for thin and extensive parts. This calculation method is referred to as 2.5D calculation, since a plane flow is assumed and a parabolic flow profile in z-direction is calculated. For FEM modeling, 2D elements – which are assigned a thickness as an attribute – can be used [31].

For a 2.5D Dual Domain model a 3D CAD model is imported into simulation software such as Moldflow Plastics Insight (MPI), Autodesk, USA where the external shell of the parts is meshed with planar triangular elements. This is far simpler than the alternative midplane model, where the part geometry is described with midplanes of the part's surface, which have to be created in a time-consuming process. For a successful simulation with the 2.5 D Dual Domain model, it is important that facing elements match. Figure 5 shows an example for good and bad matching.

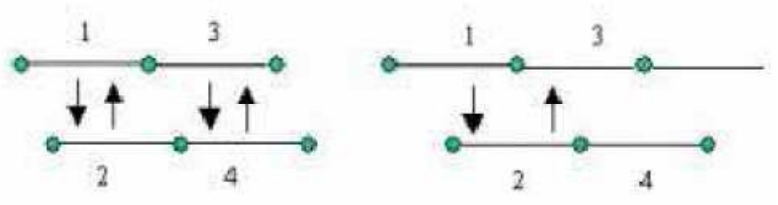

Figure 5: Good (left) and bad (right) matching of elements in a Dual Domain mesh [31].

But there are flow phenomena which cannot be described with the Hele-Shaw assumption. Some examples are given in Figure 4. The melt front cannot be described accurately since one has a fountain flow in this area leading to mass flow in z-direction. Steps in wall thickness or junctions (e.g., ribs) are bound to lead to three-dimensional flows. Such events can only be described using 3D models with three-dimensional finite elements (e.g., tetrahedrons) [31].

2.1.4.2 Calculation approach for shrinkage and warpage simulation

The calculation approaches, used by MPI, are: the residual strain model, the residual stress model and the CRIMS model, a hybrid model describing a correction scheme using measured shrinkages [24]. These models are presented in the following paragraphs.

2.1.4.2.1 Residual strain model

The residual strain model was introduced in 1988 and is defined as [57]:

$$S^{\parallel} = \sum_{i=1}^{i=5} a_i M_i^{\parallel} \qquad (7)$$

$$S^{\perp} = \sum_{i=6}^{i=10} a_i M_i^{\perp} \qquad (8)$$

where $S^{||}$ and $S^{\perp}$ are, respectively, in-plane shrinkage strains in the directions parallel and transverse to the flow direction, a_i (i= 1,…,10) are shrinkage coefficients and $M_i^{||}$ (i=1,…,5) are, respectively, measures of volumetric shrinkage, crystallization, relaxation due to mold restraint, material orientation and a constant. Similar measures $M_i^{\perp}$ (i =1,…,5) hold in the transverse flow direction.

These shrinkage coefficients can be determined empirically for any grade. For this purpose, up to 28 samples, each with different process conditions and thickness are molded. Shrinkage measurements are facilitated by a grid etched on the mold. A simulation is run for each process condition to determine the factors affecting

shrinkage $Mi^{||}$ and $Mi^{\perp}$. The shrinkage coefficients can then be obtained by regression analysis [24].

2.1.4.2.2 Residual stress model

A viscoelastic constitutive relationship is often used to define residual stress models [3, 46]. Thermal stresses, induced by freezing and further shrinkage of the material, as well as pressure-induced stresses, caused by injection and holding pressure, are taken into account [31]. One can formulate a general linear anisotropic thermoviscoelastic constitutive relationship as follows [24]:

$$\sigma_{ij} = \int_0^t c_{ijkl}\left(\xi(t) - \xi(t')\right)\left(\frac{\partial \varepsilon_{kl}}{\partial t'} - \alpha_{kl}\left(\xi(t) - \xi(t')\right)\frac{\partial T}{\partial t}\right)dt' \qquad (9)$$

with

$$\xi(t) = \int_0^t \frac{1}{a_T}dt' \qquad (10)$$

and

σ_{ij} stress tensor

ε_{ij} total strain tensor

c_{ijkl} viscoelastic relaxation modulus

t time

T temperature

α_{kl} tensor of coefficients of expansion

$\xi(t)$ pseudo time scale that accounts for the effect of temperature on material response

a_T time temperature shift factor

However, in applying equation (9) on non-isothermal systems, one is confronted with two problems. First, equation (9) assumes that the material is thermodynamically simple. Unfortunately relaxation functions satisfying the assumption of thermorheological simplicity are often not applicable on real materials. Second, particularly with systems involving semi-crystalline materials, the relaxation functions used in equation (9) depend on internal structures which themselves are affected by processing conditions [24].

A solution is to further approximate this problem with the following assumption. Above a certain temperature T_t, known as transition temperature, the material cannot

sustain any stress. Below T_t, the material can sustain stress in an elastic manner leading to [24]:

$$\sigma_{ij} = \int_0^t c^e_{ijkl}(t)\left(\frac{\partial \varepsilon_{kl}}{\partial t'} - \alpha_{kl}(t)\frac{\partial T}{\partial t}\right)dt' \qquad (11)$$

with c^e_{ijkl} as the tensor of elastic constants.

2.1.4.2.3 Corrected Residual In-Mold Stress Model (CRIMS-Model)

The main flaws affecting the accuracy of the theoretic model are [31]:

- Shrinkage reacts very sensitively to the transition temperature and pvT data, which cannot be measured in conditions corresponding to the injection molding process.
- There is no possibility to take crystallization effects into account.
- Data is lacking for a viscoelastic calculation.

For this reason, a hybrid CRIMS-model is used which takes empirically-measured shrinkage data to optimize shrinkage and warpage predictions based on theoretical models as seen in equation 9 and 11. This method proved successful for filled and unfilled polymers such as polymer blends [24].

2.1.4.3 New approaches considering crystallization

One important flaw of the models used for shrinkage and warpage simulation presented above is that the morphology of polymers is not taken into account. Since crystallization processes strongly affect the thermal and mechanical properties of the polymer, they have outspoken impact on shrinkage and warpage phenomena [31].

The implementation of crystallization into injection-molding simulation was part of Kennedy's dissertation [23]. It has to be pointed out that there is currently no commercial version of MPI available which can calculate crystallization [31].

One can see the influence of shear treatment on crystallization isotactic PP in Figure 6 [26]. Figure 6a) shows the progress of crystallization at various times with the material at a constant temperature of 140 °C. The amount of nuclei remains constant over time, but the nuclei grow to form spherulitic structures. Figure 6b) and Figure 6c) show the effect of 0.5 and 5 s^{-1} shear over a period of 10 s. The nucleation density increases and hence the crystallization rate increases dramatically due to an increase of shear rate. If the shear rate of 5 s^{-1} is applied for a longer time, as can be seen in Figure 6d) and Figure 6e), not only the crystallization rate is increased but the structure is affected too. A formation of row nuclei can be observed [23].

Although extensive research has been done in this field, still no fundamental theory has been found yet that explains exactly how flow-induced crystallization occurs and how to link it to the crystallization kinetics of the material. Several approaches to describe these phenomena can be found in literature [26, 7, 8, 10, 43].

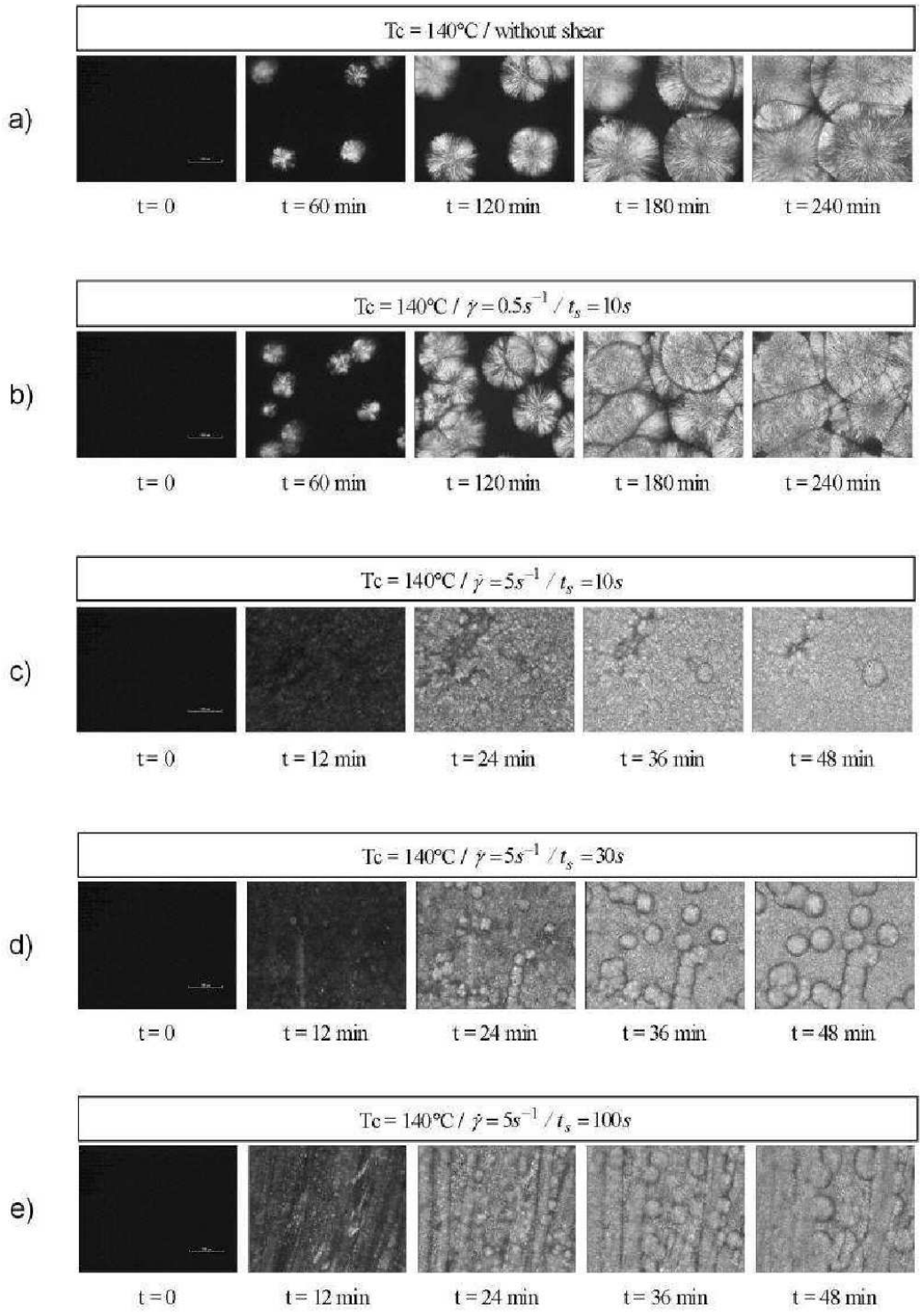

Figure 6: Crysallization of iPP for different shear treatments [26].

2.2 Aging

In the second part of this research, the reaction of a metal-coated plastic target used in mass spectrometry to different test conditions is observed. For this reason, it is important to look into the aging behavior of both the polymer substrate and different coating types. Since the impermeability and wetting behavior of the product are crucial for the application, a large part of this research will focus on surface properties.

2.2.1 General overview

2.2.1.1 Definitions

The German standard DIN 50035 defines aging in general as any – regardless if the effects are positive or negative – irreversible change of physical or chemical properties over time [33].

One has to differentiate between internal and external causes for aging. Internal causes are thermodynamic instabilities in the material. In these cases, thermal activation initiates processes leading to property changes. Possible internal causes are instable states of crystallization, internal stress due to polymer orientation, etc. In many cases, room temperature is enough to trigger significant changes. In this case, storage at higher temperatures would not be the cause of aging but an accelerating factor. External aging causes affect a material which would be stable under normal surrounding conditions. This includes all chemical and physical influences of the surrounding conditions on the material. Possible external aging causes are: temperature, oxidation, atmospheric conditions, ionic radiation, etc. [11].

The standard DIN 50035 also differentiates between chemical and physical aging processes, which often occur parallel [33].

Chemical aging processes involve changes in the chemical composition or the molecular structure of the material, the most important processes being: oxidation, hydrolysis and after-polymerization. One can differentiate between three types of chemical decomposition: change in molecular structure (reduction of molecular weight, different molecular mass distribution), formation of functional groups and separation of low-molecular products (depolymerization). Chemical aging usually leads to a reduction of mechanical properties and melt viscosity [11].

Physical aging processes are a result of thermodynamic instable conditions, caused by cooling during plastic processing [11]. According to DIN 50035, they include changes of the microstructure, post-crystallization, relaxation of internal stress and

orientations as well as changes of concentration in multi-component systems. Physical aging processes are reversible, therefore no longer detectable if the material is recycled [11].

The schematic vT-diagram in Figure 7 is well-suited to explain physical aging. If cooled rapidly, the remaining free volume between the polymer molecules will be frozen at a level greater than the thermodynamic equilibrium. Over time, the plastic will try to reach this state of equilibrium and free volume will be reduced. This change of specific volume due to a thermodynamic imbalance is an example for physical aging [22].

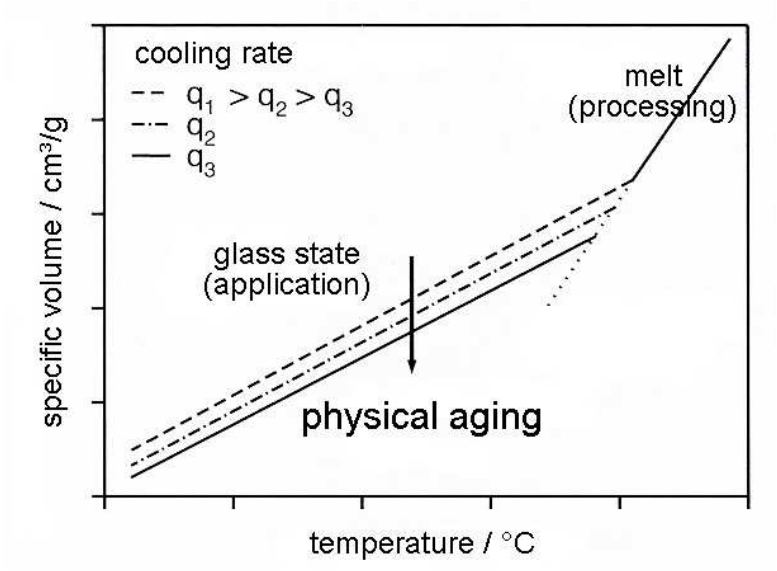

Figure 7: Schematic representation of the relationship between specific volume and temperature at different cooling rates [22].

2.2.1.2 Influencing factors

The aging of polymers is influenced by internal and external factors. For better understanding of the following chapters, the influence of temperature, oxygen, humidity and fillers are discussed in detail.

2.2.1.2.1 Influence of temperature on aging

Besides direct physical and chemical consequences, an important role of temperature in aging processes comes from its accelerating effect on any chemical reaction. According to the Arrhenius equation, the reaction rate increases exponentially with the temperature [11]:

$$k = A \cdot e^{-\frac{E_a}{RT}} \qquad (12)$$

With: E_a Activation energy
R Gas constant
k Reaction rate
T Temperature
A Constant

The “rate-temperature-rule” by Van´t Hoff based on this exponential correlation states that an increase of temperature by 10 degrees Kelvin leads to a twice as high reaction rate [48].

Besides accelerating chemical reactions in general, temperature plays an important role in the chemical degradation of the material. There are three types of mere thermal decomposition: statistical chain scission including decrease of molecular weight and the formation of low-molecular compounds, depolymerization including generation of monomers without significant decrease in molecular weight (e.g., PMMA, PS, and POM) and elimination with splitting off of side groups and formation of low-molecular compounds (e.g., PVC forming HCl). Other types of chemical degradation involving temperature are thermo-oxidative and thermo-mechanical decomposition as well as ablation [11].

2.2.1.2.2 Influence of oxygen on aging

The oxidation of polymers is influenced by [11]:

- Oxidizing agents
  - Oxygen
  - Ozone
  - Nitric oxides
- Loading
  - Thermal
  - Electrical
  - Mechanical
  - Radiation
- External catalysts
  - Copper or brass attachments (particulary polyolefins)
  - Iron

The oxidation of polymers affects both the molecular structure (chemical configuration) and microstructure (morphology) [13].

The chemical decomposition due to the influence of oxygen can cause three different mechanisms: chain scission, chain cross-linking and chain arborization. Although all reaction types can appear simultaneously, usually one mechanism is dominant [13].

The kinetic process of oxidation can be divided into four steps (see Figure 8) [11]:

I: Fast addition of oxygen at active centers

II: Latency period (depending on stabilisators)

III: Increase in oxidation rate due to radical-chain reactions with degenerated chain cross-links

IV: Decrease in oxidation rate due to decrease of active centers

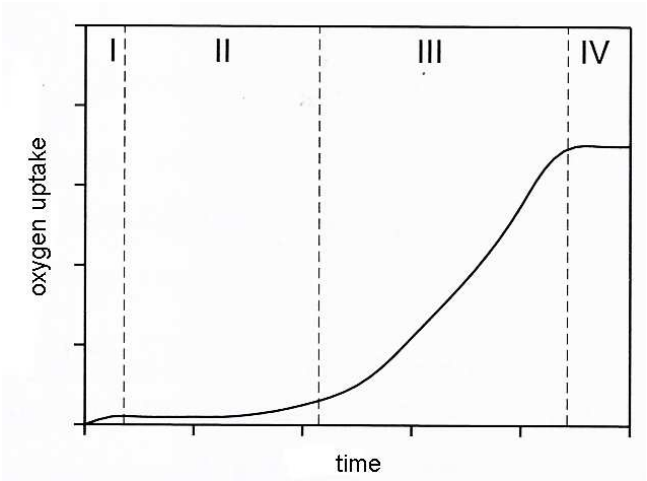

Figure 8: Kinetics of an oxidation reaction [11].

Oxidation increases the mobility of the polymer chains due to chain scission. The separated chains attach themselves to the lamellar structure, thus increasing crystallinity. This physical aging process is called chemo-crystallization [44].

2.2.1.2.3 Influence of humidity on aging

Water can influence both the polymer and included additives. Besides parts in direct contact to water, this can also play an important role for parts exposed to humidity. Soluble decomposition products or additives can be extracted from the material. Furthermore, water can act as diluent and lead to moisture expansion. Moreover, the presence of water can increase the rate of oxidation reactions [11].

Polymers with functional groups susceptible for hydrolysis in their main chain (e.g., PET, PC, PA and PU) will chemically decompose in the presence of water. Often the hydrolysis reaction is accelerated by catalytic acids and bases. Since acid groups are formed during hydrolysis, this reaction is autocatalytic. The reaction is additionally accelerated if exposed to elevated temperatures [11].

2.2.1.2.4 Influence of fillers on aging

Fillers like talcum and calcium carbonate reduce the resistance of plastics against oxygen and chemical products due to their absorption behavior [47]. On the other hand tests with weathered PE-HD shows that $CaCO_3$ can slow down the decomposition by reducing the rate carbonyl and hydro peroxide groups are formed and can act as protective coating against UV-light [44, 55]. The effect of fillers depends on their type and pretreatment [30].

2.2.1.3 Effects of aging on different materials

Polymers can react very differently to various loads. While polyolefins are quite resistant against mere thermal degradation, they react easily with oxygen and radicals. Polycarbonate, on the other hand, is very resistant against thermal loads but is very sensitive against humidity. Humidity has even worse effects on polyamides, which tend to hydrolysis. The thermal degradations of unstabilized PVC starts at temperatures as low as 100 °C through splitting off of HCl [11]. One can see that the varieties of aging phenomena are sheer endless. Therefore we want to focus on the resins used for this research: polypropylene and cyclo-olefin-polymer.

2.2.1.3.1 Polypropylene (PP)

Hermetically-sealed polypropylene does not show any signs of degradation under normal processing conditions. Under the influence of oxygen, the instable character of the hydrogen atoms connected to the tertiary carbon atom leads to significant oxidation [11].

Figure 9 shows how mechanical and rheological properties of a PP-copolymer are affected by melt temperature during injection molding. Temperatures above 280 °C lead to thermal degradation and significant molecular weight loss. This brings about a steep decrease of impact strength an increase of melt flow rate (MFR) at temperatures above 280 °C. The yield stress decreases continuously over the whole temperature range [17].

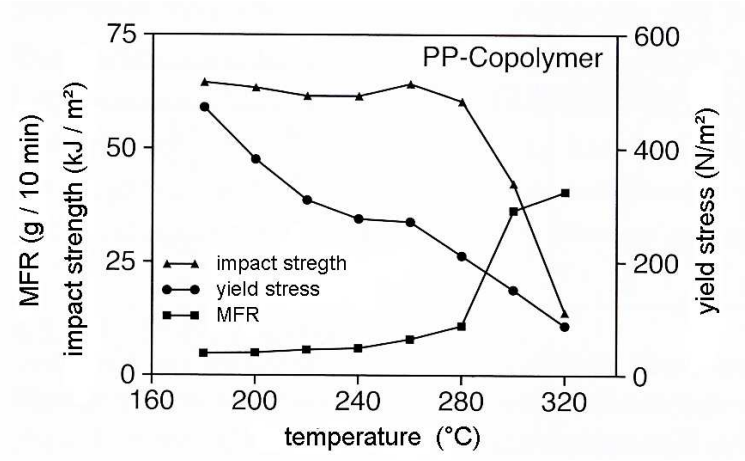

Figure 9: Influence of melt temperature during injection molding on mechanical and rheological properties of a PP co-polymer [17].

2.2.1.3.2 Cyclo-olefin-polymer (COP)

One has to differentiate between cyclo-olefin-polymers (COP) obtained by ring-opening metathesis polymerization of various cyclic monomers followed by hydrogenation on the one hand and cyclo-olefin-copolymers (COC) produced by chain copolymerization of cyclic monomers (e.g. norbornene) and ethane, on the other. The polymerization scheme for both types is shown in Figure 10. Because of the bulky cyclic olefin units attached to the polymer backbone, the polymer becomes amorphous. Typical properties are: high glass-transition temperature (T_g), optical clarity, low shrinkage, low moisture absorption and low birefringence [50].

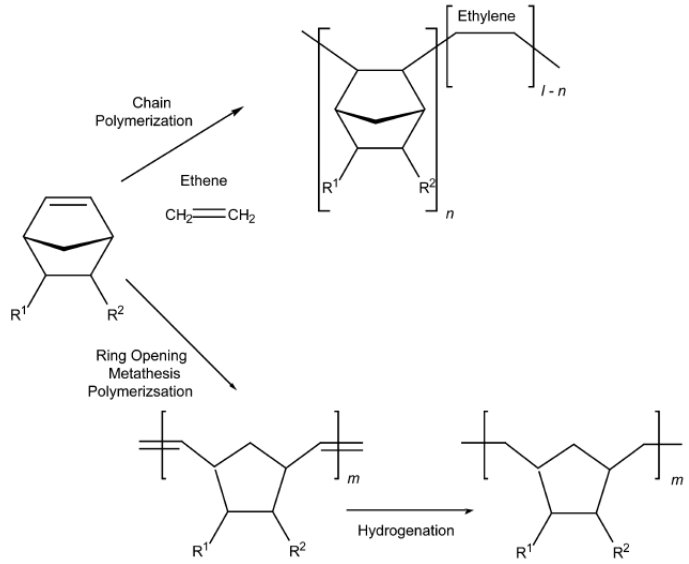

Figure 10: Typical polymerization scemes for cyclo-olefin-polymers. Top: cyclo-olefin-copolymer (COC), bottom: cyclo-olefin-polymer (COP) [50].

One can distinguish between two different phenomena if COCs are stored at high temperatures. Annealing above T_g only leads to densification due to chain reordering. Significantly (30 °K) below T_g, the COC shows two phenomena: structural relaxation (physical aging) and densification. The difference between both can be seen in Figure 11. Figure 11 (A) shows the frozen and strained chains of quenched amorphous COC. During physical aging, the strained chains (a, b and c) are loosened and glass transition enthalpy is recovered due to the softened structures (see Figure 11 (B)). The densification process on the other hand leads to fast chain relaxation and denser chain-packing resulting in substantial T_g increase (see Figure 11 (C)) [19].

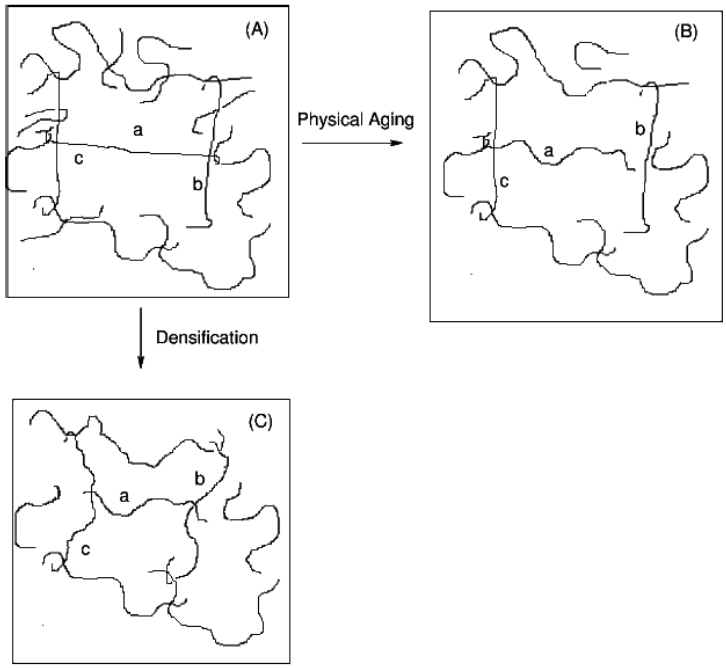

Figure 11: Schematic representation of chain motions of cyclo-olefin-copolymers during physical aging compared to densification [19].

2.2.2 Effects of aging on selected properties

The amount of properties describing a plastic is sheer endless. For each polymer and every type of loading, these properties behave different over time. The goal of the following paragraphs is to point out the typical changes under temperature loading over time for some parameters which are crucial to the application of the investigated product. Targets for mass spectrometry have to meet very accurate geometric specifications, the impermeability of their coating has to remain intact over time and their wetting behavior should not be influenced by transport or storage. This research will therefore focus on the properties connected to these specifications.

Since the quality of the surface is crucial to the application of the investigated product, properties suited to define the condition of the surface must be found. The following paragraphs define these properties and possible aging phenomena.

2.2.2.1 Roughness

In general, the surface roughness of a plastic part is determined by the roughness of the mold cavity [9]. Amplitude parameters are commonly used to characterize the surface roughness. The most important are: R_a (arithmetic average), R_q (also called R_{RMS}, root mean squared) and R_z (the average distance between the 5 highest peaks and 5 lowest valleys within the assessment length) [52].

Since surface roughness is not crucial to many applications of plastics, there is hardly any research focusing on the effects of aging on roughness. One study shows changes in roughness after aging for some polymers used in dental medicine while most remained unchanged [15].

In general, surfaces of amorphous polymers are expected to become smoother through physical aging. The surface of semi-crystalline polymers, on the other hand, may become rougher, since post-crystallization leads to an increasingly coarse microstructure [56].

2.2.2.2 Wetting behavior

Wetting behavior strongly influences adhesion and coating of polymers. Wetting is defined as the interaction of a liquid with a solid. Possible interactions are: the formation of a contact angle at the interface between both media, the spreading of the liquid over the solid's surface, or the penetration of a liquid into a porous solid medium [16].

The macroscopic behavior of interfaces can well be explained with the classical thermodynamic and mechanical description of capillarity as shown by Gibbs, Laplace and Young in the nineteenth century. Interfacial tension, key part of the classical theory of capillarity, describes the free energy necessary to increase the contact area between two different phases and is an important thermodynamic parameter to predict the wetting and adhesion properties of polymer materials [16].

Since the molecules in a solid surface are immobile, solid surface tensions cannot be measured directly. From several independent approaches to estimate surface free energies of solids, contact angle measurements are believed to be the simplest. The most common techniques to measure contact angles are the Wilhelmy balance

technique and the measurement of contact angles from sessile drops or adhering bubbles [16].

Thermodynamically, one has to differentiate between complete and partial wetting (see Figure 12). In the case of complete wetting, the contact angle is zero, the liquid (marked l) forms a very thin film on the solid surface (marked s) and molecular interactions must be taken into account, as in Figure 12 (c). If the contact angle is finite and the liquid does not spread over a large area, one speaks of partial wetting, see Figure 12 (a) and (b). In this case, the shape of a liquid drop is determined by a combination of surface tension and gravity effects [16].

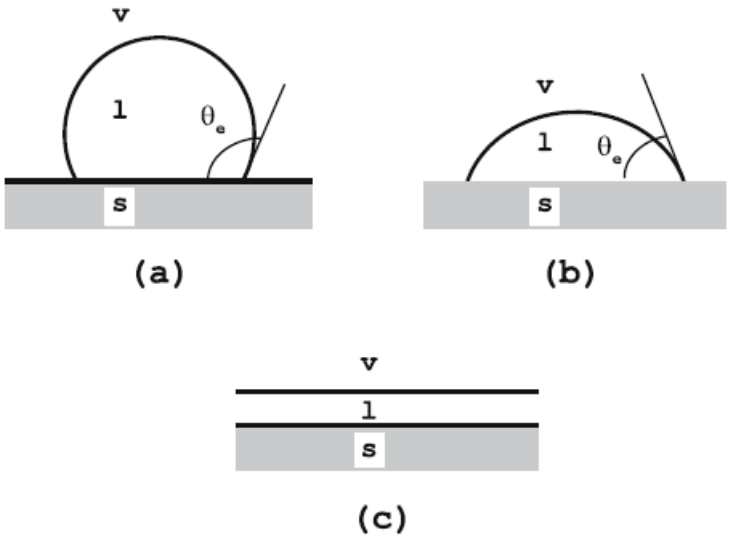

Figure 12: Different wetting situations: (a) and (b) correspond to partial wetting, (c) shows complete wetting; v: vapour, l: liquid, s: solid [16].

Classical theory of capillarity assumes that the solid's surface is smooth, homogeneous, isotropic and insoluble. Therefore, a unique contact angle is expected for a given solid-liquid system. However, this is not consistent with observations in dynamic contact angle experiments. If liquid is added to a drop on a solid, the contact angle stays constant while the radius of the drop increases. The contact angle in this case is called advancing. Respectively, if liquid is withdrawn from the drop, the radius of the drop will first stay constant, while a decrease in contact angle is observed. Eventually, the contact angle will reach a minimum called receding contact angle and the radius of the drop will decrease. This behavior is shown schematically in Figure 13. The difference between advancing and receding contact angle is called contact angle hysteresis. The amount of this hysteresis increases with roughness and heterogeneity of the surface. While the situation is more complicated for heterogeneous surfaces, reproducible predictions for the influence of roughness on contact angle hysteresis exist. One of the first to discuss this influence was Wenzel

who introduced a roughness factor (which represents the relation between the true surface area and the geometric surface area). The Wenzel equation predicts that the contact angle will increase with roughness if the contact angle on a smooth surface is greater than 90° and will decrease if it is less than 90° [16]:

$$\cos\theta_w = r\cos\theta \qquad (13)$$

where θ is the equilibrium contact angle θ_w is the apparent contact angle on the rough surface and r is the ratio of the actual wetted surface area to geometric or projected surface area calculated from the radius of the wetted base.

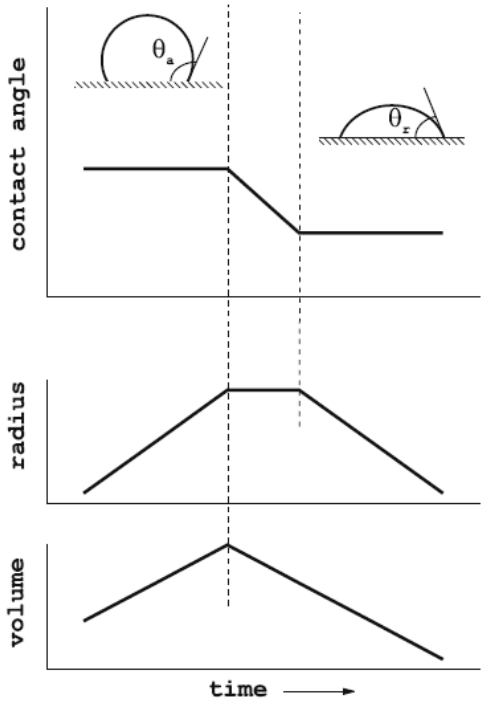

Figure 13: Representation of advancing (θ_a) (the maximum upon addition of liquid in a sessile drop) and receding (θ_r) (the minimum upon withdrawal of liquid) contact angles [16].

Since temperature affects a number of properties of both liquid and surface (e.g., viscosity, surface tension and oxidation behavior), contact angle values are sensitive to temperature. Usually viscosity and surface tension of a liquid decrease at higher temperatures, leading to increased wettability [27].

Changes in the chemical composition of the solids surface (due to oxidation or adsorption of ambivalent species) can affect contact angle values. Research done by Leezenberg et al. showed an increase of water contact angle on hydrogenated-carbon (a-C:H) films over time. After 30 days of storage at ambient conditions, films produced with different H_2 rates which originally showed contact angles from 35° to

65° all showed contact angles around 75°. The authors explained this phenomenon with adsorption of ambivalent species (especially water), since this effect was partially reversible if the samples were stored under vacuum [28].

2.2.3 Life time prediction

The complex chemical reactions superposed by physical and geometric effects make an accurate prediction of a plastic part's lifetime nearly impossible. Preconditions for a reliable life time prediction are test conditions similar to those during the use of the product and significant criteria determining failure [11].

2.2.3.1 Arrhenius equation

Nearly all models describing the aging of plastics base on the Arrhenius equation. This universal equation describes the temperature dependency of simple reactions and physical procedures. It states that the reaction rate of simple chemical reactions increases exponentially with temperature. However it can lead to false results if the Arrhenius equation is applied to processes composed of many different single reactions. The application of the Arrhenius equation therefore relies on the assumption that the aging rate of a plastic is defined by one single dominant chemical reaction or physical process [11].

The Arrhenius equation can be given as in equation (12) or as follows:

$$\ln k = \ln A - \frac{E_a}{RT} \qquad (14)$$

with: E_a = Activation energy
R = Gas constant
k = Reaction rate
T = Temperature
C = Constant

If the aging rate measured at different temperatures is plotted logarithmically against 1/T, the Arrhenius equation should give a declining straight line (as seen in Figure 14). The activation energy E_a is then obtained from the slope of the line (-E/R) [2].

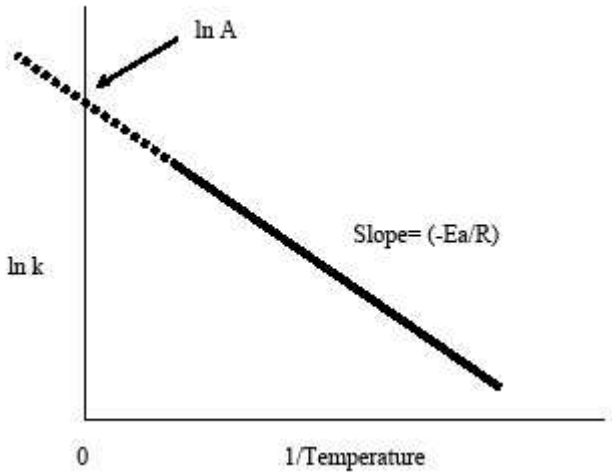

Figure 14: Schematic representation of an Arrhenius plot [2].

2.2.3.2 Time-temperature superposition

An alternative to the Arrhenius equation is time-temperature superposition. For this purpose, characteristic curves measured at different temperatures are moved along the time axis to construct a master curve at a randomly-chosen reference temperature T_0. Through superposition one can obtain a master curve over a time period significantly longer than of the single curves (see Figure 15) [11, 49].

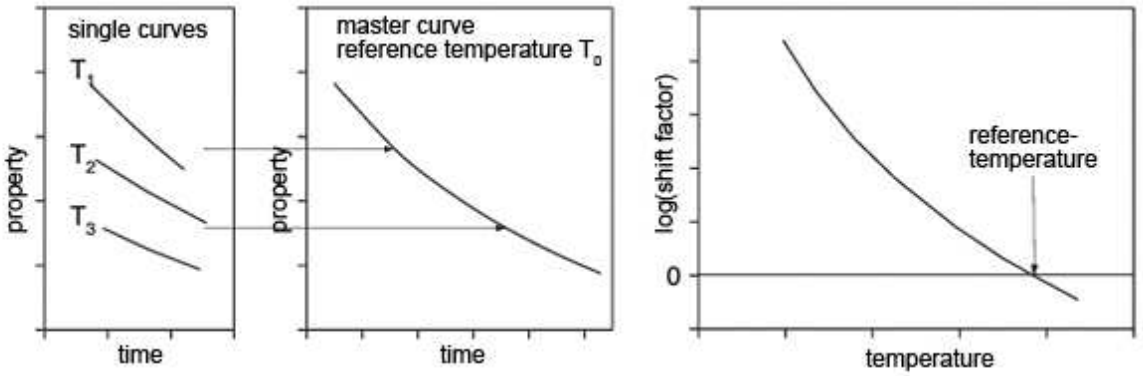

Figure 15: Left: construction of a master curve; Right: temperature shift factor against temperture [5].

The time scaling is expressed by the temperature shift factor a_t. The following equation is then valid for any property and describes the time needed to reach the same level [11]:

$$a_t = \frac{t}{t_{ref}} \qquad (15)$$

With: a_t = Temperature shift factor
t = Time needed to reach a defined identical property change
t_{ref} = Reference time to reach a defined identical property change

Mathematically, this means that the superposition is achieved by multiplying the times for each temperature with the temperature shift factor a_t and dividing the property by the same factor. The shift factor can be calculated using the Arrhenius equation (12) [11].

Using the Arrhenius equation, the temperature shift factor is described by a straight line [11]:

$$\log(a_t) = \left[-\frac{E_a}{R}\left(\frac{1}{T} - \frac{1}{T_{ref}}\right)\right] \qquad (16)$$

For most diagrams the shift factor is converted to a non-logarithmic factor by using following equations [11]:

$$a_t = 10^{k\left(\frac{1}{T}-\frac{1}{T_{ref}}\right)} \qquad (17)$$

With the activation factor k defined as follows [11]:

$$k = -\frac{E_a}{R}\log(e) \qquad (18)$$

With: a_t = Temperature shift factor
k = Activation factor
E_a = Activation energy
R = Gas constant
T = Absolute temperature
T_{ref} = Absolute reference temperature

3 EXPERIMENTAL

3.1 Materials

3.1.1 Injection molding grades

Two injection molding grades were used for this thesis. A 30 wt% carbon-black filled conductive polypropylene (Type: PP MD000E-BK1D463 (722000159), Sabic, NL) and a cyclo-olefin-polymer (Type: Zeonor 1060R, Zeon Corporation, Japan). In the following, the polypropylene will be abbreviated PP-C and the cyclo-olefin-polymer COP.

PP-C is used in applications where good electric conductivity is needed. Its semi-crystallinity and filler material make this material very challenging for shrinkage prediction. Some material data can be found in Table 1.

Table 1: Material Properties PP MD000E-BK1D463 (722000159) [39].

Property	Measurement method	Unit	Value
Specific gravity	ISO 1183	-	1.07
Tensile strength (max.)	ISO 527	MPa	26
Tensile elongation (at break)	ISO 527	%	3.7
Flexural strength	ISO 178	MPa	35
Flexural modulus	ISO 178	GPa	1.7
Surface resistivity	ASTM D257	Ohm/sq	$10\text{-}10^3$
Mold shrinkage (flow direction), 3mm	ISO 2577	%	1.3-1.8

COP is very popular for life science applications due to high transparency, low specific gravity, low water absorption, high chemical resistance, high thermal stability and low viscosity [40]. Typical properties of Zeonor 1060R can be found in Table 2.

Table 2: Relevant properties of COP Zeonor 1060R [40].

Property	Measurement method	Unit	Value
Specific gravity	ASTM D792	-	1.01
Water absorption	ASTM D570	%	<0.01
Moisture permeability	JIS Z 0280 (300µm)	g/m^2 24hr	0.29
Light transmittance	ASTM D1003 (3mm)	%	92
Glass transition temperature	DSC	℃	100
Melt flow rate	JIS K6719 (230℃)	g/10min	14
Molding shrinkage	ASTM D955	%	0.1-0.3

3.1.2 Sputtering targets

Besides testing the uncoated substrates, the aging tests were performed on coated PP-C targets. Two planar magnetron sputtering targets produced by Umicore Materials AG, Liechtenstein were used for this purpose. One target was produced out of steel 1.4301 and had a thickness of 6 mm (for detailed composition see Table 3). The other target was made of 99.99 % gold. One has to keep in mind that the gold layer was applied over a very thin steel layer to improve adhesion between coating and substrate.

Table 3: Planar magnetron sputtering steel target composition [35].

Element	Proportion / wt%
C	0.026
Cr	17.338
Fe	72.509
Mn	1.023
N	0.045
Ni	8.692
P	0.031
S	0.002
Si	0.334

3.2 Specimen

3.2.1 Shrinkage

A schematic drawing of the specimens used for the shrinkage tests can be found in Figure 16. The specimens were injection-molded out of PP-C and COP. For this part of the research, the specimens were not coated. The specimens' outer dimensions were 75 x 25 x 1 mm. Two different position marks, a cross and a circle, were engraved at four positions in the mold to allow optical dimension measurements.

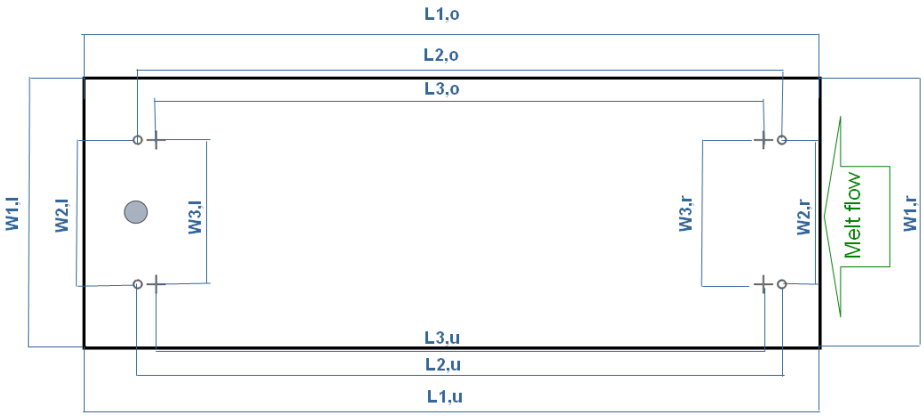

Figure 16: Shematic drawing of sample used for shrinkage experiments.

3.2.2 Aging

Other than for the shrinkage evaluation the design of FlexiMassTM-DS targets for mass spectrometry (TO-430; Shimadzu Biotech – Kratos Analytical, UK) was used for all aged samples. Not only was the layout with steel-coated PP-C tested, but also uncoated COP and PP-C substrates as well as gold-coated PP-C specimens. Shrinkage and flatness measurements were performed on 4 targets mounted in an adapter (TO-488; Shimadzu Biotech – Kratos Analytical, UK). Figure 17 shows the target and adapter as commercially available.

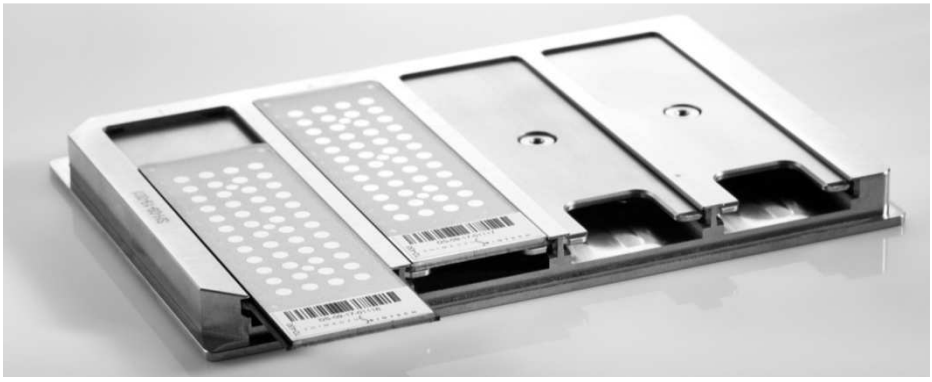

Figure 17: FlexiMassTM-DS target for mass spectrometry in adapter.

3.3 Equipment

3.3.1 Specimen production

3.3.1.1 Injection molding

All specimens were molded on the ELION 800-60 PM injection-molding machine by Netstal, CH. Due to its precision, this all electric machine is very well suited for life science products. Figure 18 depicts this 800 kN clamping force machine, some important technical data can be found in Table 4.

Figure 18: Netstal Elion 800-60 PM [36].

Table 4: Properties Netstal Elion 800-60 PM [36].

Property	Unit	Value
Clamping force	kN	800
Screw stroke	mm	100
Screw diameter	mm	18
Max injection pressure	bar	2350
Max shot weight	g	24.4
Max injection rate	cm^3/s	63.6
Screw L/D ratio	-	21.7

3.3.1.2 Coating

The coating was applied in a DC Pulse Sputtering process using the Sprinter-5 Coating System of Oerlikon Balzers AG, Vaduz, FL. The coating system and the sputtering chamber can be seen in Figure 19 and Figure 20.

Figure 19: Oerlikon Balzers Sprinter – 5 Coating system.

Figure 20: Sputtering Chamber of the Sprinter – 5 Coating System with a different target.

3.3.2 Aging equipment

The specimens were aged in following chambers, ovens or freezers:

- 80 °C/ 90 % rh: Climate chamber (PL-1KPH; espec Corp., Japan)
- 80 °C and 60 °C: Oven (KB 53; WTB Binder, Germany)
- -20 °C: Freezer (7082668-00; Liebherr Hausgeräte Ochsenhausen GmbH, Germany)
- -80 °C: Ultra Low Temperature Freezer (C340 Premium; New Brunswick Scientific, USA)

3.3.3 Testing equipment

A great variety of tests was performed at Sony DADC's plant in Anif, Austria. The tests focused on external dimensions and surface properties. The following paragraphs describe the test equipment and procedures used.

3.3.3.1 External dimensions

The optical checker Werth ScopeCheck 200 was used to determine the dimensions of the specimens. After recording a test procedure once, this checker measures the distance between measuring marks or outer borders automatically for the following targets. The measurement file is saved in the .txt format and later imported into Microsoft Excel.

For the shrinkage tests, 20 samples were examined for each process setting. The dimensions shown in Figure 16 in chapter 3.2.1 were measured and exported to the file. A comparison of the results showed that the dimensions measured between the circular position-marks proved most accurate, apparently these positioning marks were better suited for the measurement software. Therefore, these results were used for further evaluation and comparison to simulation results.

All four specimens aged under the same circumstances were inserted in an adapter and the distance between the 4 outer spots was measured for each target as shown in Figure 21. The measurement software had to be adapted to both grades (COP and PP-C) and for coated and uncoated samples.

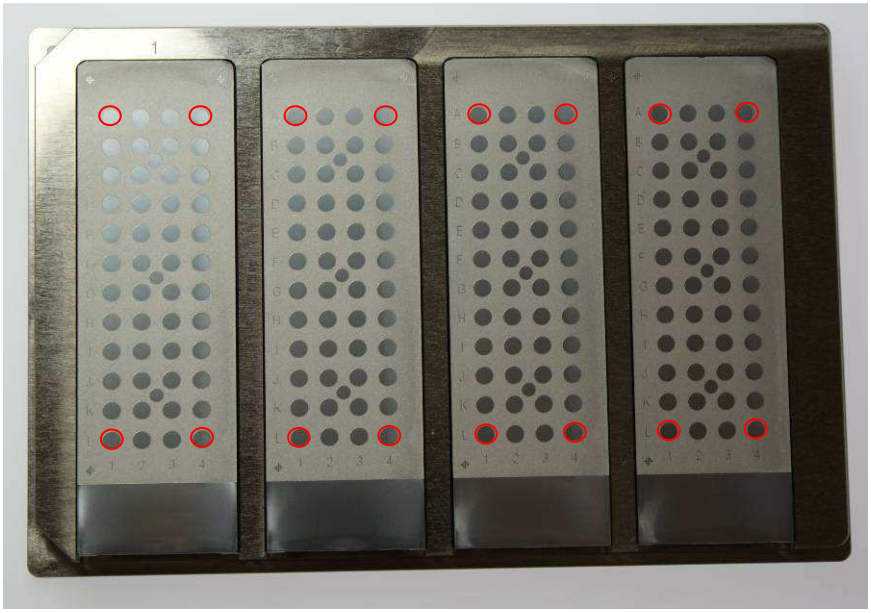

Figure 21: Four aging targets in one adapter. The red circles mark the measuring positions.

3.3.3.2 Flatness

The topography of the specimen´s surface was investigated with the FRT MicroProf 200 system equipped with the 3 mm CWL sensor (FRT GmbH, Germany). With this measuring tool and the Aquire Version 1.38 software (FRT GmbH, Germany) a 3D model of the surface topography was created and the data was used to calculate flatness. The properties of the CWL sensor can be found in Table 5.

Table 5: Properties of the 3 mm CWL Sensor [37]

Measuring range z	3 mm
Max. resolution z	30 nm
Resolution x, y	5-6 µm
Measuring angle	90° ± 15°

This test was performed on plain and coated aged specimens molded from COP and PP-C. Four targets were inserted into the adapter and a topography profile of 75 lines, each consisting of 2500 data points, was measured. The result file was converted into the .xls format via Matlab R2009. A Microsoft Excel VBA Marco picked 4 defined lines and measured the flatness results for each target. Figure 22 shows how the flatness value was calculated, Figure 23 depicts the profiles used for flatness examination.

Figure 22: Flatness measurement principle.

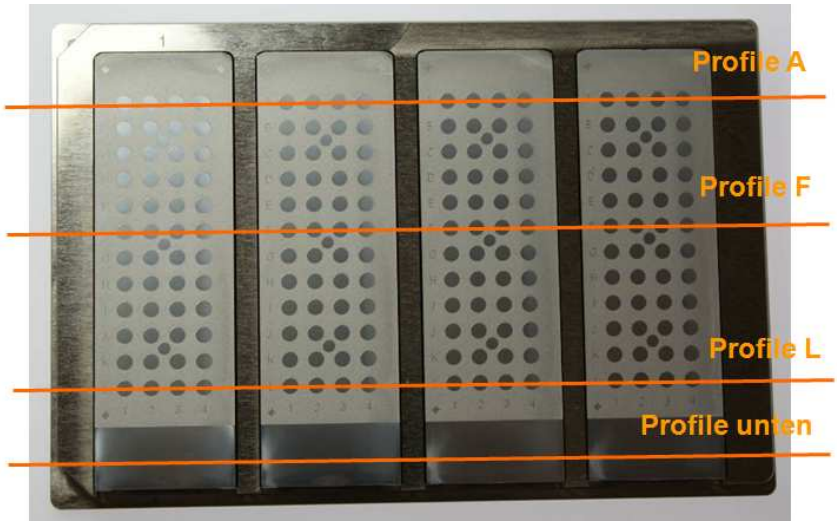

Figure 23: Flatness measurement profiles.

3.3.3.3 Roughness

The roughness of all aged specimens was measured with the FRT MicroSpy Topo, a confocal microscope designed by FRT GmbH, Germany. The tests were performed using a 20x object lens and 0.1 µm step size (properties see Table 6). Roughness measurements were done on three smooth spots and three times on the rough area outside of the spots (see Figure 24). The FRT Mark III Version 3.8.22.1 software by FRT GmbH, Germany was used to calculate the roughness values Ra, Rq and Rz and to export them to Microsoft Excel. The Ra value of the mold was 31 nm on the spots and 1.47 µm outside of the spots.

Table 6: Properties of the FRT MicroSpy Topo system with 20x lens [38].

Measuring range	400 µm
Resolution z	3 nm
Resolution x, y	1 µm

3.3.3.4 Scanning electron microscopy (SEM)

Both the coated and uncoated aged samples were examined with a (scanning electron microscope SEM) HITACHI S-4000 (Hitachi High-Technologies Corporation, Japan). Plain PP-C and COP samples had to be coated with a thin gold layer before SEM examinations. It was investigated whether any defects (e.g., cracks or delaminations) on coated samples or changes in surface appearance could be detected. For this purpose, the same spots checked during roughness evaluation (marked red in Figure 24) were examined with 40 x, 1000 x and 10,000 x magnification.

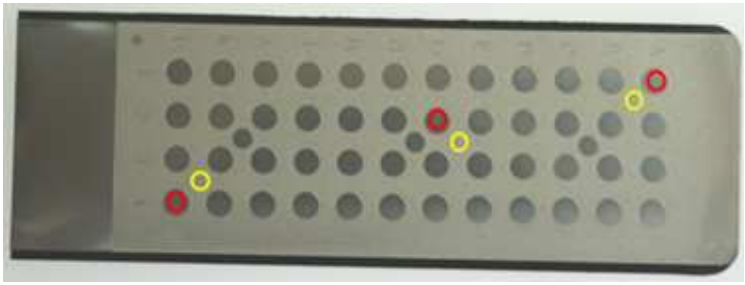

Figure 24: Red circles mark spots used for SEM and roughness measurement, yellow circles mark rough areas used for roughness measurement.

3.3.3.5 Peel test

The peel t est was the last test performed on the aged samples since it was the only destructive testing method. This test evaluates the adhesion of coatings, therefore only the coated samples were tested. In accordance with DIN EN ISO 2409, the samples were scored with a cross cut tester (ZCC 2087; Zehntner GmbH, CH, see Figure 25), an adhesive tape was taped over the scored area and pulled off evenly. The strips were pasted on white paper and the damage was examined.

Figure 25: cross cut tester (ZCC 2087; Zehntner GmbH, CH).

3.3.3.6 Contact angle

The wetting behavior of all aged targets was examined with the EasyDrop system by Krüss, Germany. A drop of water was disposed on the specimen´s surface and the angle between the drop´s contour and the surface was measured with the DSA software (Krüss, Germany). A drop volume of 2 µl and the T-1 method was used. The drops were applied on three spots of the specimen as marked in Figure 26. For each aging setting three spots on one specimen were examined.

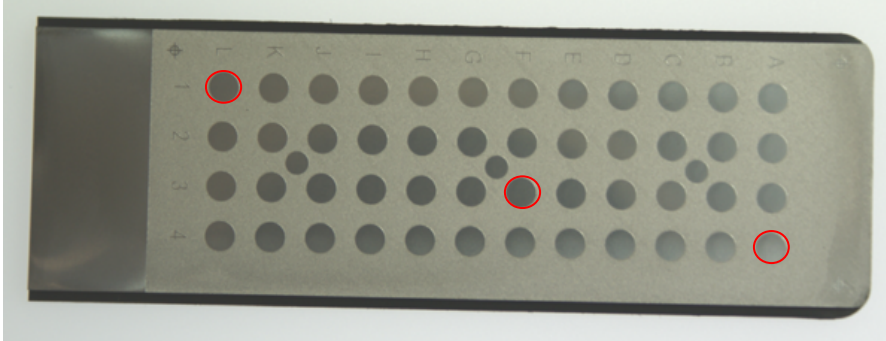

Figure 26: Spots used for contact angle measurement.

3.4 Design of experiment

3.4.1 Shrinkage

3.4.1.1 Empirical tests

3.4.1.1.1 Injection parameters

Four different parameters were chosen for this research: cylinder temperature, mold temperature, injection speed and holding pressure. For each parameter, an appropriate high and low setting was chosen. One series with all parameters on a medium level was done as reference. In total, this resulted in 17 different settings which can be seen for both materials in Table 7 and Table 8. The holding pressure profile for PP-C can be seen in Figure 27, the one for COP in Figure 28.

Table 7: Settings for experimental shrinkage tests of PP-C.

setting Nr.	cylinder temp. / °C	mold temp. / °C	inj. speed / mm/s	holding pressure / bar
1	200	40	200	400
2	200	40	200	1000
3	200	40	400	400
4	200	40	400	1000
5	200	70	200	400
6	200	70	200	1000
7	200	70	400	400
8	200	70	400	1000
9	234	40	200	400
10	234	40	200	1000
11	234	40	400	400
12	234	40	400	1000
13	234	70	200	400
14	234	70	200	1000
15	234	70	400	400
16	234	70	400	1000
17	217	55	300	700

Table 8: Settings for experimental shrinkage tests of COP.

setting Nr.	cylinder temp. / °C	mold temp. / °C	inj. speed / mm/s	holding pressure / bar
1	220	60	120	500
2	220	60	120	700
3	220	60	250	500
4	220	60	250	700
5	220	90	120	500
6	220	90	120	700
7	220	90	250	500
8	220	90	250	700
9	260	60	120	500
10	260	60	120	700
11	260	60	250	500
12	260	60	250	700
13	260	90	120	500
14	260	90	120	700
15	260	90	250	500
16	260	90	250	700
17	240	75	185	600

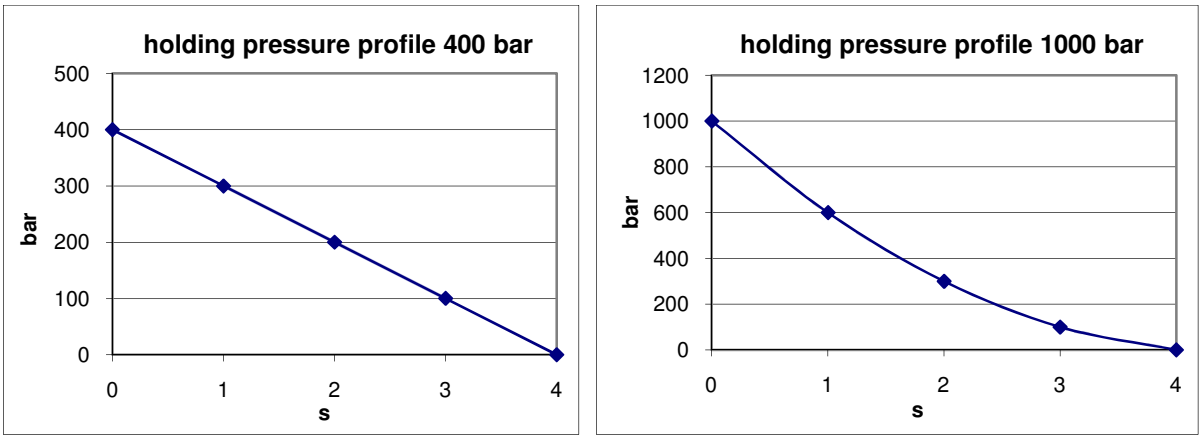

Figure 27: Pressure profiles for PP-C.

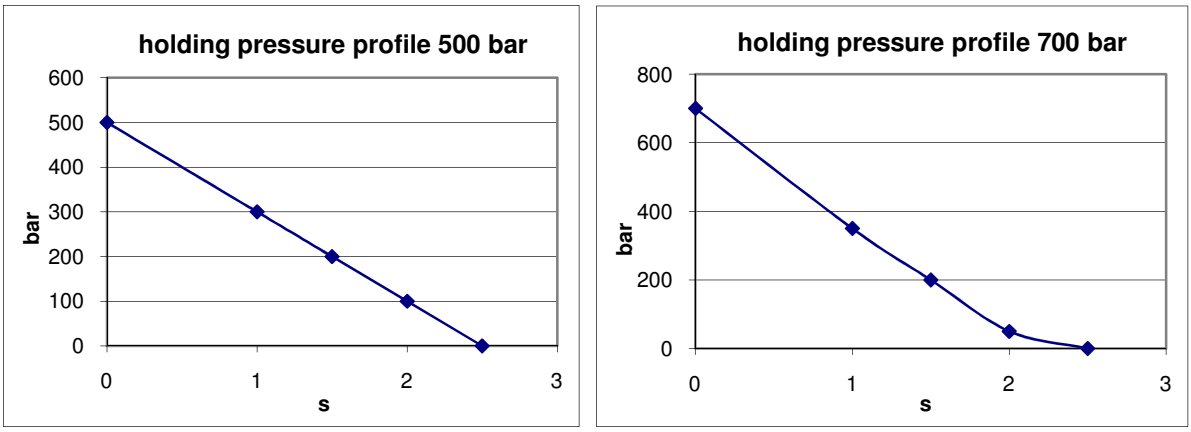

Figure 28: Pressure profiles for COP.

3.4.1.1.2 Timeline

To examine the changes in shrinkage over time, the dimensions of the specimens were measured at four different times: immediately after injection molding, 1, 16 and 47 days after injection molding. This is illustrated in Figure 29.

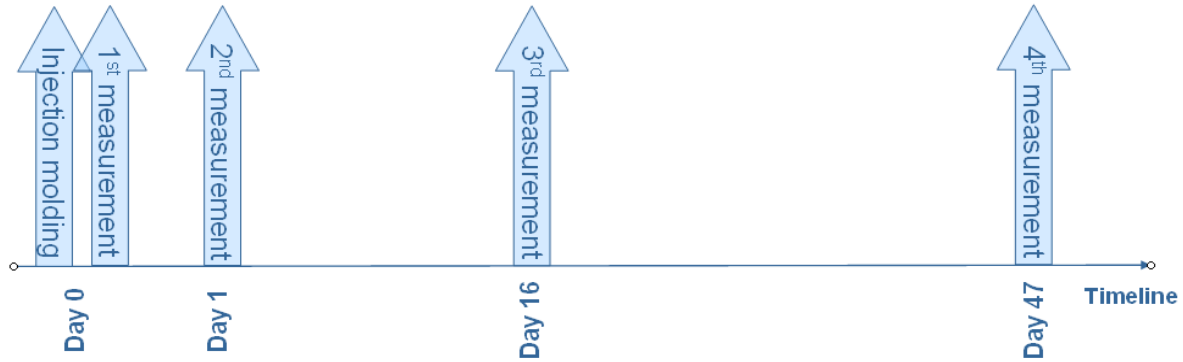

Figure 29: Timeline for shrinkage measurements.

3.4.1.1.3 Data reduction

For each parameter set, a measurement series of 20 samples was evaluated. The evaluation software created a text file with all dimensions marked in Figure 16. This file was imported in Microsoft Excel 2003 and the average, standard deviation, minimum and maximum of this series were calculated. This data was first reduced in a form as can be seen in Figure 30 and then used for different comparisons.

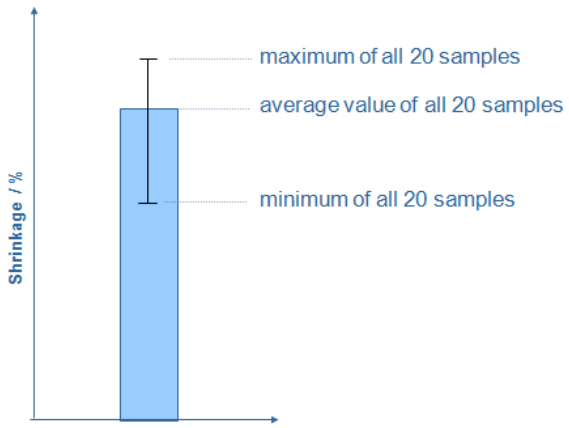

Figure 30: Data reduction for shrinkage tests.

3.4.1.2 Simulation

One goal of this research was to investigate whether simulation could be used to predict the extent of shrinkage of the specimens. Therefore, a shrinkage simulation was performed by the IKV-Institute of Plastics Processing at the University of Leoben. To get most reliable results, the experimental results were compared to two different simulation models. In addition to the injection parameters investigated in the experimental part, further parameter sets were added so that it was possible to compare the trend for all parameters investigated. The following paragraphs illustrate the approach to simulation.

3.4.1.2.1 Software

The software used for the simulations was Moldflow Plastics Insight 6.2 Rev. 3. This simulation software has found most use throughout the industry since its numerous features facilitate mold design and allow injection molders to cut costs significantly.

3.4.1.2.2 Model

A model of the specimen used in the experimental part, including the runner and cooling system, was created, as can be seen in Figure 31 and Figure 32.

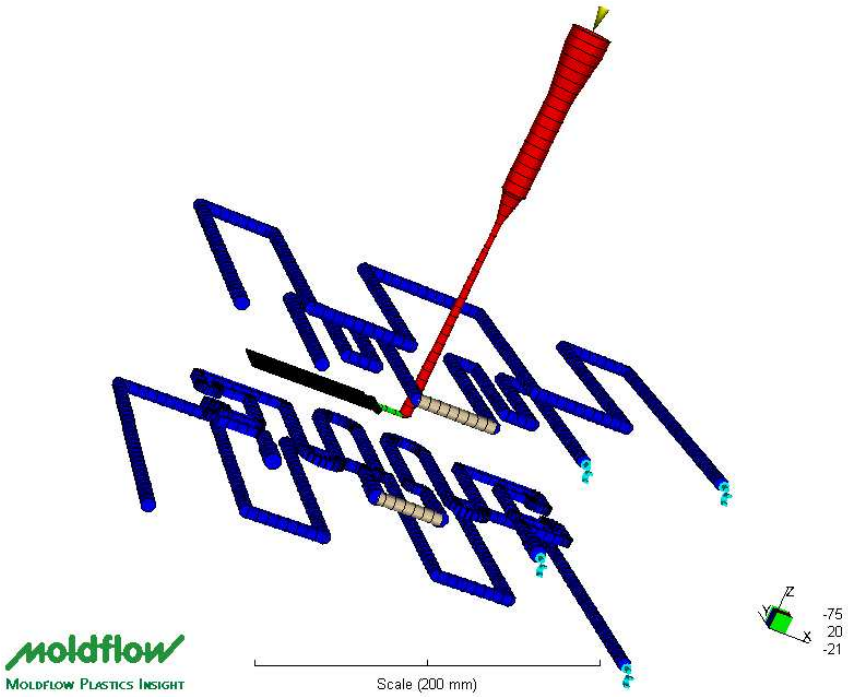

Figure 31: Simulation model including runner and cooling system.

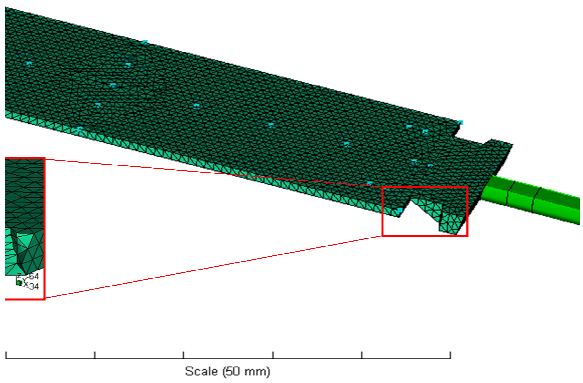

Figure 32: Detailed view of the simulation model of the part to be molded.

Since both materials have only limited commercial use, the material data required for simulation cannot be found in the usual databases. This data was measured earlier at the IKV-Institute of Plastics Processing at the University of Leoben and was then imported into Moldflow [29].

The Moldflow software allows different types of meshing. For better comparison, simulation was done for two different mesh types: a 3D and 2.5D (Dual Domain) mesh. The differences between both mesh types are explained in chapter 2.1.4.

3.4.1.2.3 Parameters

In addition to the parameter sets used for the experimental tests (see chapter 3.4.1.1.1), following combinations of parameters were investigated to observe possible non-linear trends:

Table 9: Additional parameter sets simulated for PP-C.

setting Nr.	cylinder temp. / °C	mold temp. / °C	inj. speed / mm/s	holding pressure / bar
28	217	70	400	1000
31	217	40	200	400
34	234	55	400	1000
37	200	55	200	400
40	234	70	300	1000
43	200	40	300	400
46	234	70	400	700
49	200	40	200	700

Table 10: Additional parameter sets simulated for COP.

setting Nr.	cylinder temp. / °C	mold temp. / °C	inj. speed / mm/s	holding pressure bar
28	240	90	250	700
31	240	60	120	500
34	260	75	250	700
37	220	75	120	500
40	260	90	185	700
43	220	60	185	500
46	260	90	250	600
49	220	60	120	600

3.4.1.2.4 Data reduction

The mesh of the simulated part contained nodes for calculation correlating with the positioning marks on the specimen´s surface. A VBA-macro was designed to calculate the distance between these nodes, thus giving the specimen´s simulated dimensions. This data was used to calculate the predicted shrinkage and was compared to the experimental data. Besides calculating the total deviation between the experimental and simulated values, trend diagrams showing the variation of shrinkage when changing different process parameters were created.

3.4.2 Aging

3.4.2.1 Short-term tests

Short-term tests were done out of two reasons: to investigate whether the part´s properties could be influenced by exposing the specimen to elevated temperatures over a short period of time and to examine whether the product is damaged by transportation phenomena. For this purpose, two different types of tests were done, static conditioning tests, where the specimens were exposed to a constant temperature up to 3 days and cyclical tests, where the samples were frozen overnight (16 h) and left at room temperature during the day (8 h). Short-term tests were performed on uncoated PP-C and COP targets, as well as steel coated PP-C specimens. The exact design of experiment for these tests is defined in the following paragraphs.

3.4.2.1.1 Static tests (conditioning)

Static conditioning tests were done with temperatures ranging from -80 °C to 120 °C with durations starting from 1 min up to 3 days. Furthermore, the influence of humidity was tested for selected temperatures. Table 11 shows which tests were done for each temperature. For tests done in climate chambers (only tests lasting 24 hours and longer) an exact humidity value is given, for tests done in ovens, refrigerators or at room temperature, humidity is marked as undefined (undef.).

Table 11: Testing parameters for static conditioning tests.

Temperature / °C	Duration	Humidity
120	1, 5, 15, 30 and 45 minuntes 1 and 6 hours	undef.
80	15, 30 and 45 minutes 1, 3, 6, 9, 14, 24, 48 and 72 hours	undef.
	24, 48 and 72 hours	90 % rh
40	1, 2, 3, 4, 6, 12, 24, 48 and 72 hours	undef.
	24, 48 and 72 hours	90 % rh
25	24, 48 and 72 hours	undef.
	24, 48 and 72 hours	90 % rh
-20	24, 48 and 72 hours	undef.
-80	24, 48 and 72 hours	undef.

3.4.2.1.2 Cyclical tests

Two cyclical tests were performed. One varied between -20 °C and room temperature, the other between -80 °C and room temperature. In total, the specimens were subjected to 5 cycles stretching over 7 days. Figure 33 schematically shows how the cyclical tests were performed.

Figure 33: Procedure for cyclical tests.

3.4.2.2 Long-term tests

3.4.2.2.1 Specimen preparation

As with the short-term tests, uncoated and coated samples were used. Additionally, some coated targets were pre-conditioned, meaning they were heated to 120 °C for 10 minutes or 80 °C for an hour prior to the long-term aging tests. This way it was investigated whether preconditioning had any effect on the long-term behavior of the product. In total, this resulted in 6 different types of specimens as listed in Table 12.

Table 12: Types of specimens used in long-term tests.

Substrate	Coating	Conditioning
PP-C	none	none
PP-C	steel	none
PP-C	steel	120 °C / 10 min
PP-C	steel	80 °C / 1 hour
PP-C	gold	none
COP	none	none

A total of ten boxes containing four specimens were aged for each type of specimen and test condition (see Table 13). Over the 14 week testing period, the specimens were examined after eight removals; two boxes were kept as reserve. Table 14 shows the aging time before each removal.

3.4.2.2.2 Test parameters

Table 13: Test conditions long term tests.

Temperture / °C	Humidity / % rh
80	undef.
80	90%
23 (RT)	undef.
-20	undef.
-80	undef.

Table 14: Aging time before each removal.

Box	Aging time / weeks
1	1
2	2
3	3
4	4
5	6
6	8
7	11
8	14

4 RESULTS AND DISCUSSION

4.1 Shrinkage

The following chapters show the results of the empirical and simulated shrinkage examination. Both results are compared and a conclusion is drawn whether in this case the simulation tools used are applicable for shrinkage prediction.

4.1.1 Average experimental shrinkage

PP-C

In Figure 34, one can see that the average shrinkage of all investigated PP-C samples is quite extensive. Significant post-mold-shrinkage can be observed. While the shrinkage over the length is not quite 1 % immediately after injection molding, it increases to over 1.1 % in 47 days. It can be observed that the width near the gate shrinks approximately 0.1 % less than the width away from the gate.

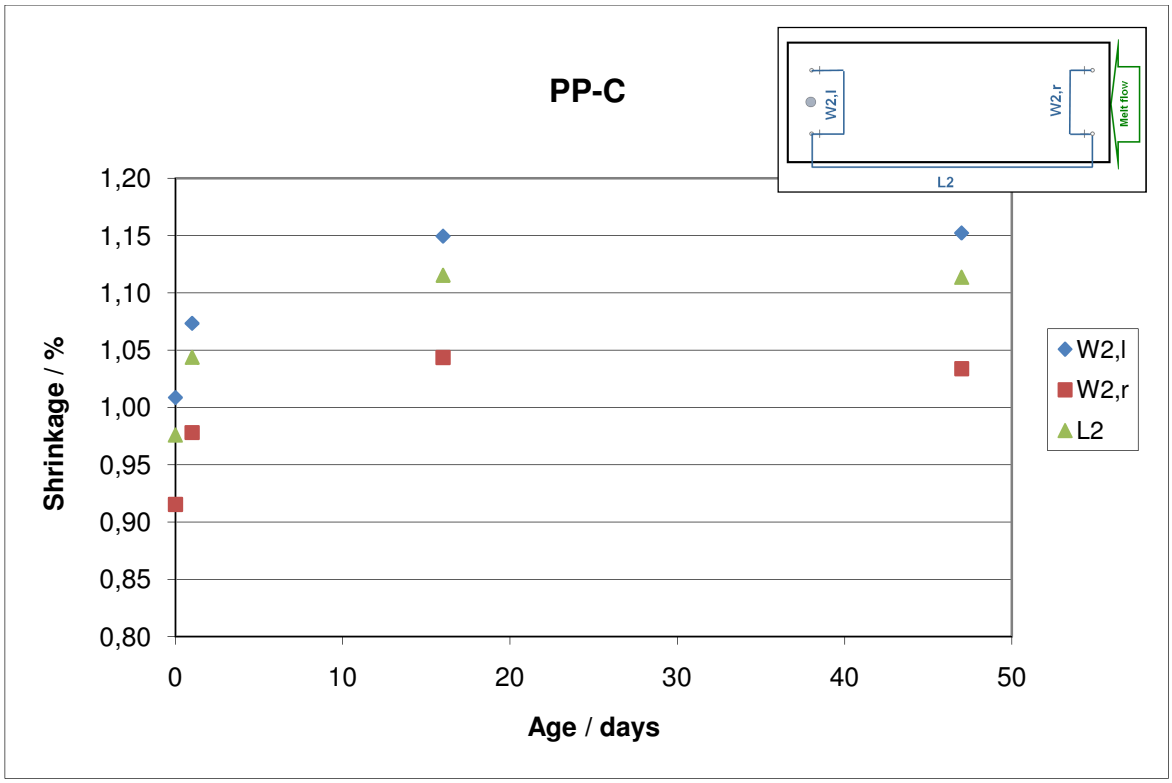

Figure 34: Average shrinkage of PP-C samples over time.

COP

As seen in Figure 35, the amorphous COP shows hardly any change in shrinkage over time, just a slight increase in shrinkage during the first day after injection molding, and shrinkage values are nearly the same (between 0.3 and 0.35 %) for all examined dimensions.

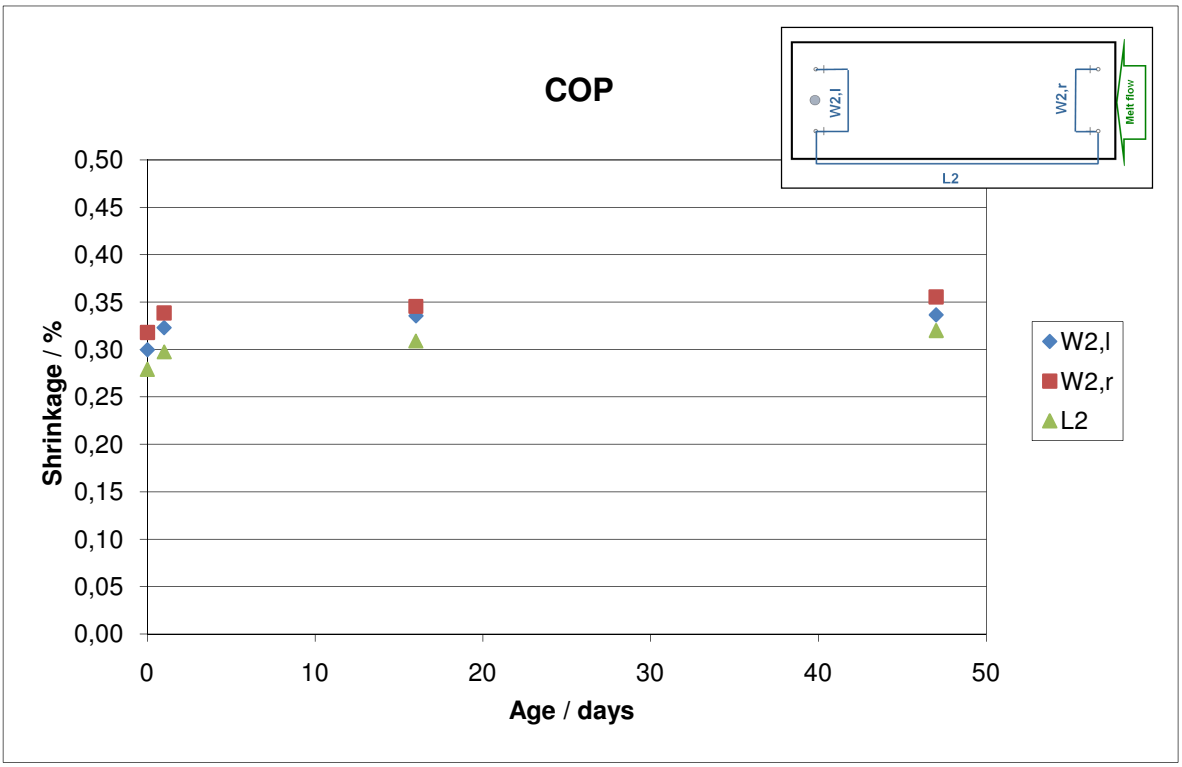

Figure 35: Average shrinkage of all COP samples over time .

Overall, one can see that the two materials used for this research show great differences in their shrinkage behavior. This was expected since COP is an unfilled amorphous and PP-C is a highly filled semi-crystalline polymer. Figure 36 summarizes all shrinkage data obtained during the experimental part. The average, minimum and maximum of the shrinkage values measured for all 17 settings are shown for both materials. Not only the absolute shrinkage values (as can be seen PP-C shrinks three to four times more than COP) show significant deviations, but there are also differences in the shrinkage behavior over time and between the investigated dimensions of the sample.

This correlates to predictions by literature [12] stating great differences between amorphous and semi-crystalline materials. Overall semi-crystalline resins shrink more, their shrinkage increases after injection molding due to post-crystallization and depends on molecule-orientation which also influences the crystallization process.

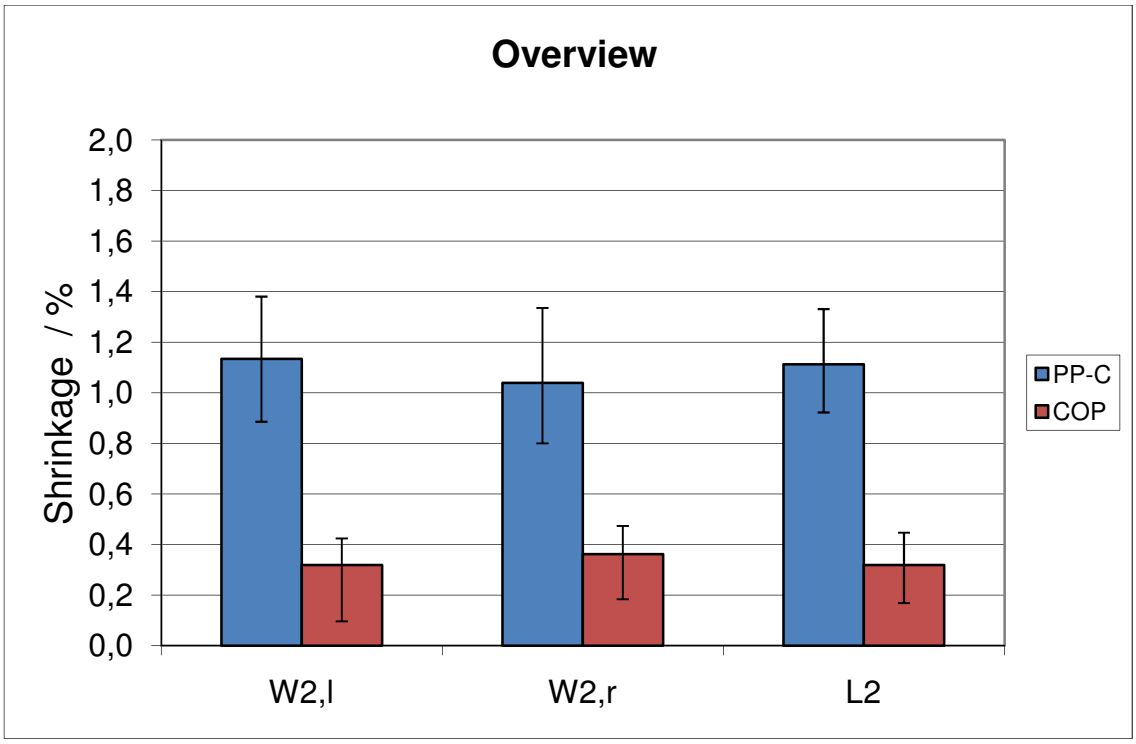

Figure 36: Average of all samples after 47 days. The error bars show the minimum and maximum values of all measured samples.

4.1.2 Comparison of absolute shrinkage values

To examine the applicability of simulation for the targets, first the predicted absolute values were compared to our experimental data. In the next chapter, the trends for each investigated parameter will be adressed.

Since significant differences between the two examined materials could be observed the results will be discussed for each material separately. Figure 37 and Figure 38 show the shrinkage optically measured after one day and the results predicted with both simulation models for both materials and all parameters.

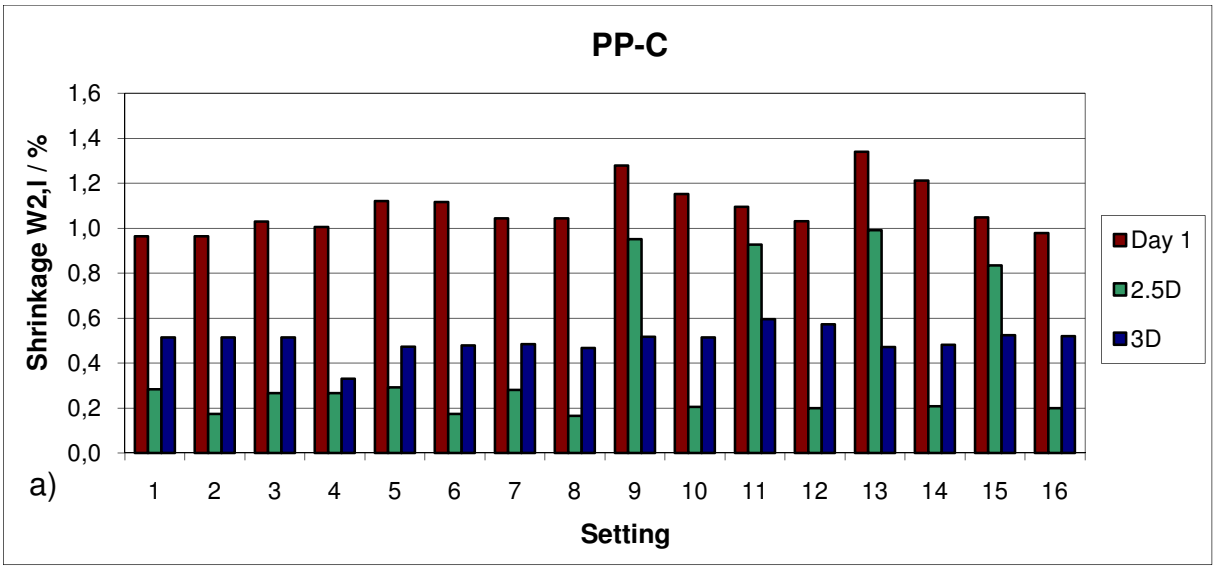

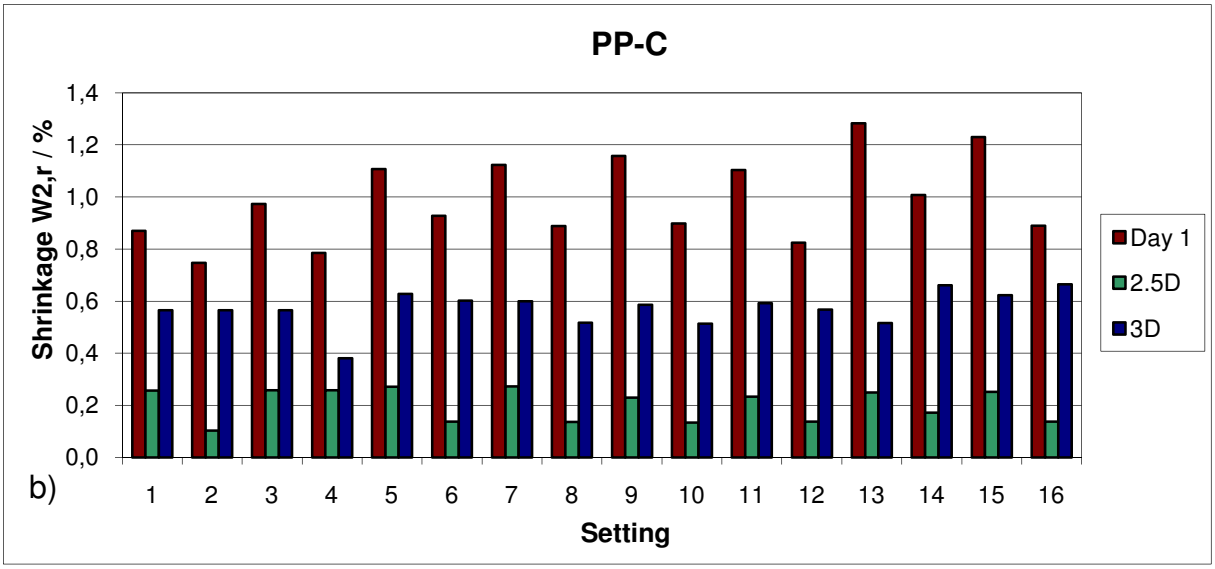

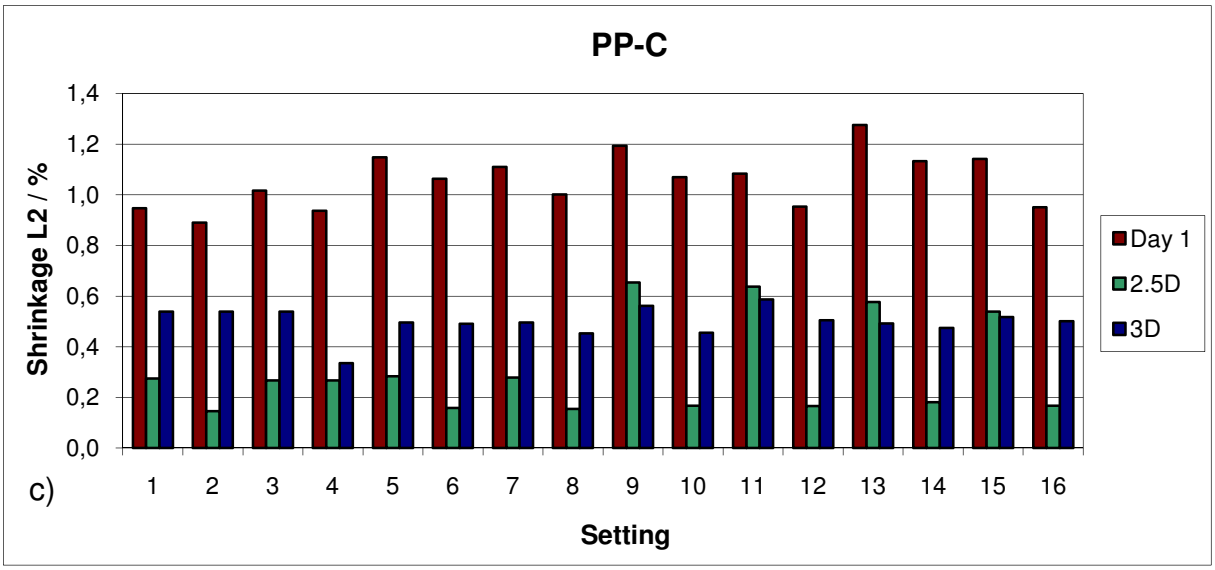

Figure 37: Experimental shrinkage (after 1 day) and shrinkage predicated by both simulation methods for all parameter settings (PP-C).

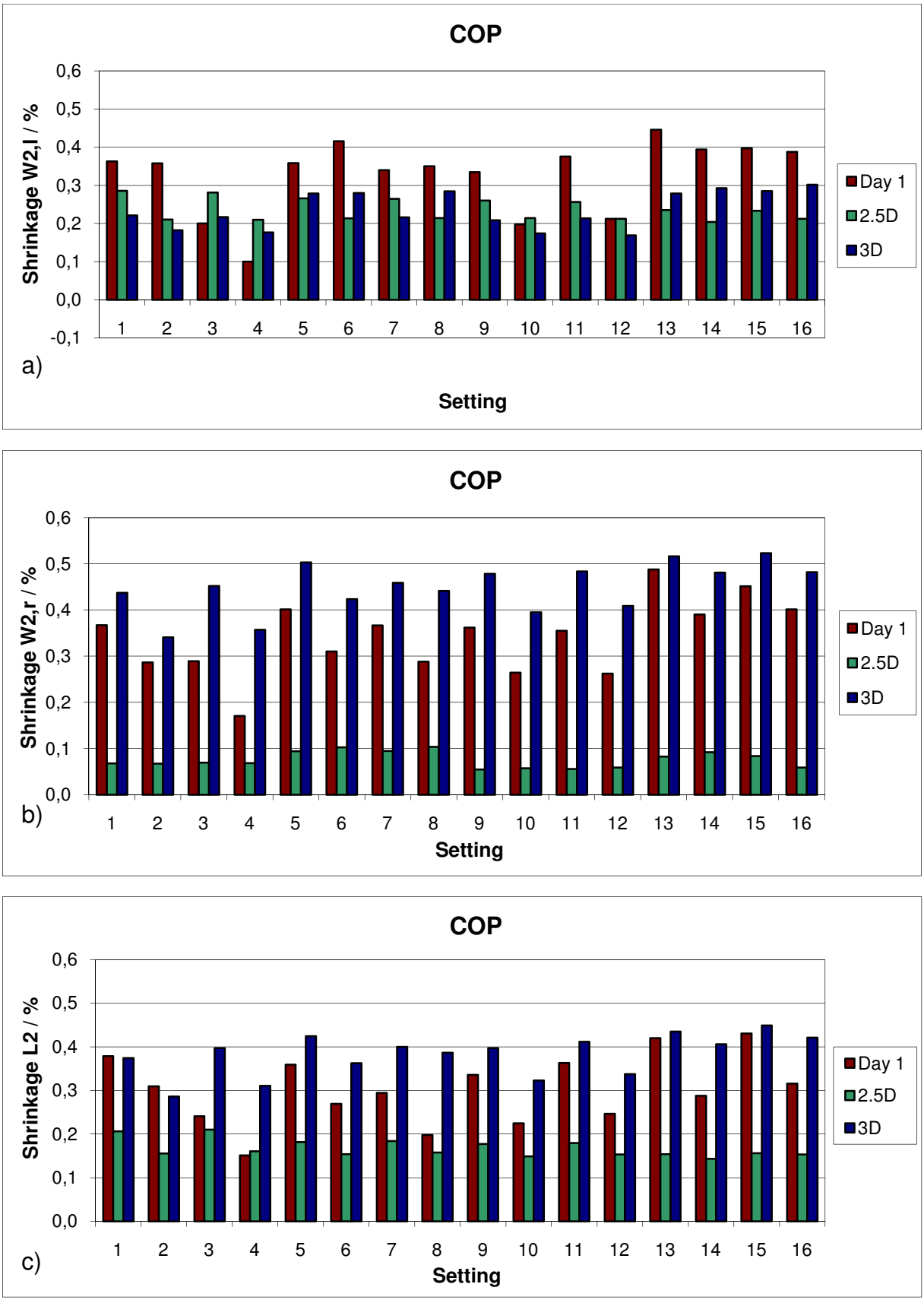

Figure 38: Experimental shrinkage (after 1 day) and shrinkage predicated by both simulation methods for all parameter settings (COP).

Comparison and conclusions

Figure 39 illustrates the mean deviation of the predicted shrinkage from the experimental results for both materials and simulation models, with error bars showing the minimum and maximum deviation. The error bars in Figure 39 and detailed results in Figure 37 and Figure 38 show that, while simulation and experiment are consistent in few cases, there are very large deviations between all parameters and dimensions. In general, the 2.5D Dual Domain model predicts less shrinkage than the 3D model and larger fluctuations between the results.

PP-C

In Figure 39, one can see that both simulation models underestimate shrinkage of PP-C clearly. The 2.5D model averaged a deviation of 0.75 % (minimum: 0.08 % maximum: 1.09 %), and the 3D model of 0.52 % (minimum: 0.10 % maximum: 0.91 %) from the experimental value. This means that while shrinkage results were predicted quite precisely for a few parameter sets and dimensions, it was underestimated drastically in others (keeping in mind that the total average shrinkage for PP-C is approximately 1.1 %).

Looking at the detailed shrinkage predictions for each parameter set in Figure 37, it becomes apparent that the 2.5D model is not suited for shrinkage prediction in this case, since it displays great variations between different parameter sets and dimensions. Even though shrinkage is underestimated clearly by the 3D model, its results appear to be more constant.

To a certain extent, less accurate simulation results were to be expected for this semi-crystalline material, since filler content and morphology complicate shrinkage prediction in this case [23, 31].

COP

Focusing on the results for COP, which are also summarized in Figure 39, one can see that the overall deviation between simulation and experiment is quite small. The prediction is less accurate with the 2.5D model. Only regarding the mean value of predicted shrinkage however one could argue that the values simulated with the 3D model are quite precise. Unfortunately a glance at the detailed results dismantles this hypothesis. Already the error bars in Figure 39, showing a maximum deviation of shrinkage of ± 0.25 % between the simulated and experimental results, suggest great differences for certain parameters or dimensions. One has to consider that the average shrinkage for COP, which amounts to 0.3 %, is nearly as high as the total deviation between the experiment and simulation. A closer look at Figure 38 shows the cause of these great deviations. Both models give accurate predictions for a few

parameter sets, but never for the same parameter set for all three investigated dimensions. While experimental results show maxima and minima for the same parameter set for all dimensions, both simulation models predict different parameter sets with minima or maxima for each dimension. Generally, the 3D model predicts higher shrinkage values than the 2.5D model. Curiously, the 2.5D model predicts great deviations in shrinkage for the three dimensions, ranging from 0.05 % for the width near the gate to 0.25 % away from the gate.

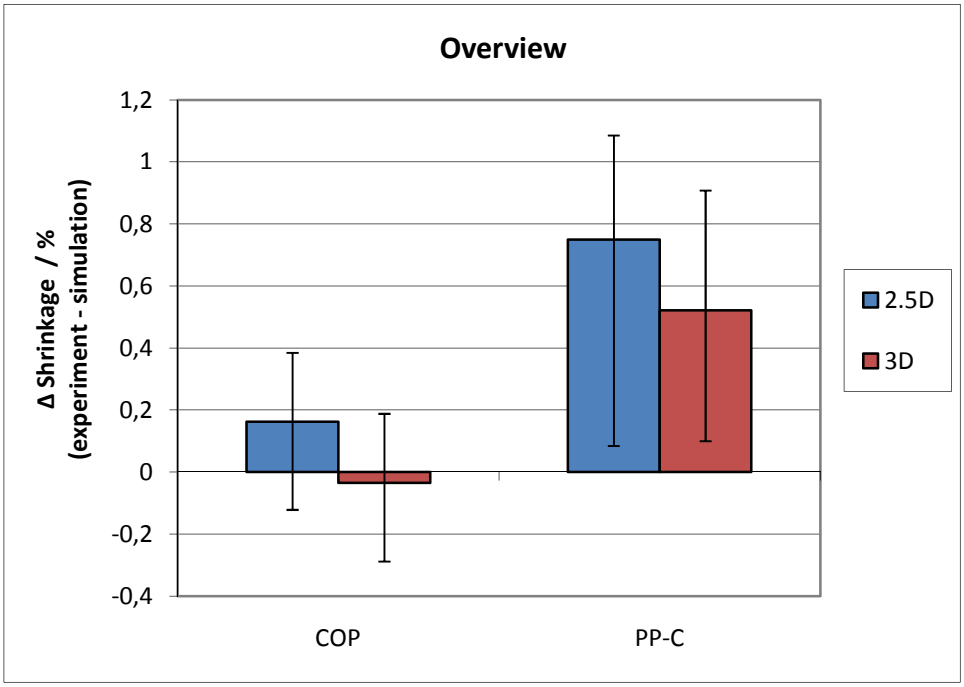

Figure 39: Shrinkage comparison between experiment and simulation.

Choosing a setting where simulation showed the best results for the material COP, Figure 40 demonstrates the variations in shrinkage for different dimensions. In fact, literature predicts greater shrinkage away from the gate than near the gate [12]. This is consistent with the results of both simulation models and the experimental results. However this effect is drastically overestimated by simulation. The 2.5D model predicts 0.144 % more absolute shrinkage away from the gate, the 3D shows similar results with 0.158 % deviation, while the experiment only shows a difference of 0.071 %.

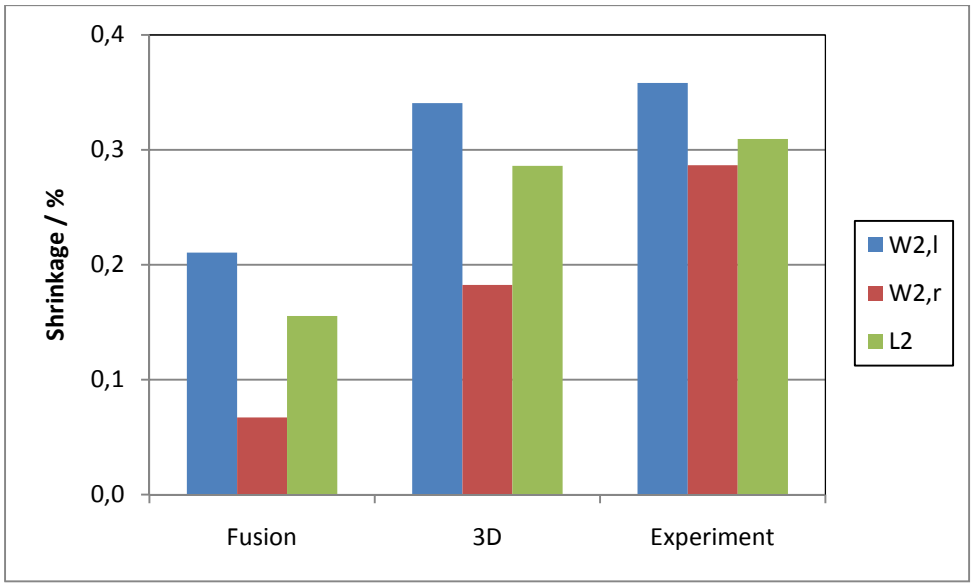

Figure 40: Fluctuations of shrinkage between different dimensions.

4.1.3 Parameter study

After comparing the absolute values of shrinkage predicted by simulation to those measured in the experiment, it is now necessary to examine whether the simulation results follow the same trend when altering one injection parameter. The trend comparison was done by leaving all other parameters on either a low (marked “Rest low” in the following diagrams) or high (marked “Rest high”) level and altering the examined parameter over three different levels (simulation) or just the high and low level (experiment). In the following paragraphs, these trends will be compared for both materials and each process parameter separately. Since the results appeared to be more accurate, only simulation results done with the 3D model were used for these trend comparisons.

4.1.3.1 Cylinder temperature

The following paragraphs demonstrate the influence of cylinder temperature on shrinkage as seen in the experimental results as well as in simulation.

Figure 41 and Figure 42 demonstrate how shrinkage of PP-C is influenced by cylinder temperature. Simulation and experiment correlate in neither of the two cases for PP-C. Keeping all other parameter on a low level, simulation predicts no influence due to changes in cylinder temperature, while experimental results show an increase in shrinkage due to higher cylinder temperature for all dimensions. On the other hand, when all other parameters are kept on a high level, simulation predicts a slight increase in shrinkage, while experimental results show decreasing shrinkage for all dimensions.

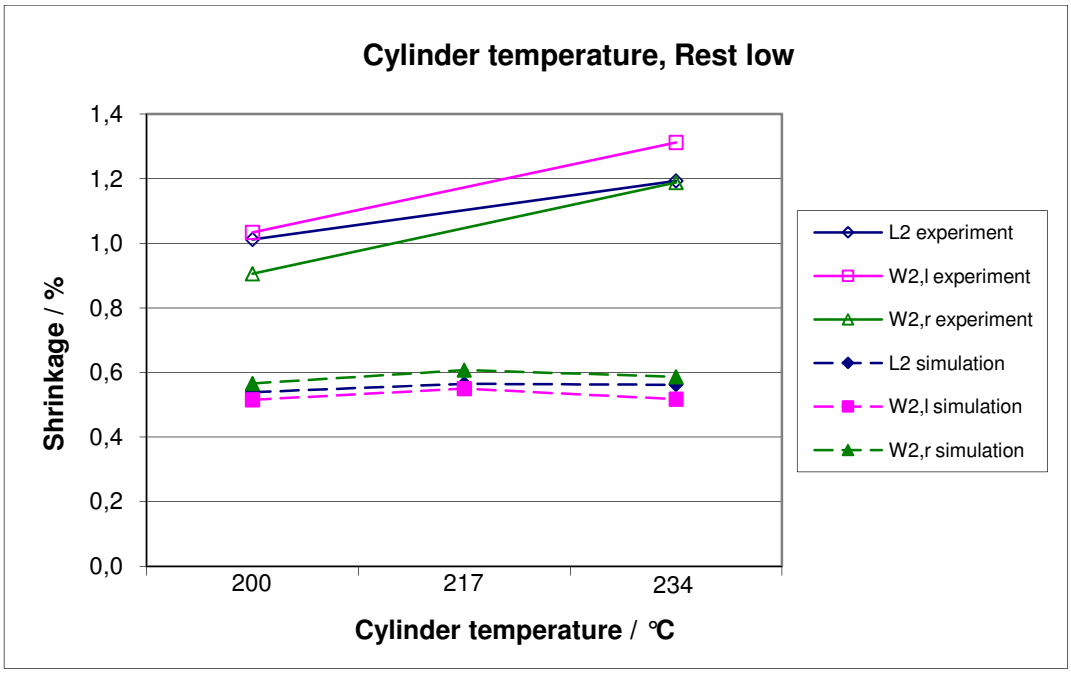

Figure 41: Change in shrinkage of PP-C due to variation of cylinder temperature while keeping all other parameters at a low level.

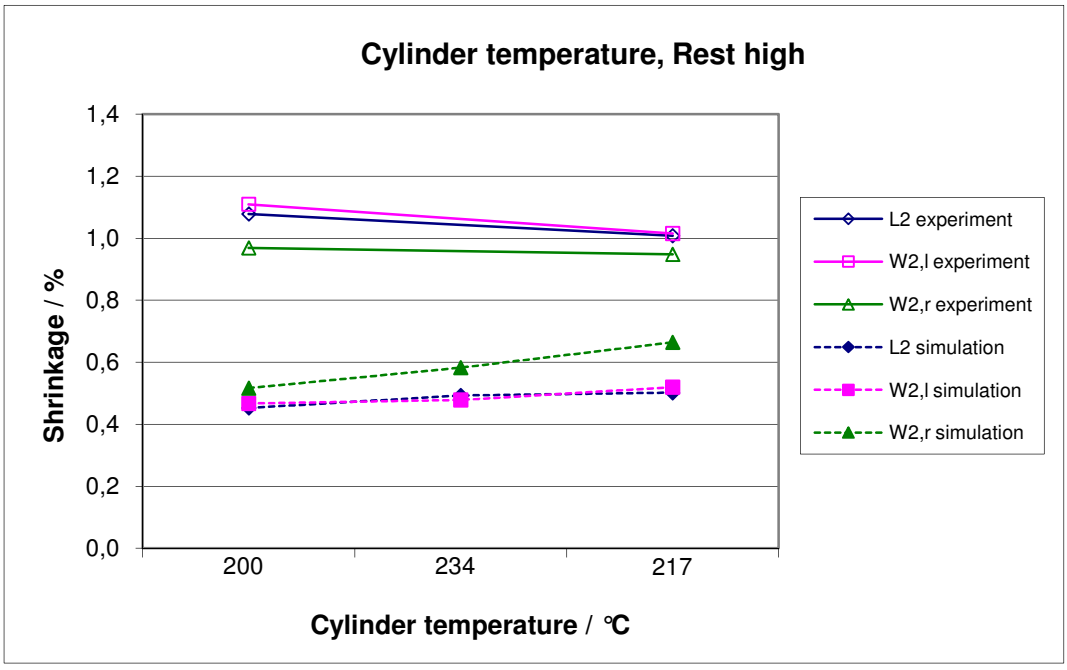

Figure 42: Change in shrinkage of PP-C due to variation of cylinder temperature while keeping all other parameters at a high level.

Focusing on the results achieved for COP in Figure 43 and Figure 44, if all other parameters are kept on a low level simulation predicts a slight increase in shrinkage for the width away from the gate and the length, while the width close to the gate is predicted to stay constant. For this case the experiment showed more or less

constant shrinkage for all dimensions. If all other parameters are kept on a high level both experiment and simulation show an increase in shrinkage at higher cylinder temperatures. A particularly steep increase was observed for the length and the width near the gate during the experiment.

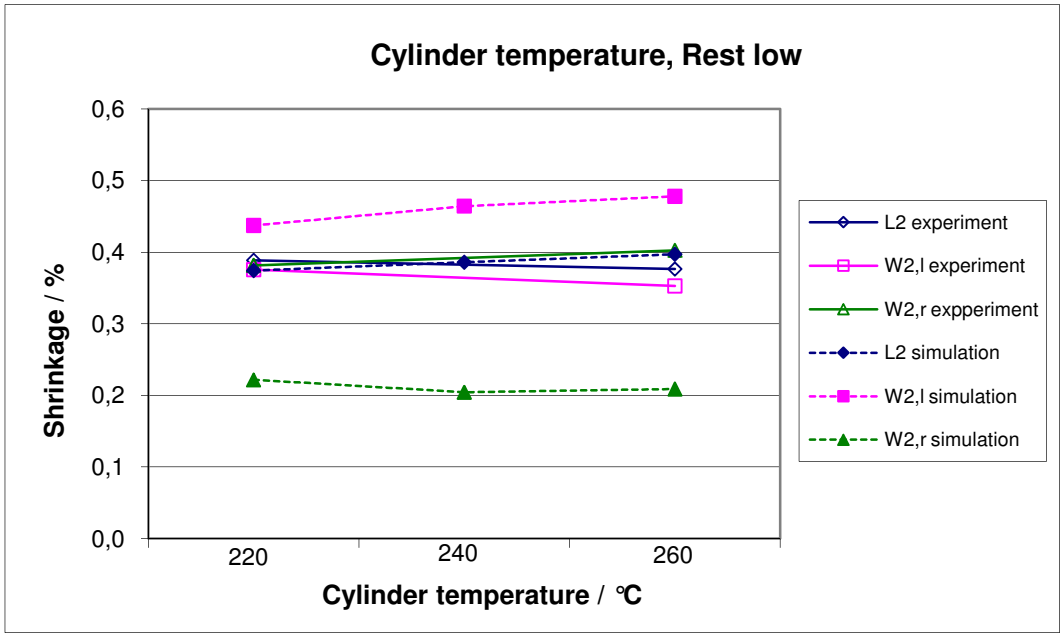

Figure 43: Change in shrinkage of COP due to variation of cylinder temperature while keeping all other parameters at a low level.

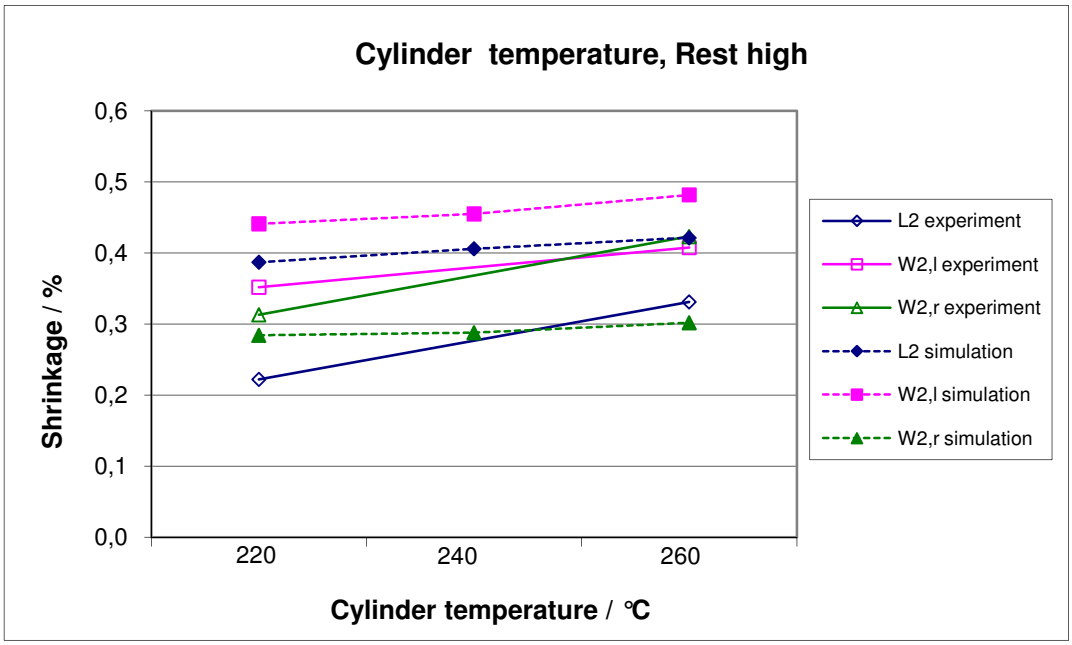

Figure 44: Change in shrinkage of COP due to variation of cylinder temperature while keeping all other parameters at a high level.

4.1.3.2 Mold temperature

The influence of mold temperature on shrinkage of PP-C is illustrated in Figure 45 and Figure 46. Simulation suggests no significant influence of mold temperature on shrinkage (predicting a slight increase for the width near the gate and decrease in shrinkage away from the gate). The experiment supports the simulated results if all other parameters are kept at a high level, but shows significant increase in shrinkage with the other parameters at a low level.

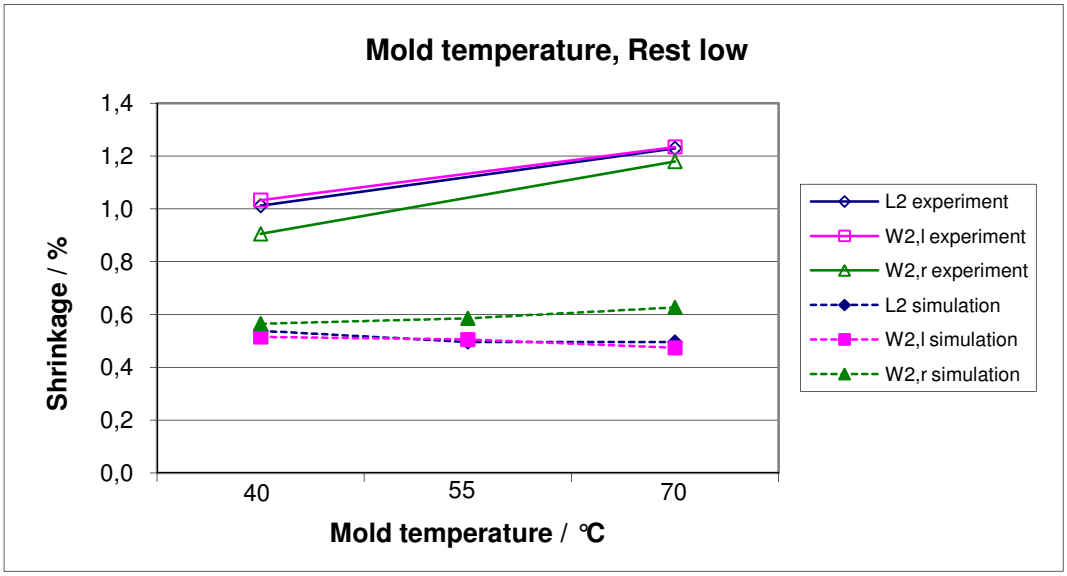

Figure 45: Change in shrinkage of PP-C due to variation of mold temperature while keeping all other parameters at a high level.

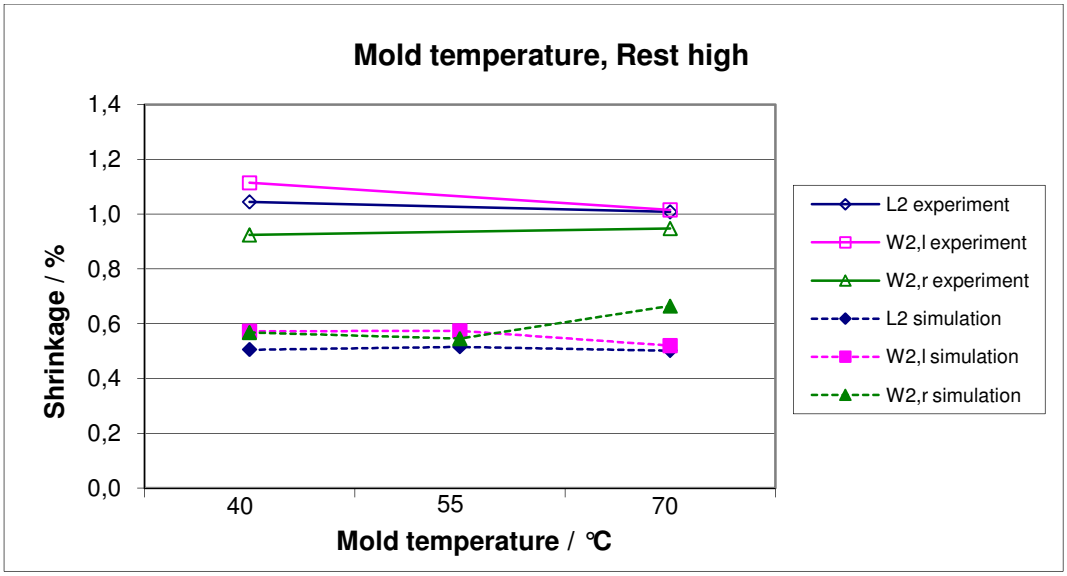

Figure 46: Change in shrinkage of PP-C due to variation of mold temperature while keeping all other parameters at a high level.

The influence of mold temperature on the shrinkage of COP is demonstrated in Figure 47 and Figure 48. Simulation predicts an increase in shrinkage at higher mold temperatures in all cases. This is consistent with the experimental results if all other parameters are kept on a high level. If the other parameters are kept on al low level, only a slight increase in shrinkage can be observed for the width near the gate, while the other dimensions remain more or less unchanged.

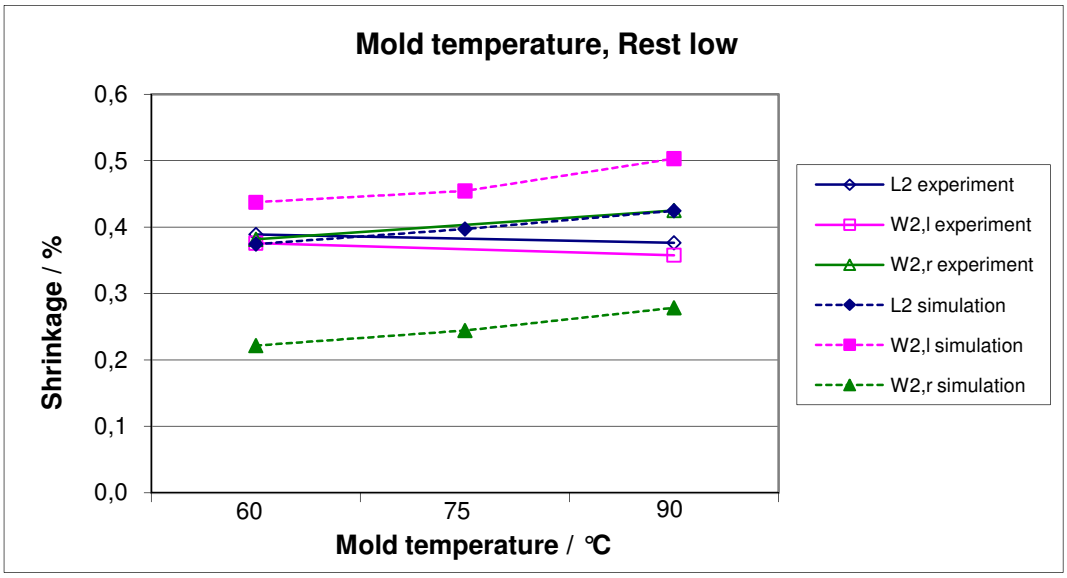

Figure 47: Change in shrinkage of COP due to variation of mold temperature while keeping all other parameters at a low level.

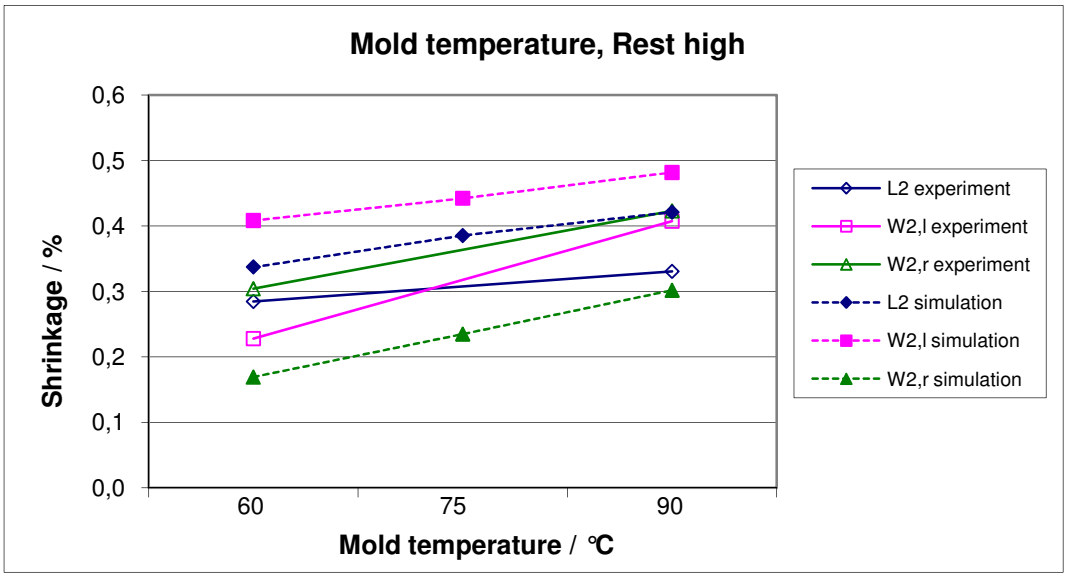

Figure 48: Change in shrinkage of COP due to variation of mold temperature while keeping all other parameters at a high level.

4.1.3.3 Injection speed

Figure 49 and Figure 50 show how shrinkage of PP-C is influenced by injection speed. Simulation shows a V-shaped trend for the length and the width away from the gate, while the shrinkage of the width near the gate remains unchanged. Since only two parameter sets were tested in the experiment, the identification of non linear trends is not possible in this case. Overall the experimental results show a slight increase in shrinkage at higher injection speeds.

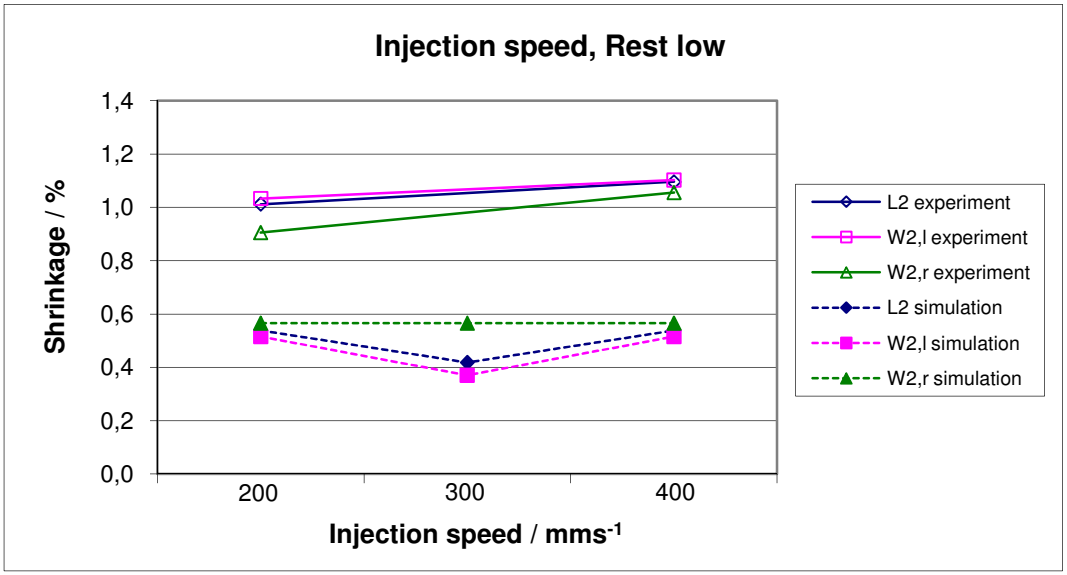

Figure 49: Change in shrinkage of PP-C due to variation of injection speed while keeping all other parameters at a low level.

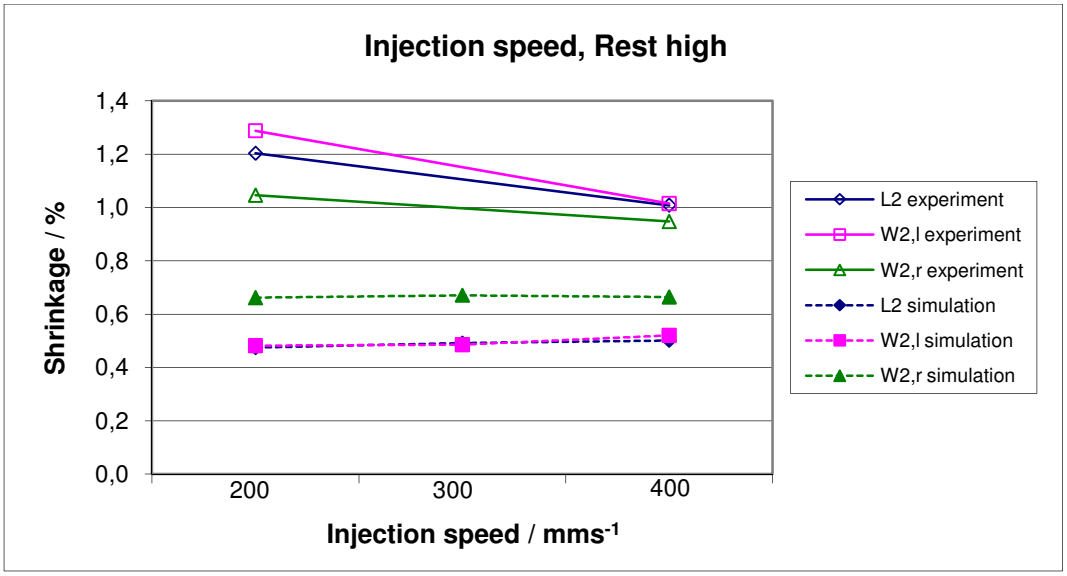

Figure 50: Change in shrinkage of PP-C due to variation of injection speed while keeping all other parameters at a high level.

Shifting the attention to COP in Figure 51 and Figure 52, one can see that in both cases, simulation predicts hardly any change due to variations of injection speed. While this is consistent with the experimental data if the other parameters are kept at a high level, the experiment suggests decreasing shrinkage when increasing injection speed and keeping all other parameters low. This phenomenon is particularly strong for the width away from the gate.

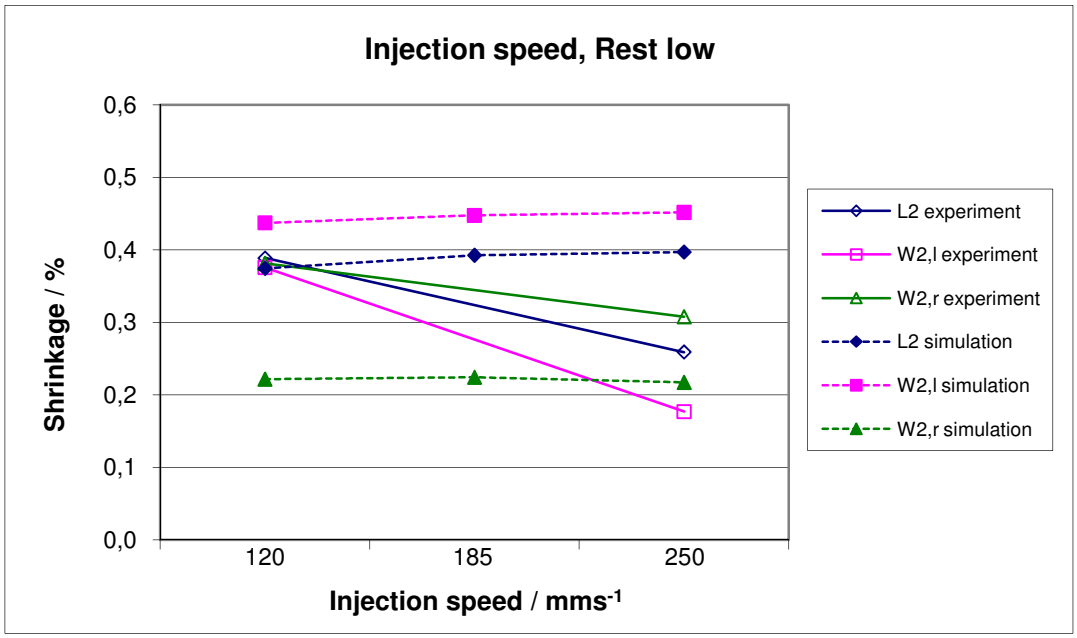

Figure 51: Change in shrinkage of COP due to variation of injection speed while keeping all other parameters at a low level.

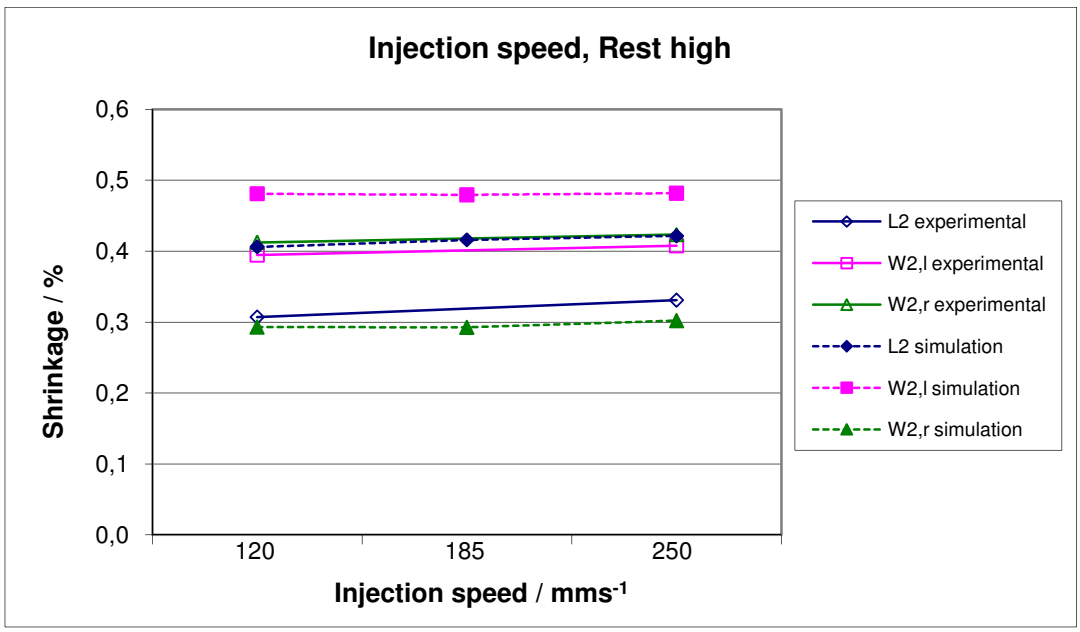

Figure 52: Change in shrinkage of COP due to variation of injection speed while keeping all other parameters at a high level.

4.1.3.4 Holding Pressure

The influences of changes of holding pressure on shrinkage of PP-C are illustrated in Figure 53 and Figure 54. If all other parameters are kept on a high level experimental results show decreasing shrinkage when holding pressure is increased. This effect is particularly strong near the gate. If all other parameters are at a low level no change due to higher holding pressure can be observed for the length and width away from the gate. Curiously, simulation predicts hardly any influence of holding pressure on shrinkage.

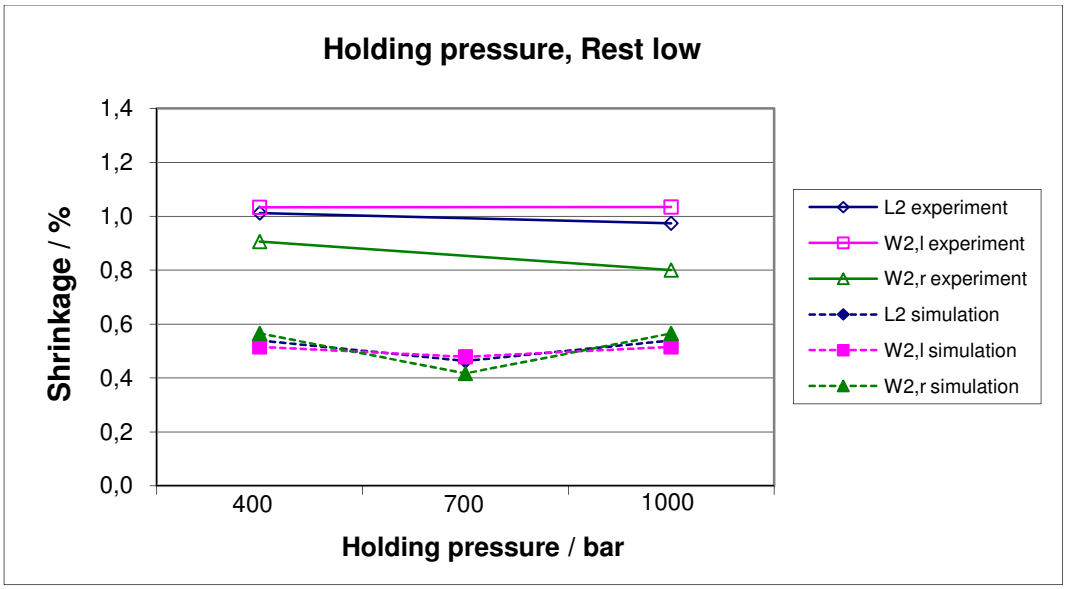

Figure 53: Change in shrinkage of PP-C due to variation of holding pressure while keeping all other parameters at a low level.

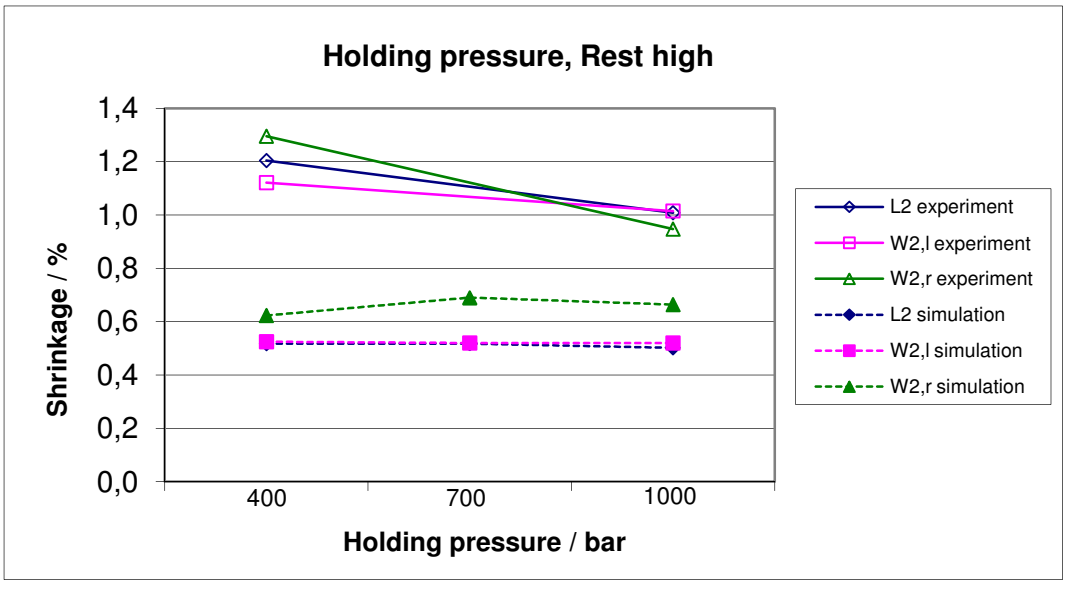

Figure 54: Change in shrinkage of PP-C due to variation of holding pressure while keeping all other parameters at a high level.

Figure 55 and Figure 56 look into the influence of changes in holding pressure on shrinkage of COP. Both simulation and experiment suggest a decrease of shrinkage with increasing holding pressure if all other parameters are kept on a low level. The results are less consistent if all other parameters are kept at a high level. While shrinkage predicts hardly any influence of holding pressure, a significant decrease in shrinkage over the length was observed during the experiment.

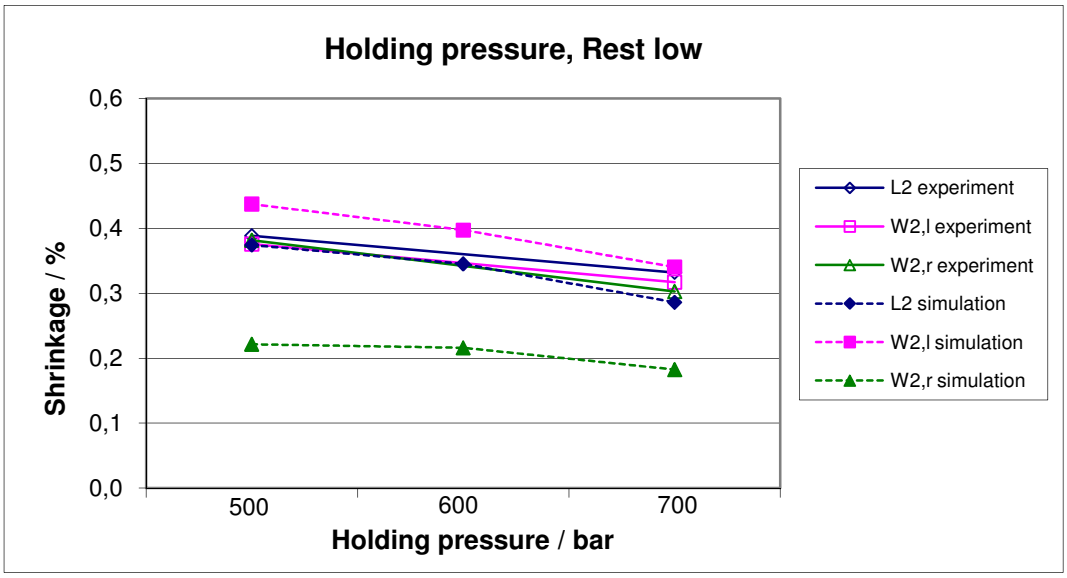

Figure 55: Change in shrinkage of COP due to variation of holding pressure while keeping all other parameters at a low level.

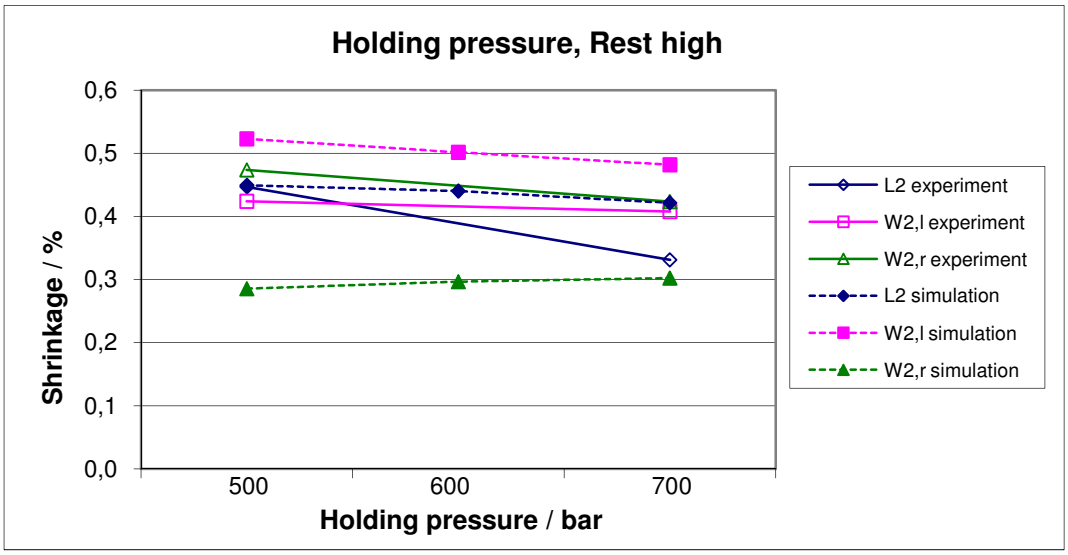

Figure 56: Change in shrinkage of COP due to variation of holding pressure while keeping all other parameters at a high level.

4.1.3.5 Comparison and conclusions

Table 15 compares the experimental results to simulation (3D model). If the trend for one dimension are consistent the box is marked green, if not, red.

Table 15: Comparison of trends (change of shrinkage due to variation of one injection molding parameter) between experiment and simulation. Green: trends are consistent, red: trends differ.

		PP-C			COP		
	Rest	L2	W2,l	W2,r	L2	W2,l	W2,r
Cylinder temp.	Low						
	High						
Mold temp.	Low						
	High						
Inj. Speed	Low						
	High						
Pressure	Low						
	High						

The results show that one can use simulation to predict how changing one parameter would influence shrinkage for COP at most times. However, it would be unwise to rely on simulation to predict changes in shrinkage for PP-C, since the trends do not correlate in this case.

Investigating the results obtained with PP-C, some flaws of current simulation programs become evident. PP-C is a very sophisticated grade since it has very high carbon-black content and is a semi-crystalline grade. These two factors affect many thermal and mechanical properties and have therefore great influence on shrinkage. Although extensive research has been performed in this area (see chapter 2.1.4.3), no appropriate model predicting the influence of crystallization on shrinkage has been found and implemented into software until today.

In Figure 57 and Figure 58, the effect of varying the process parameters is shown for both investigated materials. It is apparent that simulation underestimates the impact of each parameter on shrinkage. The difference between the minimum and maximum amount of shrinkage for each observed parameter is always greater in experiment than in simulation.

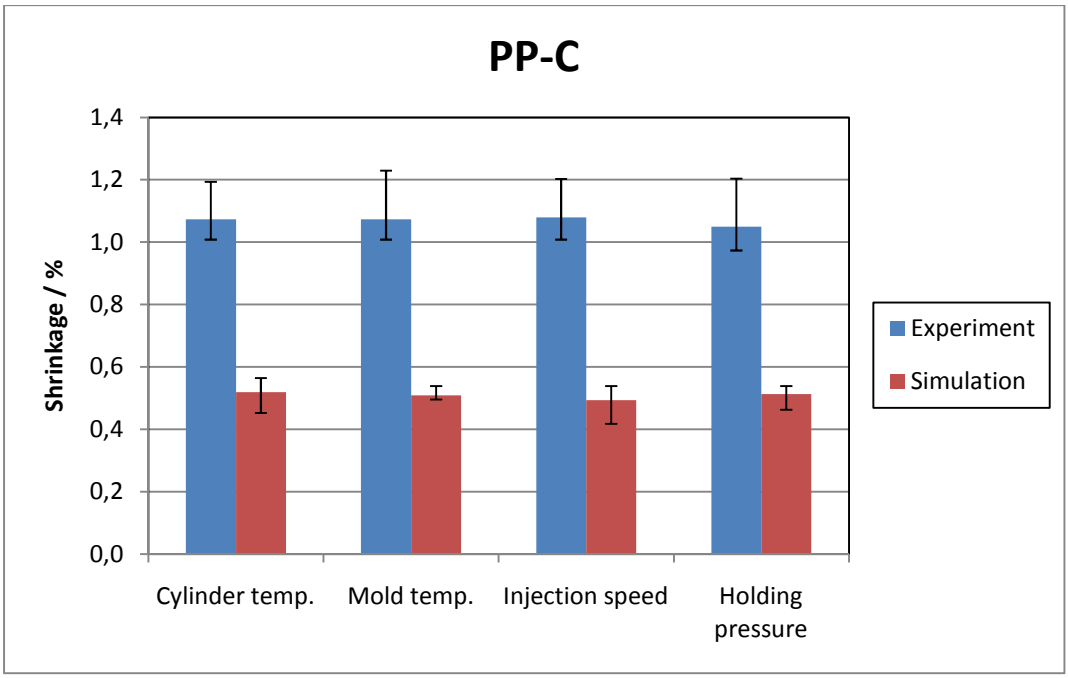

Figure 57: Average, minimum and maximum shrinkage over the length (L2) while varying one injection molding parameter for PP-C.

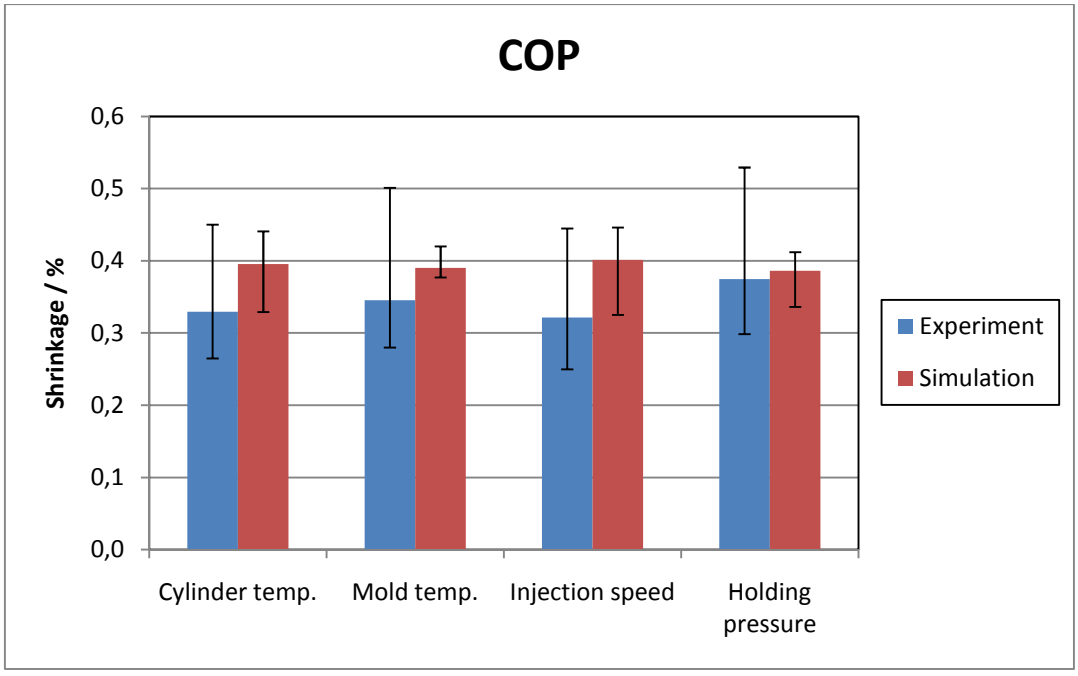

Figure 58: Average, minimum and maximum shrinkage over the length (L2) while varying one injection molding parameter for COP.

4.2 Aging

After examining how different injection molding parameters influenced the shrinkage of two thermoplastic resins used for various medical science products, another goal was to examine the reactions of one specific product used in mass spectrometry to different environmental conditions. Besides using two different coated designs (steel- and gold-coated), the reactions of the uncoated substrates molded from the two grades investigated in the previous chapter were examined. Short-term tests were done to investigate conditioning and transportation phenomena, long-term tests to look into life time at high temperatures and the possibility of archiving at low temperatures. The examined properties were shrinkage, flatness, roughness, wetting behavior (contact angle), surface evaluation (with SEM) and adhesion of the coating (with peel test). Results from the static tests are discussed once in detail for PP-C. For COP and all coating types, long-term results are only shown if they differ to those found for PP-C. Cyclic tests did not show any significant deviations from the static tests. These tests results are only discussed in detail for coated targets, since they investigate the possibility of archiving, primarily relevant for the coated design.

4.2.1 Uncoated substrates

4.2.1.1 Carbon-black filled polypropylene (PP-C)

In the following paragraphs, the reactions of carbon-black filled polypropylene to different test conditions are observed. This material is discussed in detail since it is most relevant as a substrate for the investigated product.

4.2.1.1.1 Shrinkage

The specimens used for the long-term tests were produced two months prior to the start of this test series (also the reference point for the age given in the following diagrams). As can be seen in Figure 59, specimens stored at room temperature and below shrank additional 0.05 % compared to the amount of shrinkage at the star of the testing period. The specimens stored at 80°C shrank an additional 0.15 % compared to the samples stored at room temperature during the first two week of testing. At the end of the testing period the samples stored at 80 °C showed 1.28 % shrinkage, while the samples stored at room temperature only shrank 1.12 %. No long-term tests were performed with specimens stored at 40 °C therefore, only the three short-term measurements are shown in Figure 59. No significant deviation from the specimens stored at room temperature was observed in this short time period. No difference between the substrates stored at high (90 %) and those stored at low

(undefined humidity in oven) relative humidity could be observed (see Figure 60). The extent of after-shrinkage is less than observed in literature, where additional after-shrinkage of 0.27 % could be observed for unfilled polypropylene [12]. This could be due to the presence of large amounts of carbon-black, which reduces shrinkage. Still an additional after-shrinkage of 0.15 % is a problem, since the high claims for geometric accuracy in this case would no longer be met.

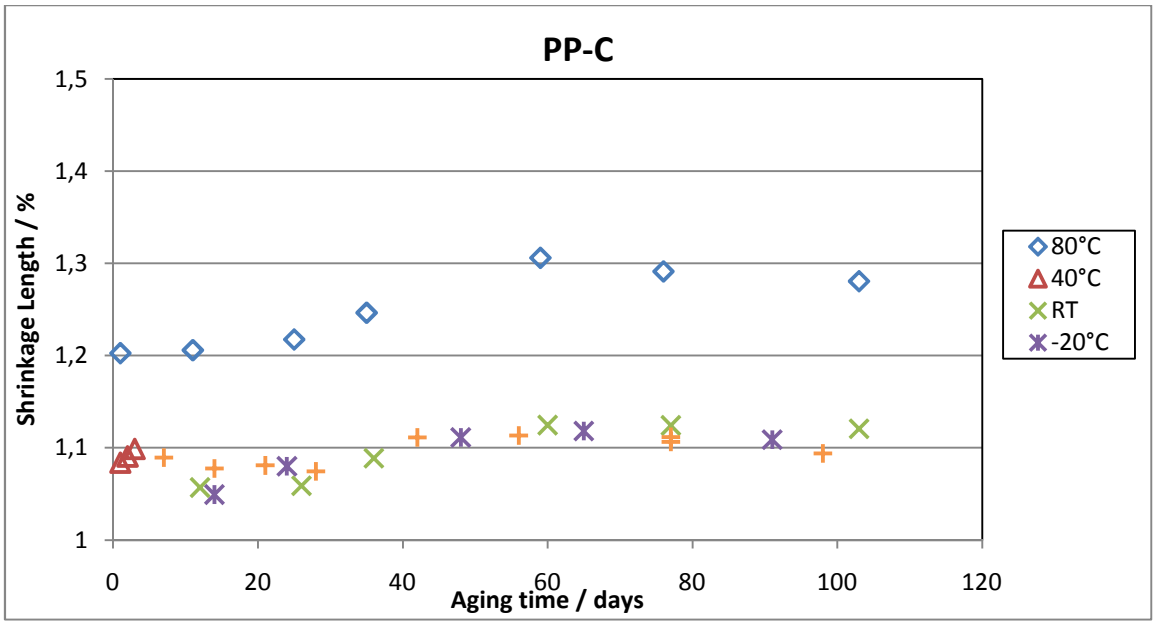

Figure 59: Shrinkage of uncoated carbon-black filled polypropylene along length stored at various temperatures during the testing period.

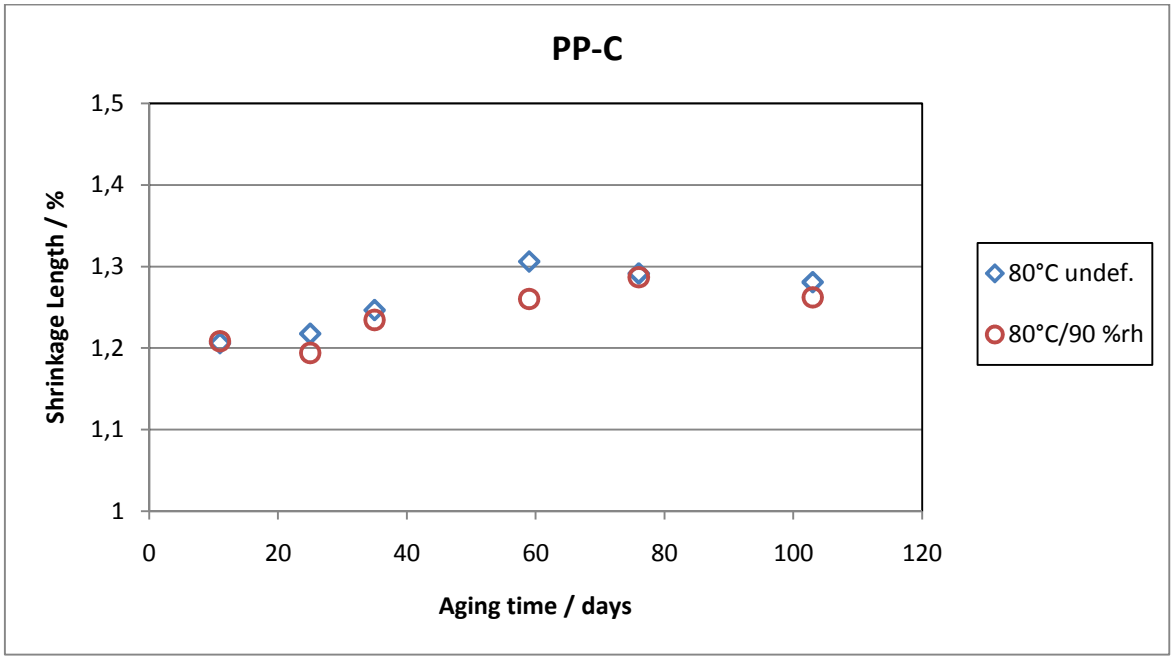

Figure 60: Shrinkage of uncoated carbon-black filled polypropylene along length stored at 80 °C at high and low humidity during the testing period.

4.2.1.1.2 Flatness

The flatness of carbon-black filled polypropylene substrates proved to not be influenced by the testing conditions (i.e., temperature and humidity). As seen in Figure 61 and Figure 62, a flatness value of approximately 50 µm was measured for all specimens. No significant difference in flatness was observed for any testing condition.

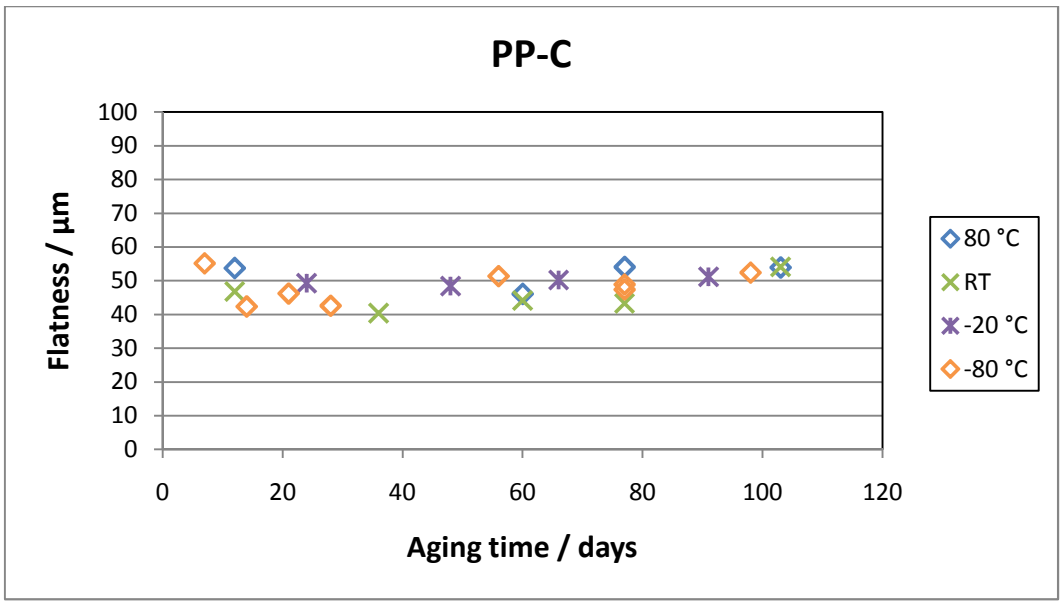

Figure 61: Flatness of PP-C samples after aging at various temperatures.

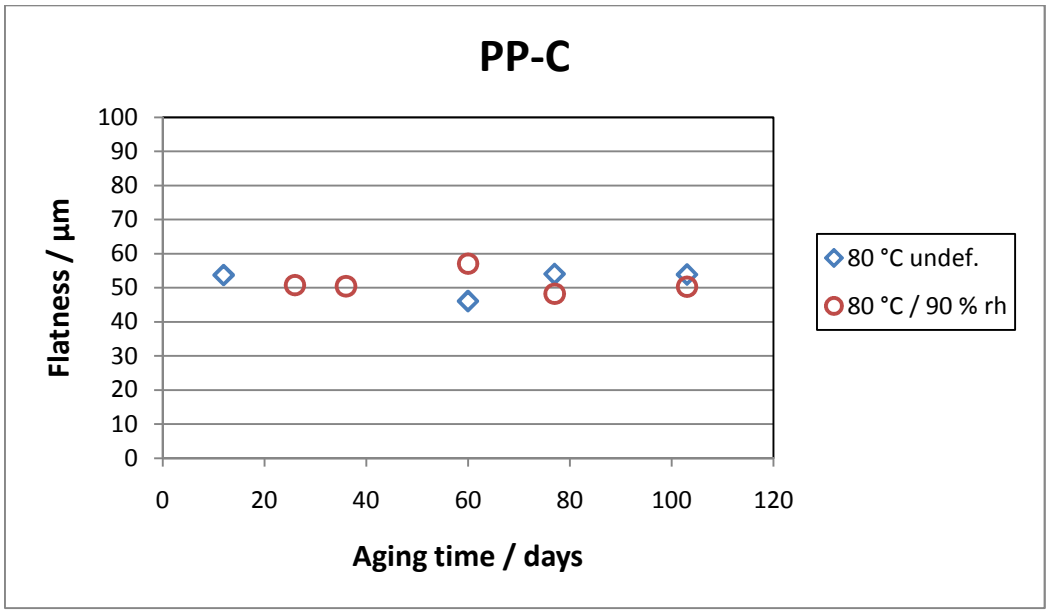

Figure 62: Flatness of PP-C samples after aging at 80 °C at different humidity levels.

4.2.1.1.3 Roughness

The roughness of PP-C stayed constant for all examined test conditions over the whole testing period. Ra, Rq and Rz values were examined both on the smooth area of the spots and on the rough area outside of the spots on the target. Altough the absolute values varied, the trend was the same for all three roughness values. Therefore only the Ra values measured on the spots are shown in Figure 63. Table 16 and Table 17 show a comparison between all examined roughness values. Humidity did not have any effect on roughness either, as can be seen in Figure 64.

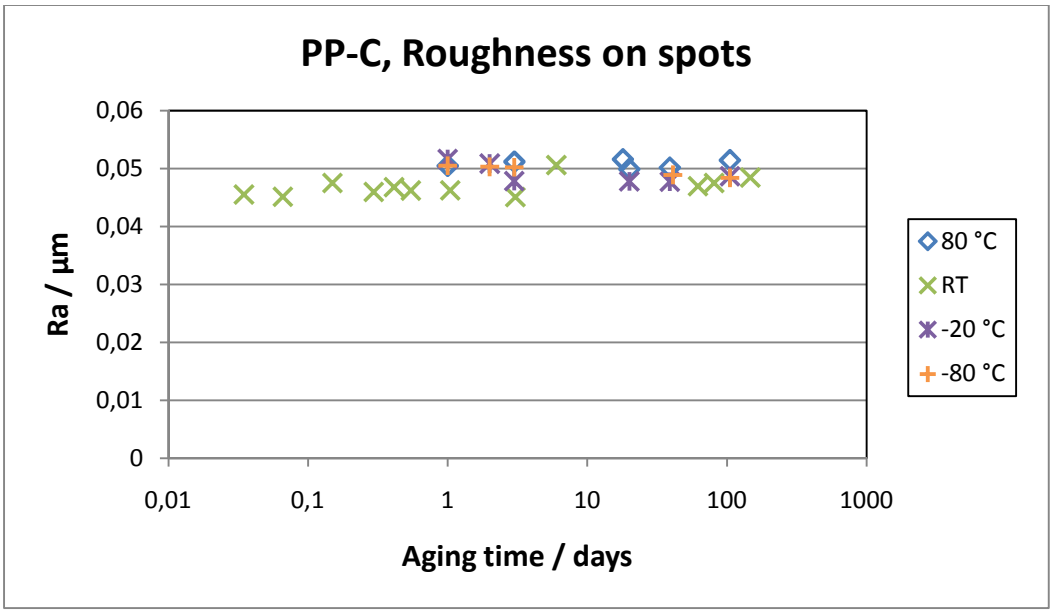

Figure 63: Roughness of PP-C samples after aging at various temperatures.

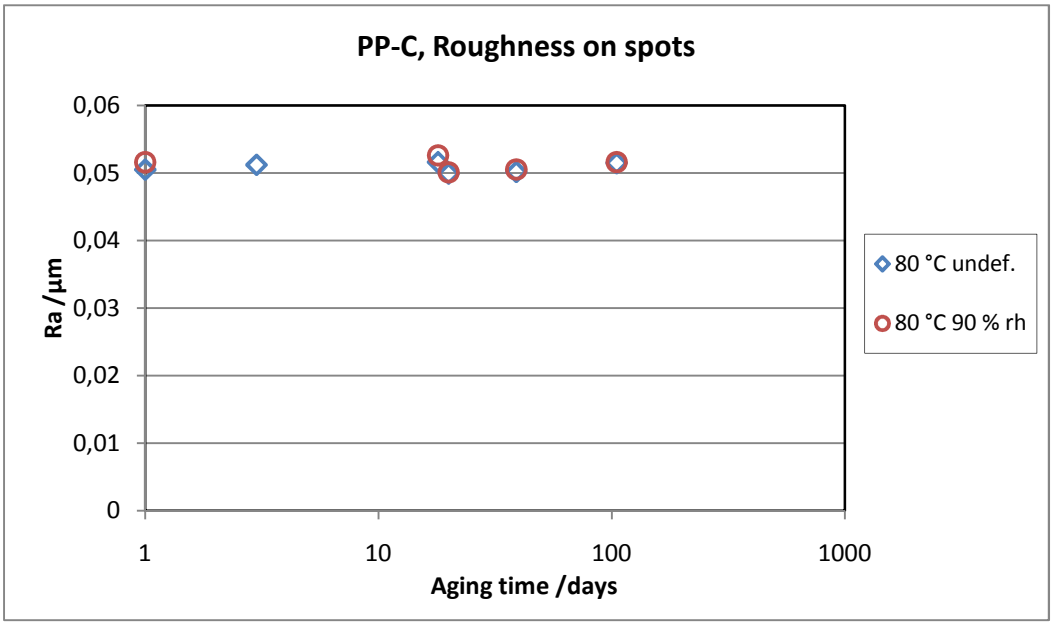

Figure 64: Effect of humidity on the roughness of aged PP-C samples.

Table 16: Comparison of different roughness values measured on spots for steel-coated PP-C targets conditioned three days at 25 °C.

	Ra / µm	Rq / µm	Rz / µm
Mean value	0.048	0.063	0.619
Std. deviation	0.008	0.01	0.122

Table 17: Comparison of different roughness values measured outside of spots for steel-coated PP-C targets conditioned three days at 25 °C.

	Ra / µm	Rq / µm	Rz / µm
Mean value	1.432	1.802	13.533
Std. deviation	0.040	0.059	0.422

4.2.1.1.4 Scanning electron microscopy (SEM)

SEM investigations were done to observe if the target's surface changed due to aging phenomena. For this purpose, pictures with magnifications of 40x, 1000x and 10000x were compared. As can be seen in Figure 65, a magnification of 10000x shows many local defects due to the injection molding process. Cracks or delaminations are rather large defects. It proved better to use pictures with a magnification of 40x and 1000x, since these defects require a better overview.

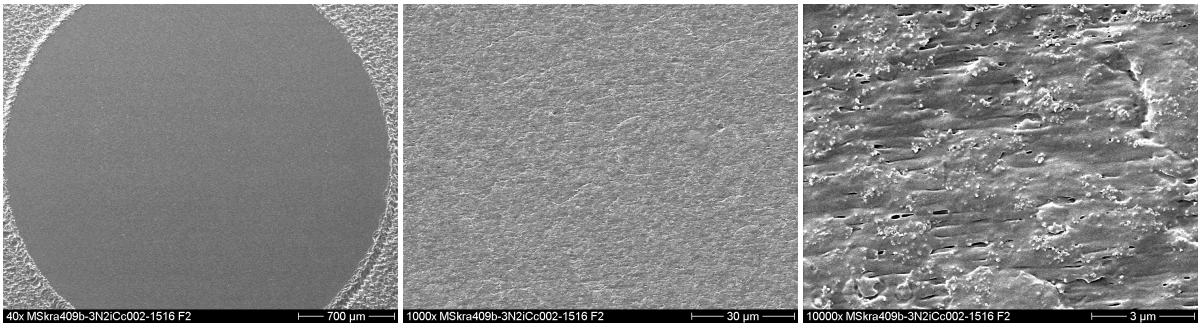

Figure 65: SEM pictures of the same spot and sample taken with various magnifications (from left to right: 40 x, 1000 x and 10000 x).

Figure 66 and Figure 67 compare SEM pictures (with a magnification of 40x and 1000x) taken after 19 and 103 days of aging at various conditions. No changes could be observed. This is consistent with the roughness examinations above which did not show any change in surface properties.

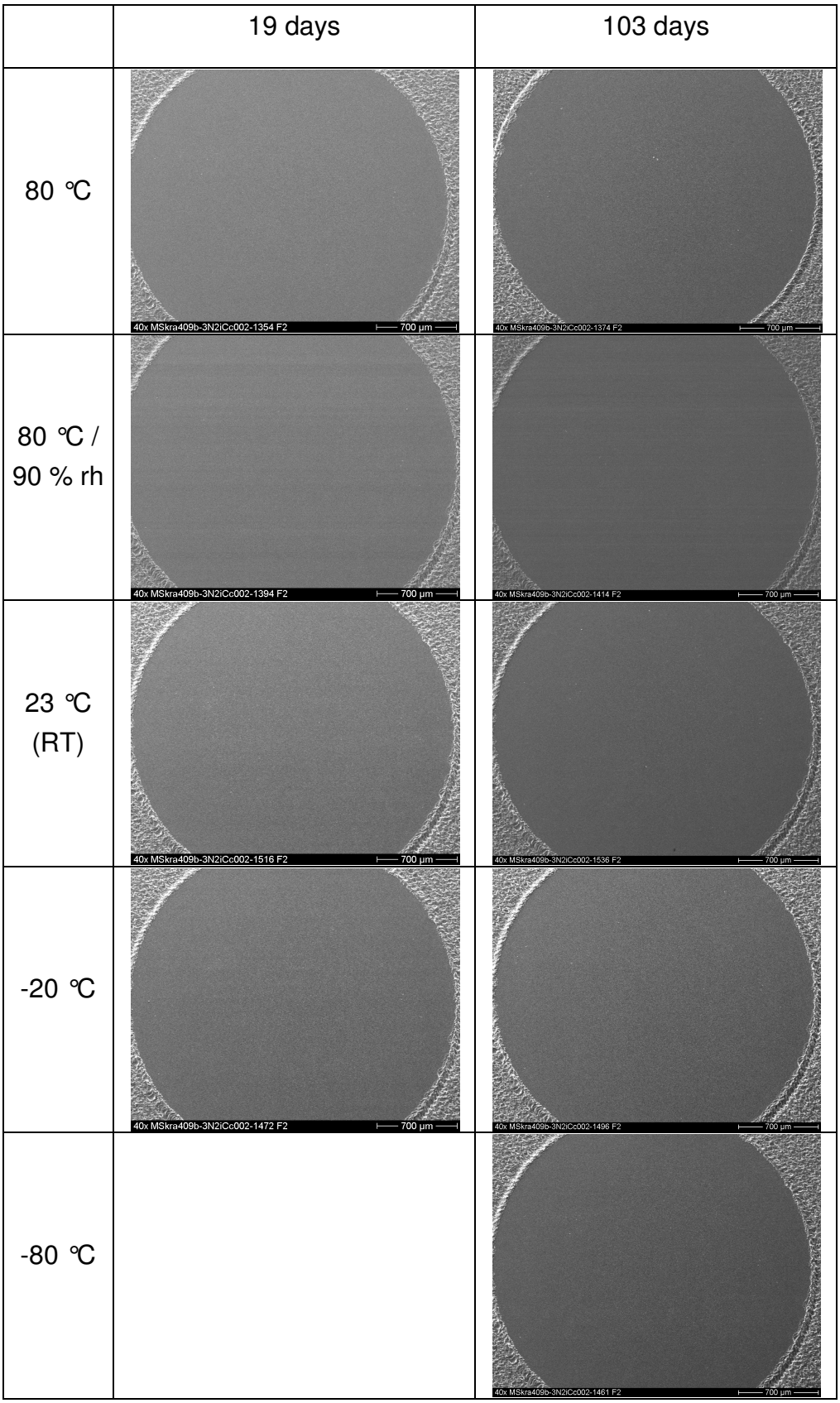

Figure 66: Comparison of SEM pictures taken after 19 and 103 days of aging at various conditions, 40x magnification.

	19 days	103 days
80 °C	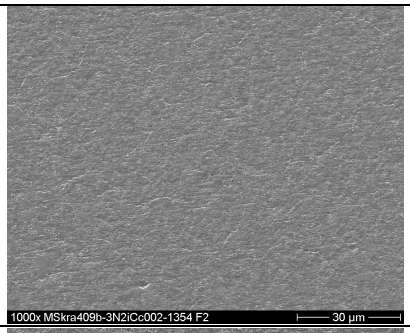	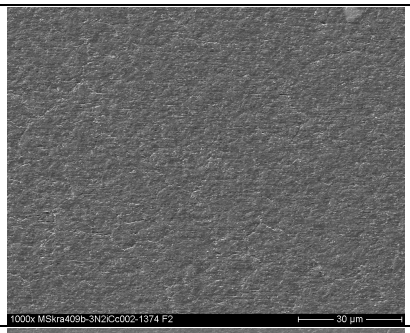
80 °C / 90 % rh	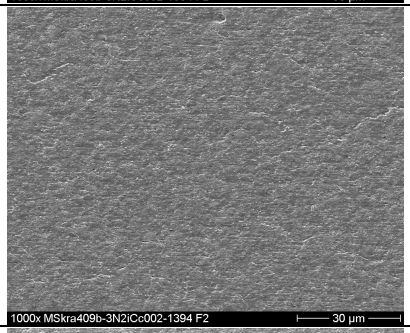	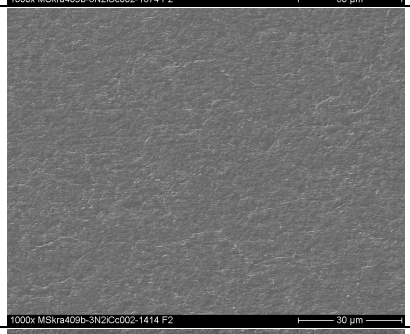
23 °C (RT)	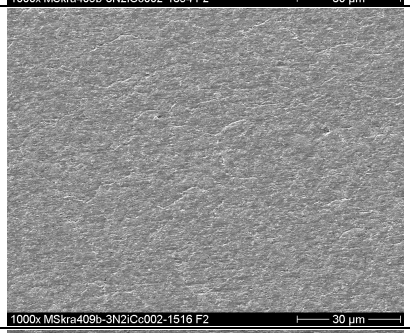	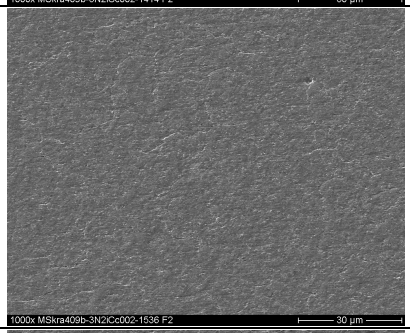
-20 °C		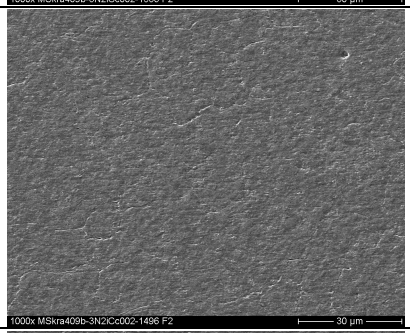
-80 °C		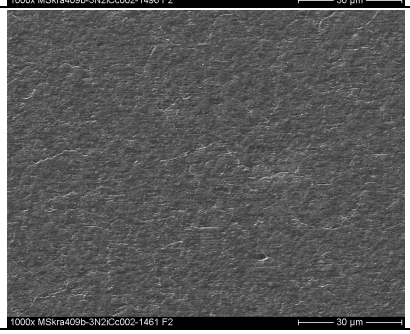

Figure 67: Comparison of SEM pictures taken after 19 and 103 days of aging at various conditions, 1000x magnification.

4.2.1.1.5 Wetting behavior

The wetting behavior of uncoated PP-C is not influenced by any examined aging conditions. As seen in Figure 68, the contact angle of all examined specimens lay around 110°. No influence of temperature or humidity could be identified.

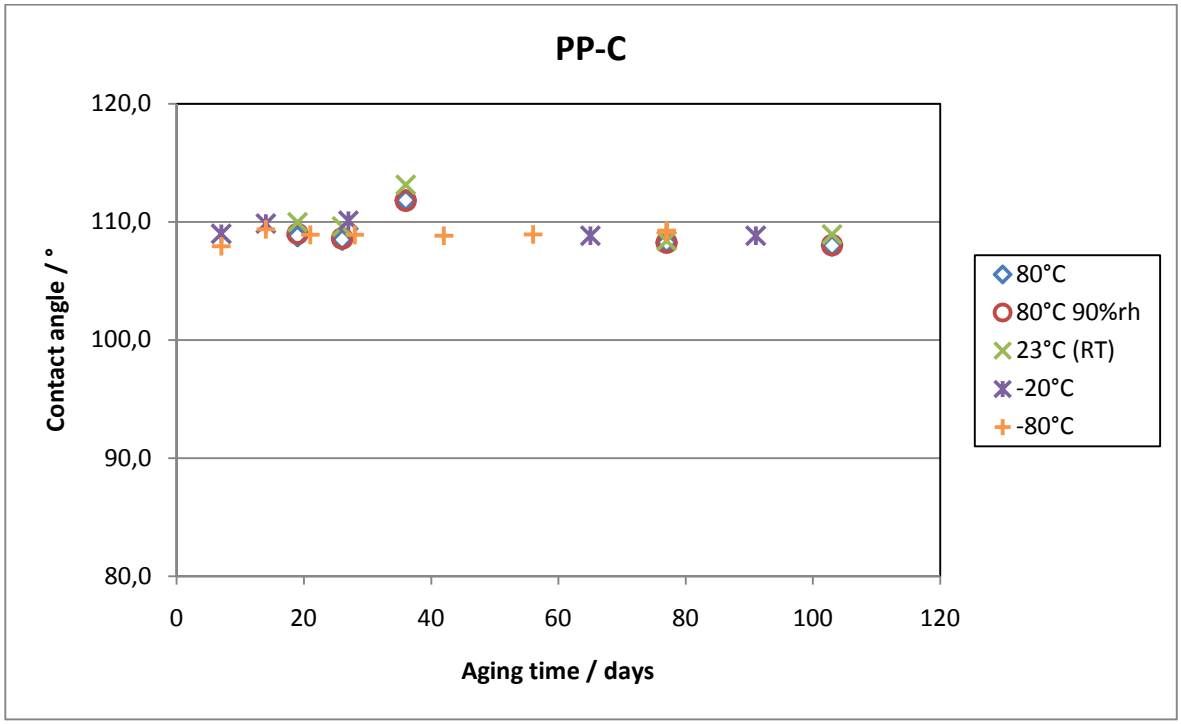

Figure 68: Contact angle of PP-C during aging period.

4.2.1.1.6 Conclusions

Altogether, the only reaction of carbon-black filled polypropylene to the aging tests conducted within the framework of this thesis was increased shrinkage, if stored at higher temperatures (80 °C). One has to point out that the tests conducted for this research focused on geometrical and surface properties. Mechanical properties, although the center of attention in many other publications [11], were not examined since they are not crucial for the application of this product. Since this grade is used as a substrate for the final, coated product, it is of utmost importance to know that ambient conditions as can be found during storage, archiving or transport all over the world cannot influence the product in any way troublesome for the later application. Since this substrate is used for all coated versions, the results for the coated layouts and for the amorphous grade are only discussed in detail if a deviation from the findings achieved with PP-C is observed.

4.2.1.2 Cyclo-olefin-polymer (COP)

Most examinations done with the amorphous COP, excluding the wetting behavior at high humidity as will be discussed later, show the same trends as seen with PP-C, but differ in the absolute values. In the following paragraphs, these results are discussed and a comparison to PP-C is drawn.

4.2.1.2.1 Shrinkage

Similar to PP-C, investigations done with the amorphous COP showed a significant increase in shrinkage for specimens stored at 80 °C (see Figure 69). While specimens stored at room temperature and below shrank approximately 0.45 %, the shrinkage was 0.1 % higher (a total of around 0.55 %) for those kept at 80 °C. Since no long-term tests were performed with samples stored at 40 °C, the shrinkage of these specimens was only evaluated during a period of three days. Possible explanations are the reduction of internal stress and polymer orientations at higher temperatures [12].

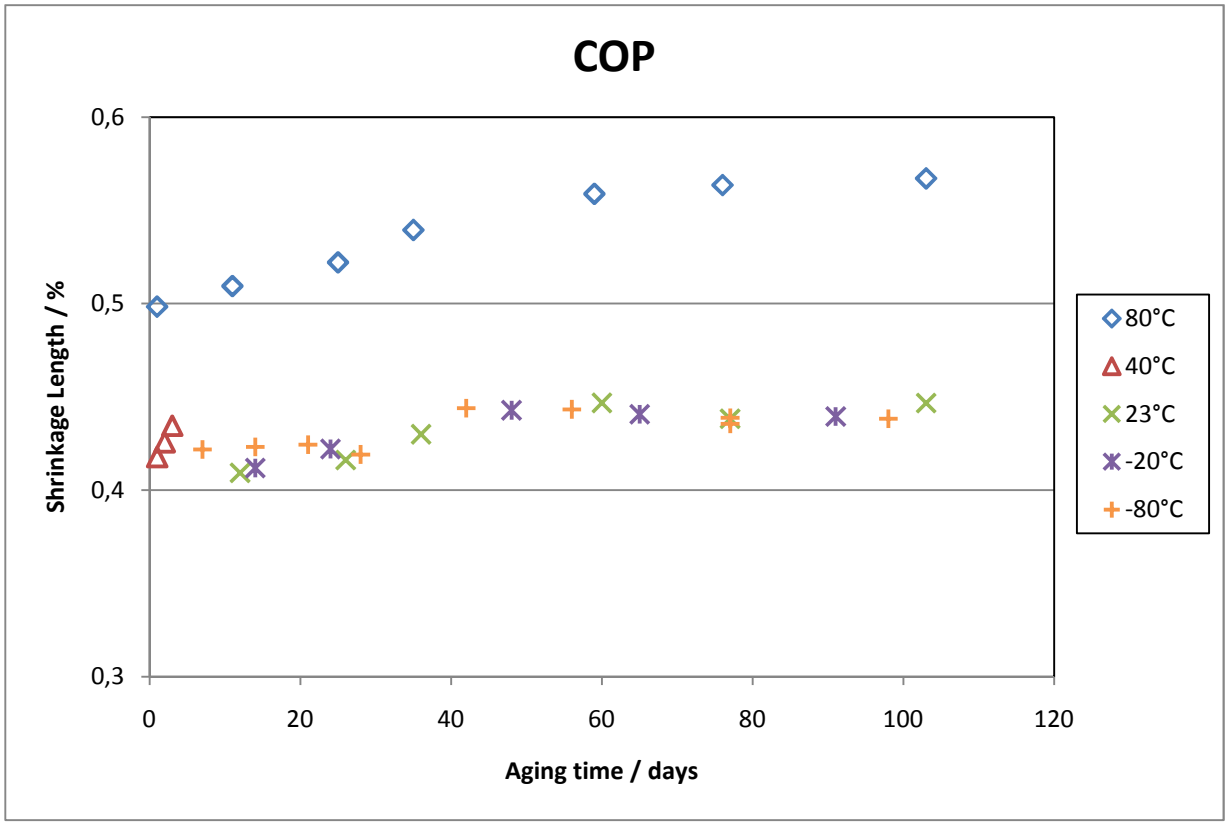

Figure 69: Shrinkage of COP measured over the length of the target during aging testing.

4.2.1.2.2 Flatness

Consistent with the observation for PP-C, COP did not show any change in flatness over time in any of the test conditions examined in the course of this research. However, Figure 70 points out a considerable difference in flatness between specimens molded from semi-crystalline polypropylene and amorphous Zeonor. While the maximum deflection over the width of the target is roughly 50 µm for PP-C, it is only about 35 µm for COP. A possible explanation for this effect is the far greater shrinkage of the semi-crystalline material compared to the amorphous grade.

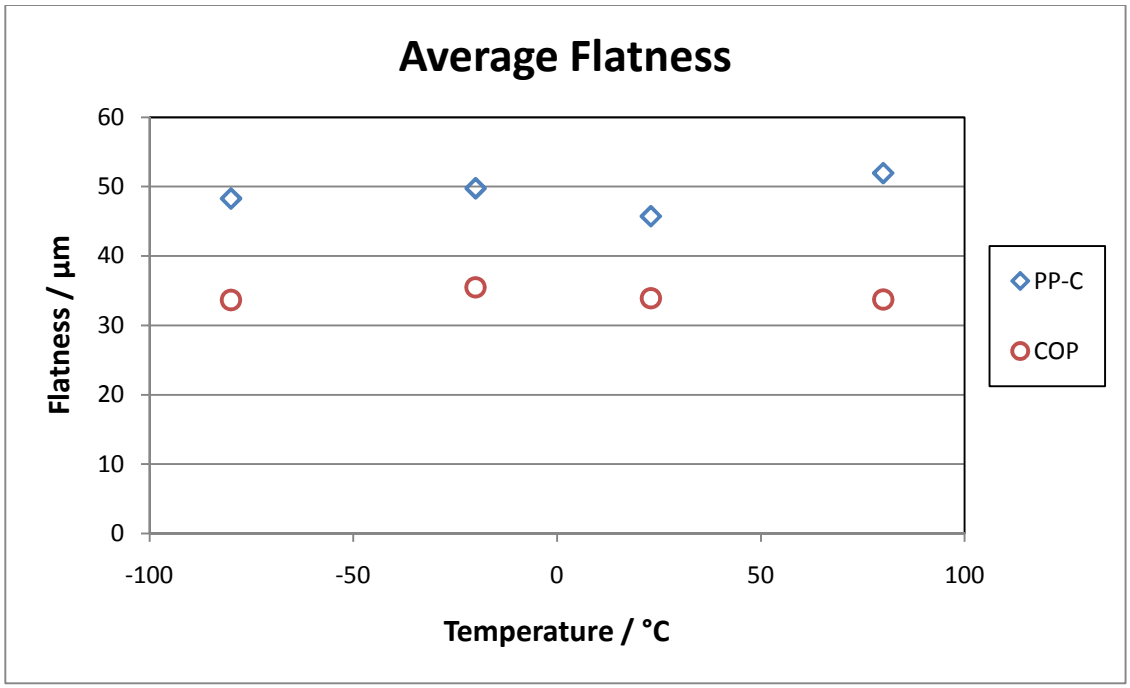

Figure 70: Flatness measured after 103 days of aging at various temperatures.

4.2.1.2.3 Roughness

Likewise, the roughness of COP does not vary over time or temperature. However, the absolute values are clearly lower than those of PP-C, which can be explained by the lack of carbon-black particles located at the surface. In Figure 71, one can see that the Ra value measured on the spots of the target lies around 30 nm for COP and 50 nm for PP-C, independent of aging conditions.

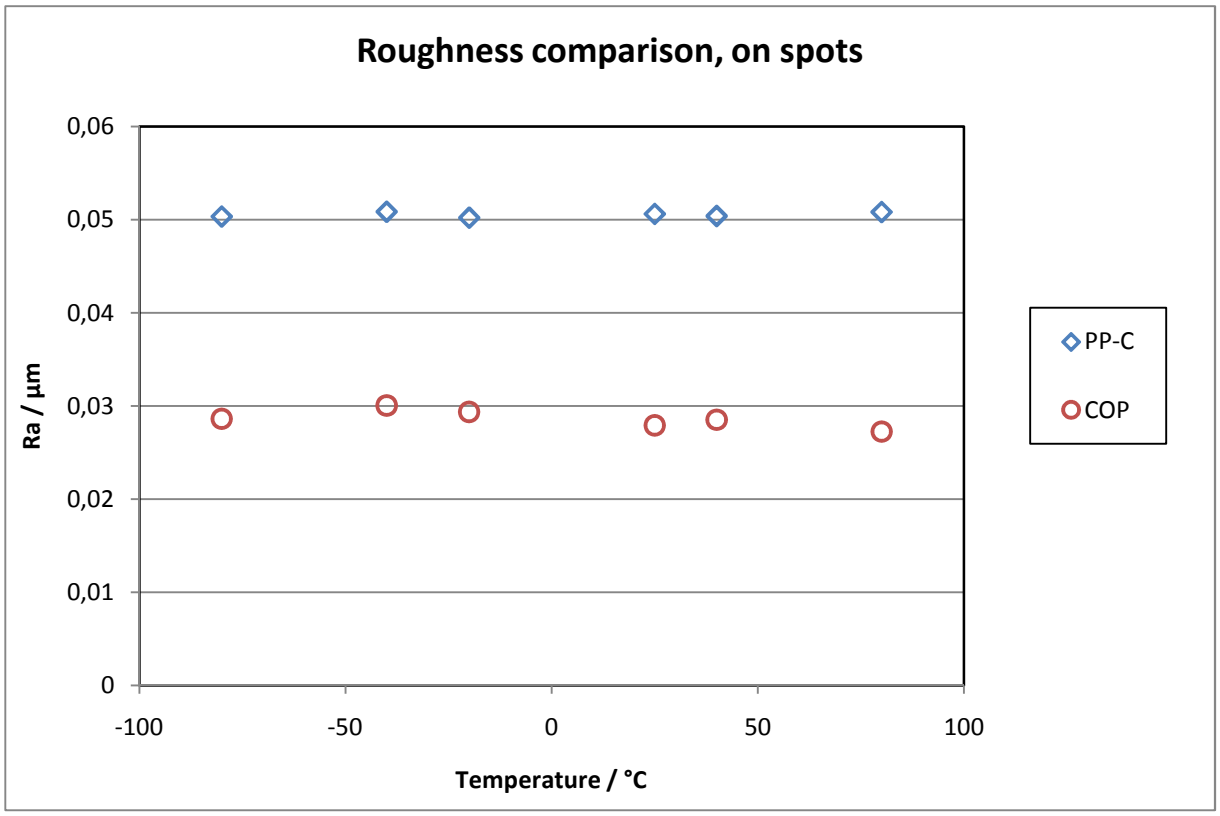

Figure 71: Roughness measured after 103 days of aging at various temperatures.

4.2.1.2.4 SEM

For both materials, scanning electron microscopy pictures showed no apparent change over time with any test condition. When compared (as in Figure 72), one can see that the surface of the unfilled amorphous material appears smoother than that of the carbon-black filled polypropylene.

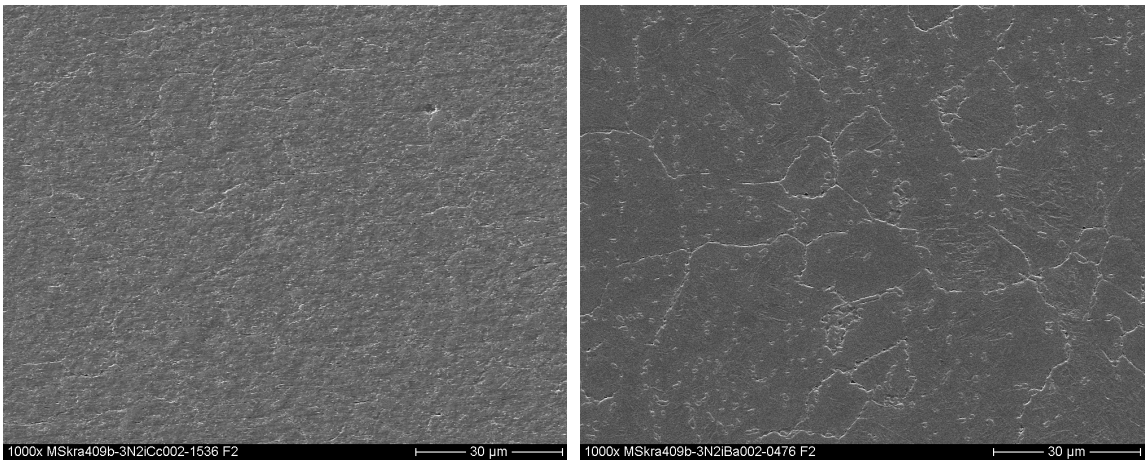

Figure 72: SEM pictures taken of the same spot on the target after 103 days of storage at room temperature (left: PP-C; right: COP).

4.2.1.2.5 Wetting behavior

Contact angle measurements performed with COP showed interesting results for targets stored at high temperature and humidity. While, similar to PP-C, no changes could be observed if humidity is undefined (Figure 73 illustrates that the contact angle values for all COP test series performed at undefined humidity levels vary around 97 °), Figure 74 and Figure 75 show a different picture if humidity is at a high level.

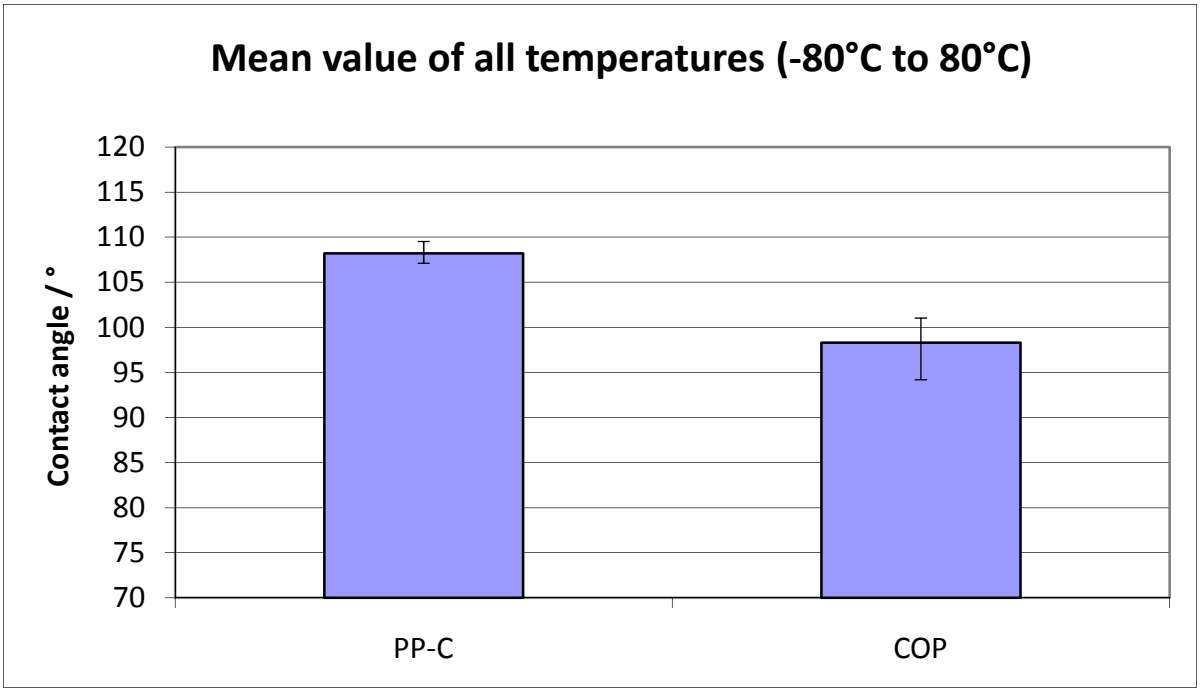

Figure 73: Average, minimum and maximum of all contact angle measurments for all temperatures, disregarding series with high (90 % rh) humidity.

Figure 74 demonstrates the contact angle values measured during short-term conditioning (maximum 3 days). The specimens were stored at three temperatures and two humidity settings. Contact angle measurements were performed after each removal (one every day). One can observe that while the results are stable for all other settings, contact angle values dropped during the conditioning period for samples aged at 80 °C and 90 % relative humidity. After conditioning the specimens were stored at room climate and remeasured twice during the following three weeks. One can see that the sample which aged three days at 80 °C and 90 % rh regained higher contact angle values, not quite reaching the original level of above 95 ° after 600 hours.

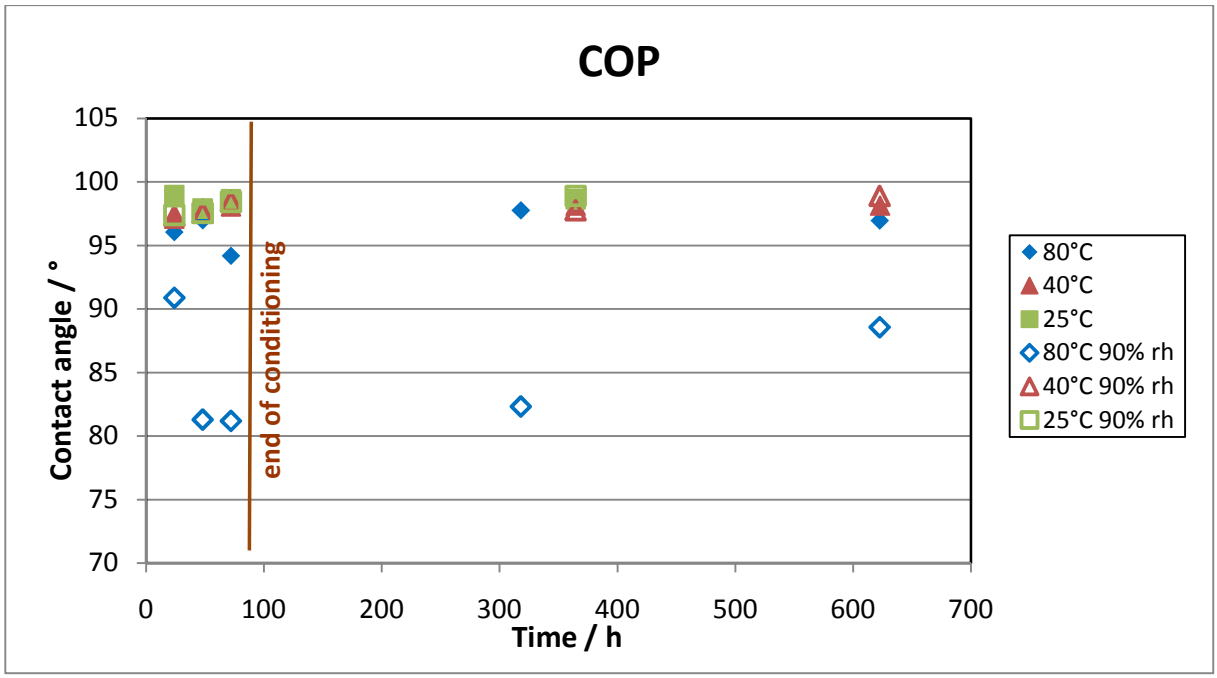

Figure 74: Short-term conditioning tests: contact angle values measured immediately after take-out up to the brown line. After conditioning, the samples were stored at room climate. The specimens which were conditioned three days in the climate chamber were then measured again, giving the values on the right side of the brown line.

Long-term aging tests illustrated in Figure 75 showed yet another trend. While there was still no change in contact angle for all settings without defined humidity level, the contact angle of the samples aged at 80 °C and 90 % rh (the only setting with high humidity observed during the long-term tests) first dropped to the level of around 80 ° observed during the conditioning tests. After three weeks, though, it appeared to become more hydrophobic again, and regained a contact angle level of approximately 100 ° after 5 weeks of aging like all other test settings. A possible explanation for this phenomenon could not be found in literature or in discussion with experts in this field.

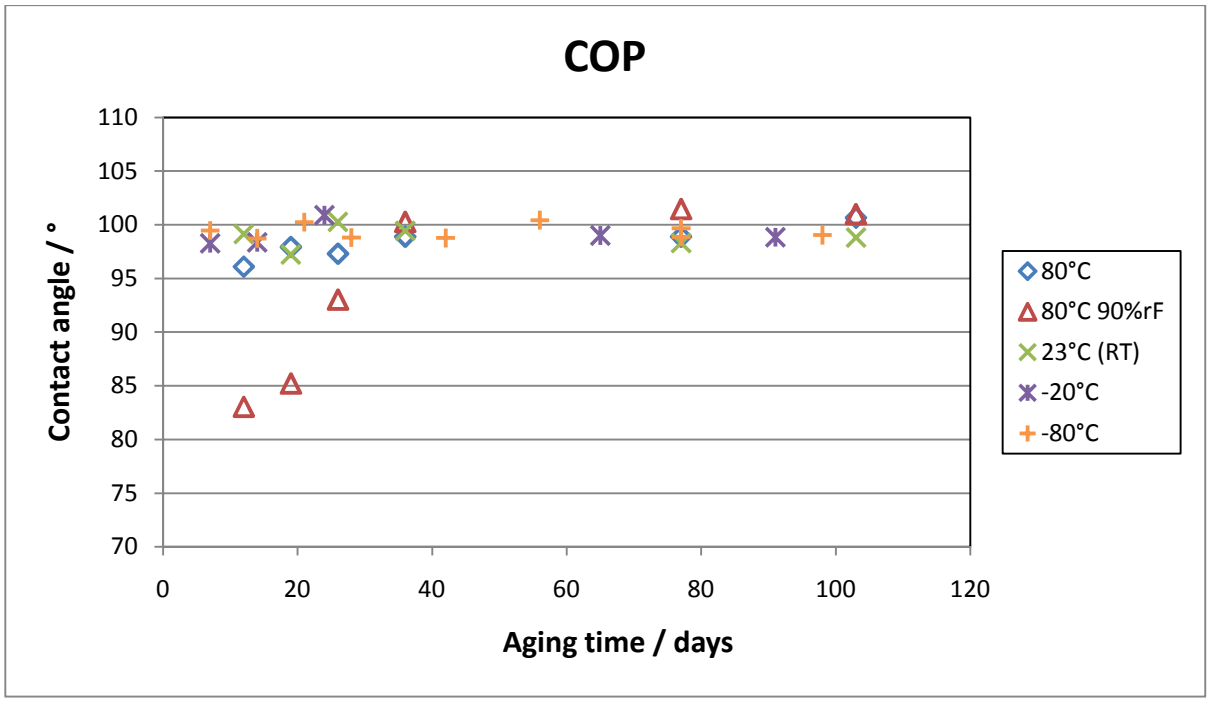

Figure 75: Long-term aging tests: contact angle values of samples aged at various conditions, measured immediately after removal.

4.2.2 Coated substrates

For the target's application in mass spectrometry, an impermeable conductive top layer is of great importance. This research focused on steel-coated carbon-black filled polypropylene targets. Most accurate target preparation for later mass spectrometry tests requires high geometric accuracy and reproducible wetting behavior. The goal of this research was to examine whether storage at different temperatures and climate conditions had any effect on the target's functionality.

4.2.2.1 Steel coating

The following paragraphs illustrate the effects of different surrounding conditions on steel-coated black carbon filled polypropylene targets. Results deviating from the behavior of the uncoated substrates will be emphasized. For all tests at and below room temperature, targets pre-conditioned in three different ways were examined: one month at room temperature (referred as unconditioned), one hour at 80 °C and 10 minutes at 120 °C. Short-term conditioning results discussed later showed similar contact angle values for all three conditioning types.

4.2.2.1.1 Shrinkage

Figure 76 compares the shrinkage of the coated (conditioned at room temperature) target to the uncoated substrate. As could be expected, a steel layer of barely 100 nm did not influence shrinkage in any way and both versions show the same increase in shrinkage (about 0.15 additional percent compared to samples stored at room climate) for targets stored at 80 °C.

As illustrated in Figure 77, the short pre-conditioning cycles had no detectable influence on shrinkage. The mean values determined for all targets of the same conditioning type aged at the same temperature are approximately the same. Minima and maxima of these series, illustrated through the error bars, demonstrate possible deviations within the series.

In Figure 78 one can see that no significant difference in shrinkage between samples tested under static and cyclic conditions could be detected. At the end of the testing period the samples stored at static conditions shrank 1.08 %, those tested under cyclic conditions displayed 1.06 % shrinkage.

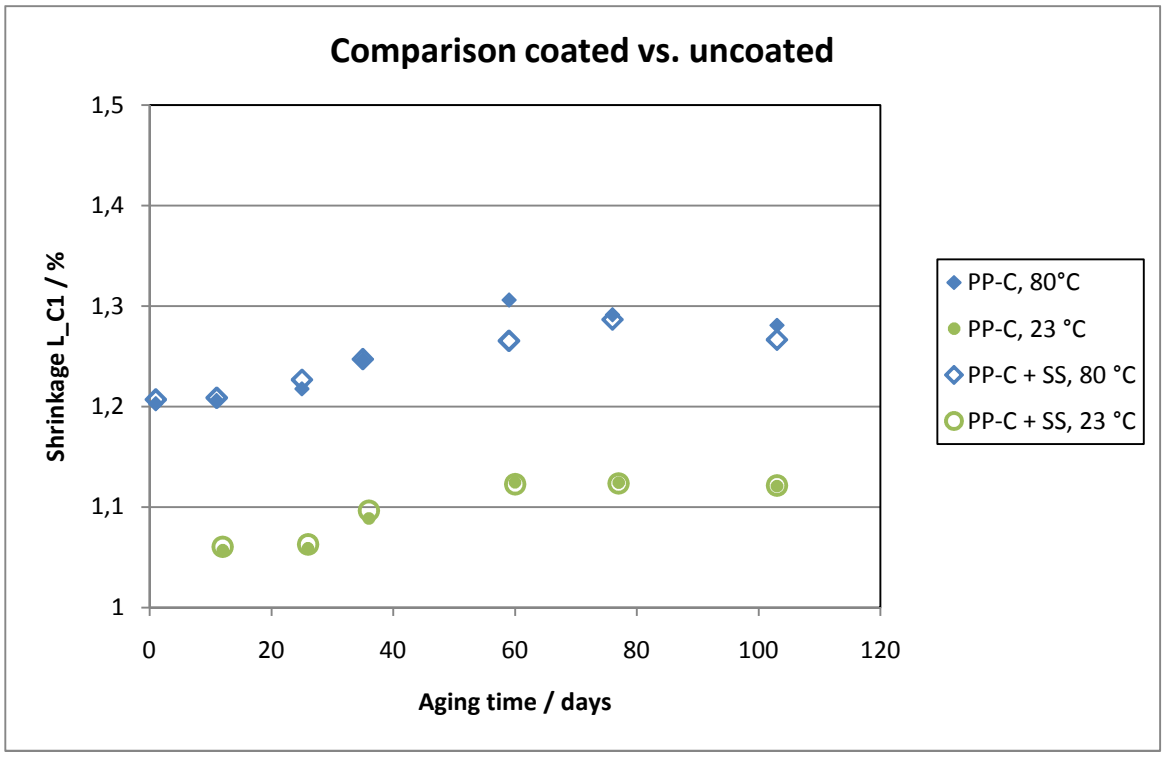

Figure 76: Shrinkage of unconditioned coated and uncoated PP-C.

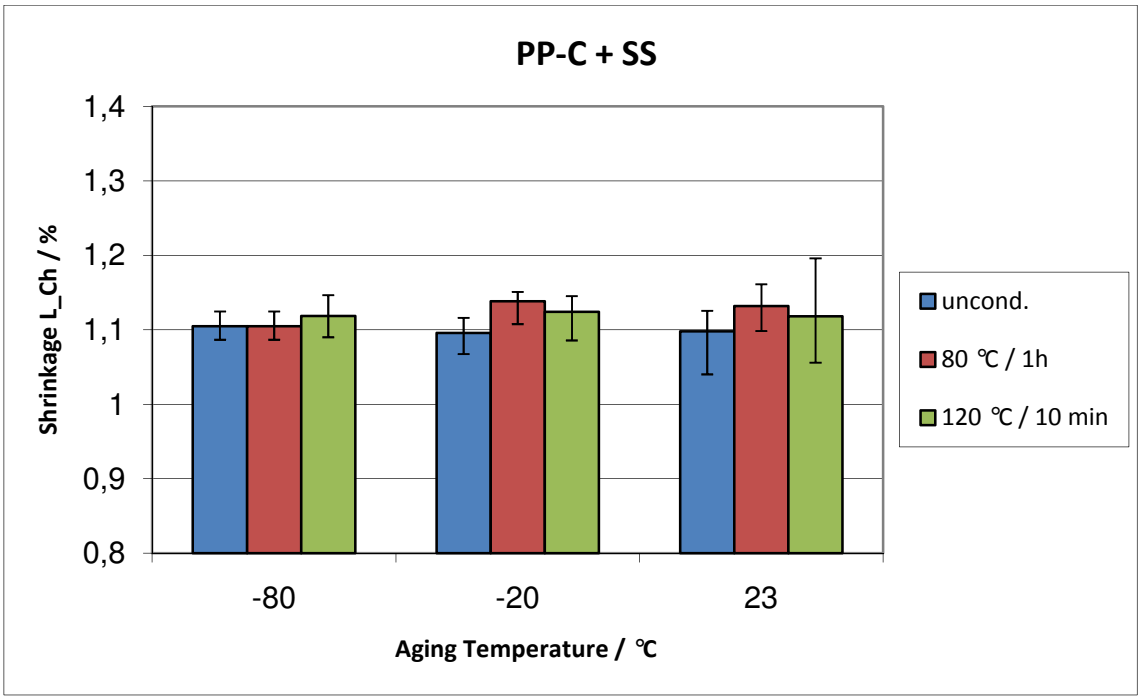

Figure 77: Mean value of shrinkage for all three conditioning versions determined over the whole testing period of aging at different temperatures. Error bars showing minima and maxima.

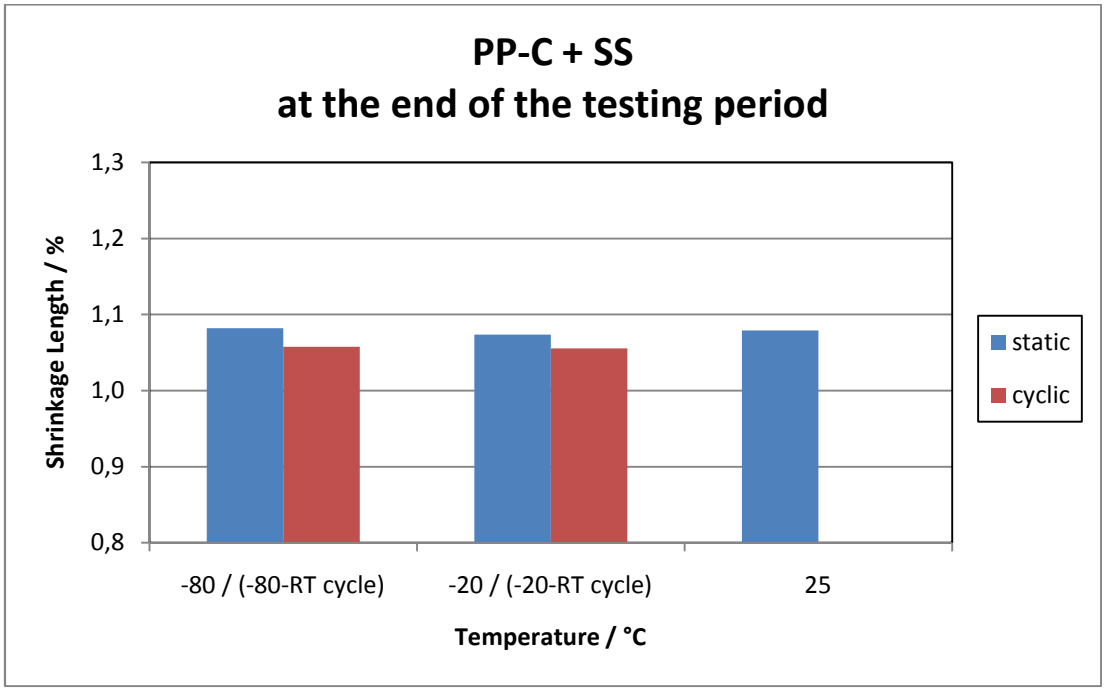

Figure 78: Shirnkage comparison between short-term static and cyclic tested samples at the end of the testing period (3 days static, 7 days cylic).

4.2.2.1.2 Flatness

Consistent with the shrinkage results above, the steel coating did not influence the target's flatness in any way. Figure 79 and Figure 80 show mean flatness values measured after 103 days of aging at different temperatures for both, uncoated and coated specimens. Independent of preconditioning and test conditions, a flatness of approximately 50 µm was measured. No influence of the coating could be identified. Figure 81 compares the flatness of static and cyclic tested specimens at the end of the testing period. No significant deviations between was testing types were identified and the flatness values and variations are consistent with those seen in the long-term tests.

4.2.2.1.3 Roughness

Likewise, no significant difference in roughness between coated (all three conditioning types) and uncoated substrates could be found. Analog to the flatness evaluation, Figure 82 and Figure 83 illustrate the results measured after 103 days of aging. A Ra value of approximately 50 nm was measured on the spots, regardless of preconditioning and test temperature. Coated targets were slightly less rough in each case than uncoated targets. As seen in Figure 84 no difference in roughness between static and cyclic tested targets could be identified.

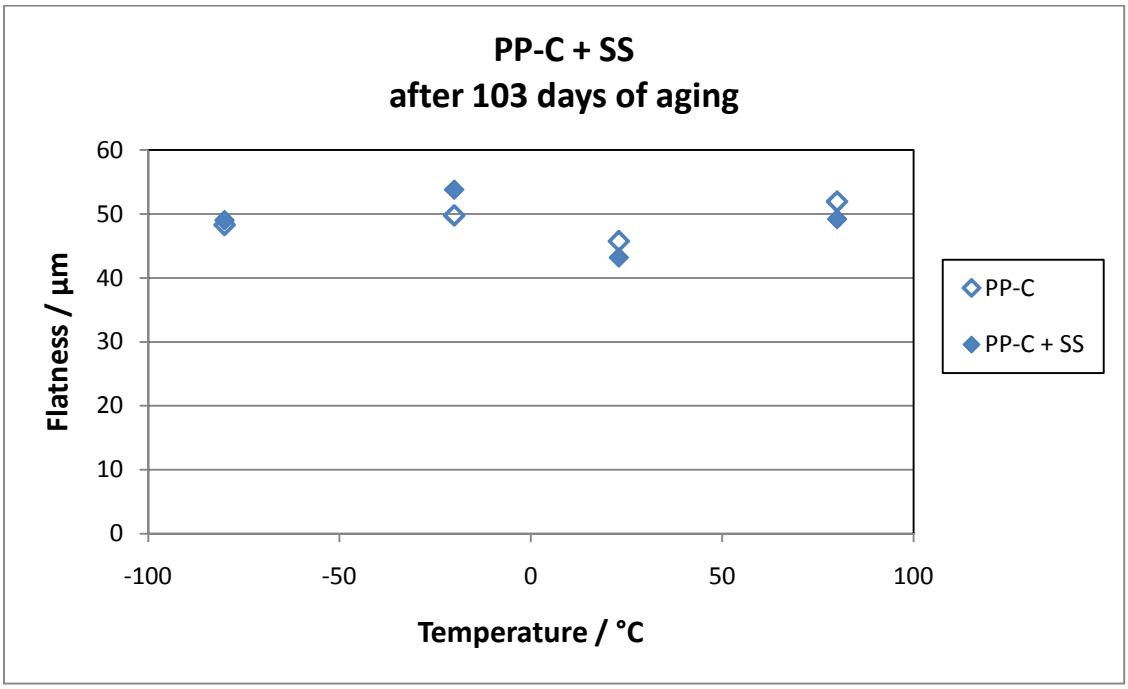

Figure 79: Flatness of coated and uncoated PP-C targets after 103 days of aging at different temperatures.

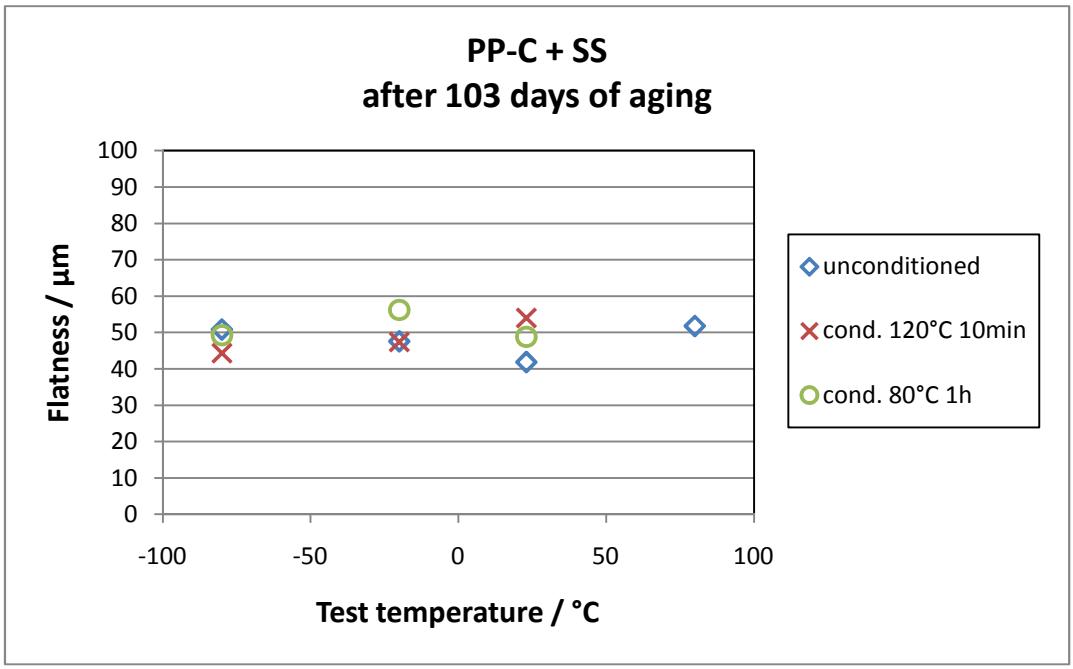

Figure 80: Flatness of all three conditioning types after 103 days of aging at various temperatures.

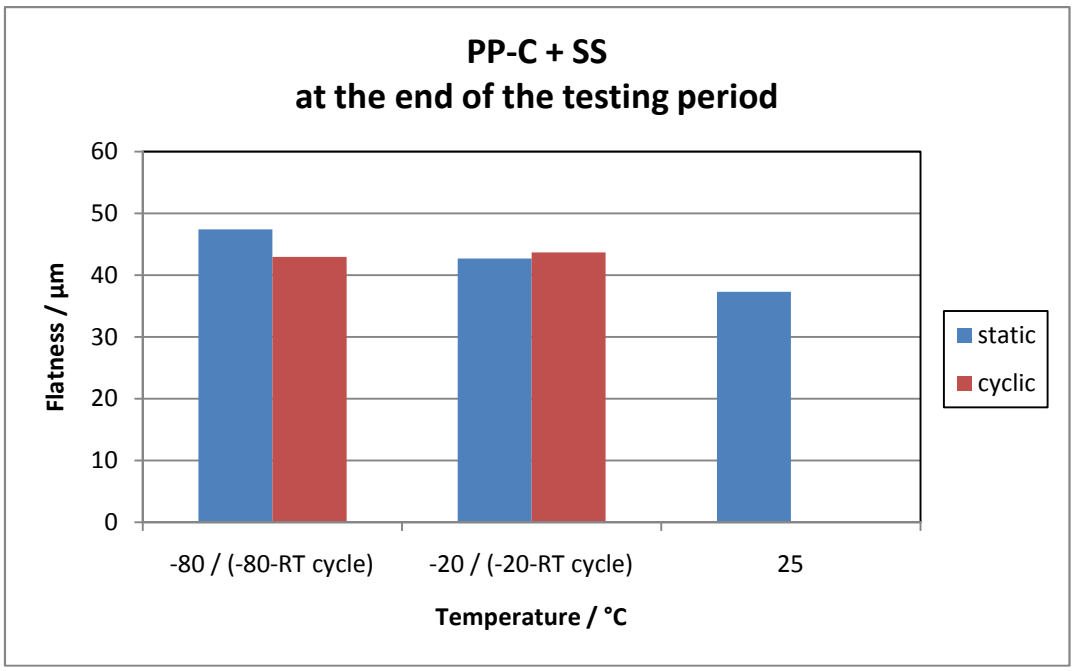

Figure 81: Flatness comparison between short-term static and cyclic tested samples at the end of the testing period (3 days static, 7 days cylic).

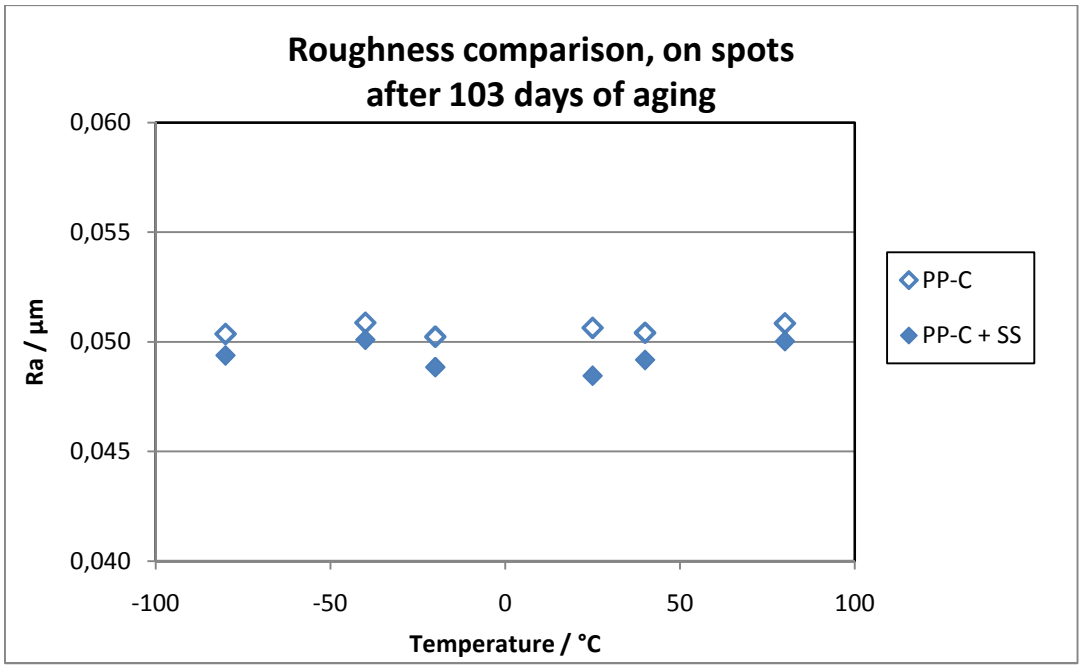

Figure 82: Roughness of coated and uncoated PP-C targets after 103 days of aging at different temperatures.

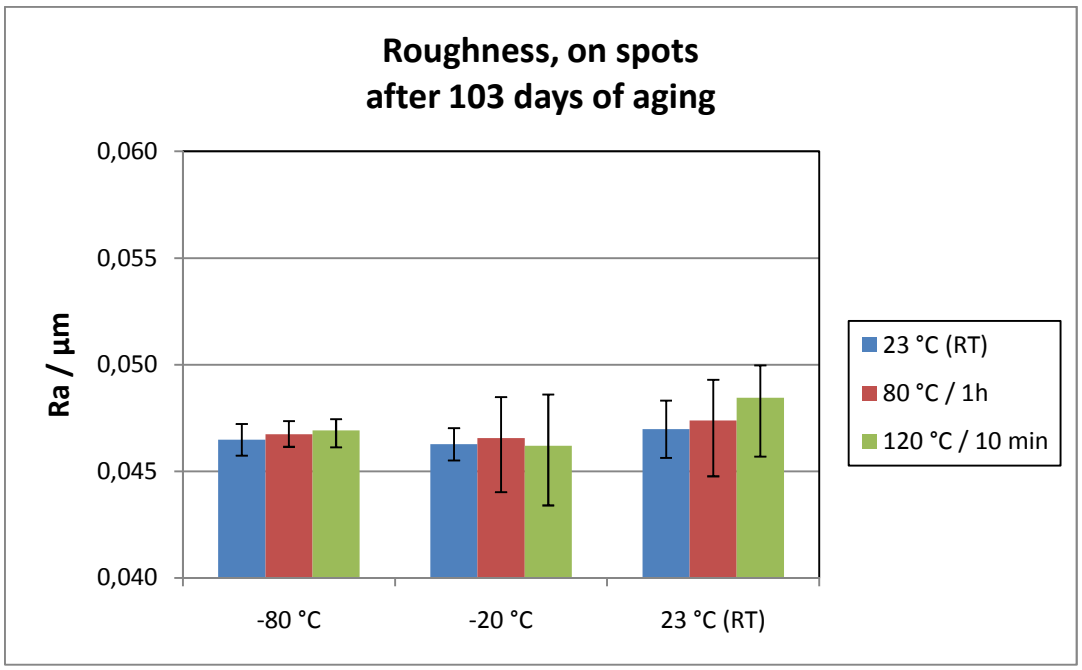

Figure 83: Mean value of roughness for all three conditioning versions determined over the whole testing period of aging at different temperatures. Error bars showing minima and maxima.

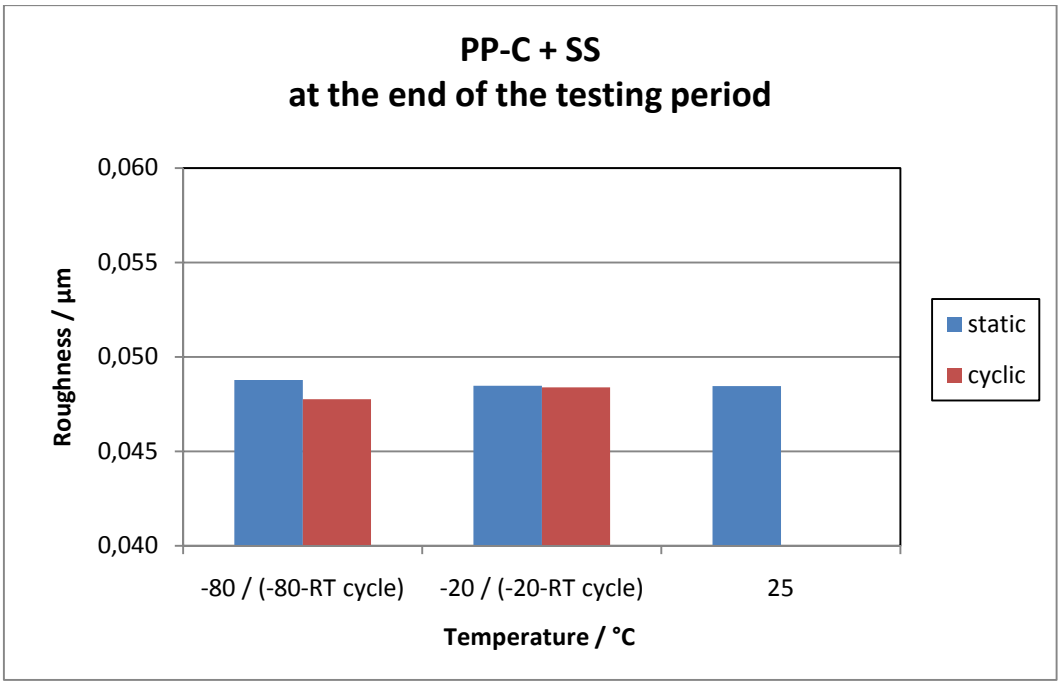

Figure 84: Roughness comparison between short-term static and cyclic tested samples at the end of the testing period (3 days static, 7 days cylic).

4.2.2.1.4 SEM

The purpose of the scanning electron microscope investigations was to determine whether any apparent change to the surface could be observed. The impermeability of the surface is crucial to the application. Therefore three spots were examined for cracks or delaminations, which would indicate a possible failure of the target. Figure 85 shows the surface of the same spot of an uncoated and coated target stored at room temperature for 19 days. Compared to the same spot of two targets stored 103 days at 80 °C in Figure 86, it is apparent that neither time nor temperature caused any identifiable change during the aging period. In total, both the coated and uncoated surface are quite similar and show the same marks resulting from the injection molding process. All pictures taken from targets during the long-term aging tests showed the same results.

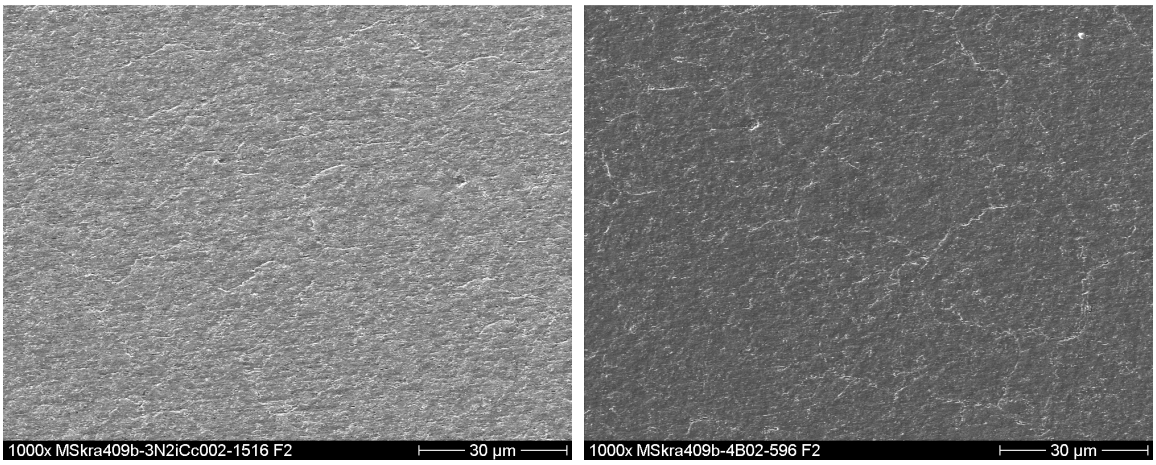

Figure 85: SEM pictures taken after 19 days of storage at room temperature. Right: uncoated substrate; Left: steel-coated target.

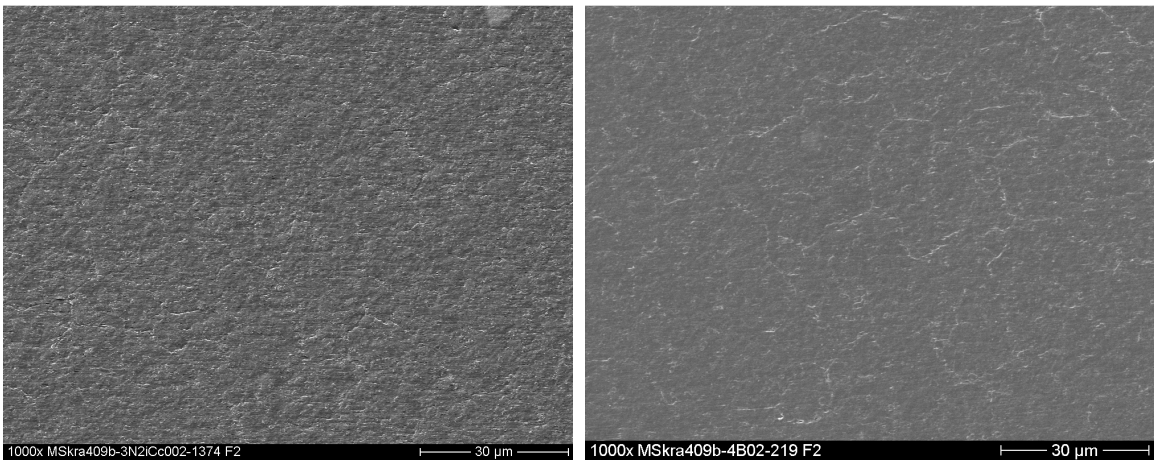

Figure 86: SEM pictures taken after 103 days of storage at 80 °C. Right: uncoated substrate; Left: steel-coated target.

The only abnormality observed was seen on a sample from a short-term conditioning test. Figure 87 shows a spot at 1000x magnification of a sample conditioned six hours at 120 °C. One can see that the surface's appearance has changed. Elongated bubbles cross the spot normal to the injection direction of the target. This could indicate damage to the coating at this point and be a possible starting point for cracks. No changes of the surface of the specimens tested under cyclical conditions was observed.

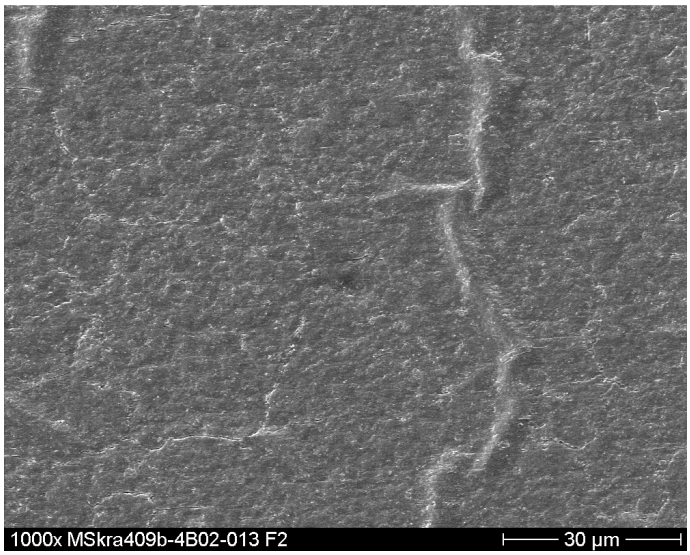

Figure 87: Steel-coated target, conditioned 6 hours at 120 °C.

4.2.2.1.5 Peel Test

The peel test confirms the suspicions raised by the SEM pictures. As seen in Figure 88 the only test setting showing delaminations was performed with the same target conditioned 6 hours at 120 °C. None of the other tested targets showed any sign of damage to the surface whatsoever.

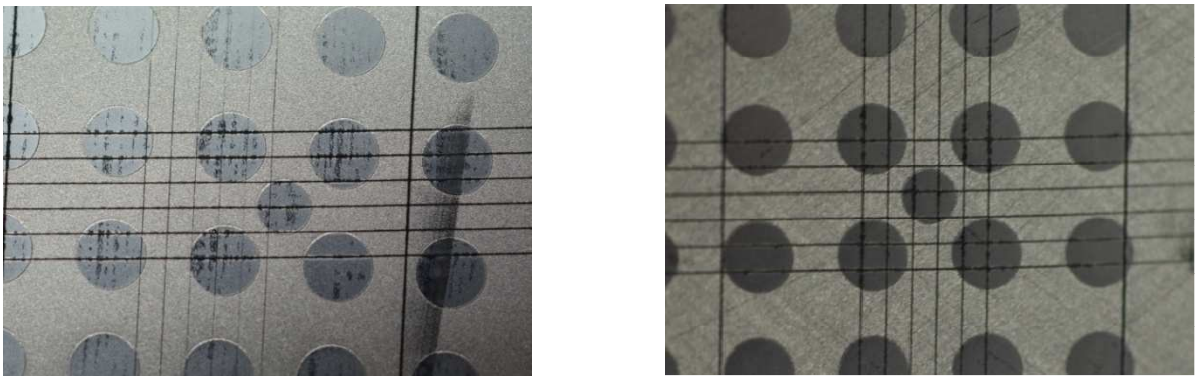

Figure 88: Peel test of two different steel-coated PP-C targets. Left: Target conditioned 6 hours at 120 °C, elongated delaminations across the target; Right: test done after four months storage at room temperature.

4.2.2.1.6 Wetting behavior

In mass spectrometry, the sample is dissolved and dropped on the spots of the target. For the application, it is crucial that the sample is evenly distributed over the surface of the spot. At higher contact angles, the area covered by a drop dosed on the spots decreases and the density of crystals on the spot increases. A contact

angle of at least 80 ° is required for a 2 µl drop to stay in the defined area. Previous examinations showed that the contact angle increases slowly, starting at approximately 40 ° immediately after sputtering, and reaches a constant level above 100 ° after two weeks of storage at room temperature. Oxidation is suspected to be responsible for this behavior. Currently, tests are performed to confirm this suspicion. First examinations showed that this process can be accelerated by storing the targets at higher temperatures. The goal of this research was to determine possible conditioning settings for the acceleration of this process.

First, possible options for short-term conditioning were examined. Immediately after coating, samples were stored at various temperatures and the contact angle was measured after different conditioning times. Figure 89 shows the increase of contact angle during conditioning at different temperatures. Note that the time axis is logarithmic. The contact angle increases rapidly first; with progressing time, the increase rate diminishes and a constant level is reached. On a logarithmic time scale, this growth appears nearly linear. It is apparent that the rate of increase can be increased significantly by storing the sample at higher temperatures. This is consistent with research done by Leezenberg et al., which showed an increase in water contact angle for a-C:H films stored at ambient temperatures over time [28]. One can see that the time needed to reach a constant level at around 110 ° can be reduced significantly by conditioning at higher temperatures and varies from a few minutes, if stored at 120 °C, up to three weeks at room temperature. If the time needed to reach this plateau is plotted (as done in Figure 90), one can observe a logarithmic dependency between the conditioning time needed and the storage temperature. In order to calculate the activation energy of this process, an Arrhenius plot was compiled for this behavior (see Figure 91). As discussed in Chapter 2.2.3, the activation energy can be calculated from the slope of the straight line in the Arrhenius plot. For this combination of materials, the activation energy is 61.32 kJ / mol. The activation energy was then used to calculate the temperature-shift factors (Table 18) to create a contact angle master curve as seen in Figure 92.

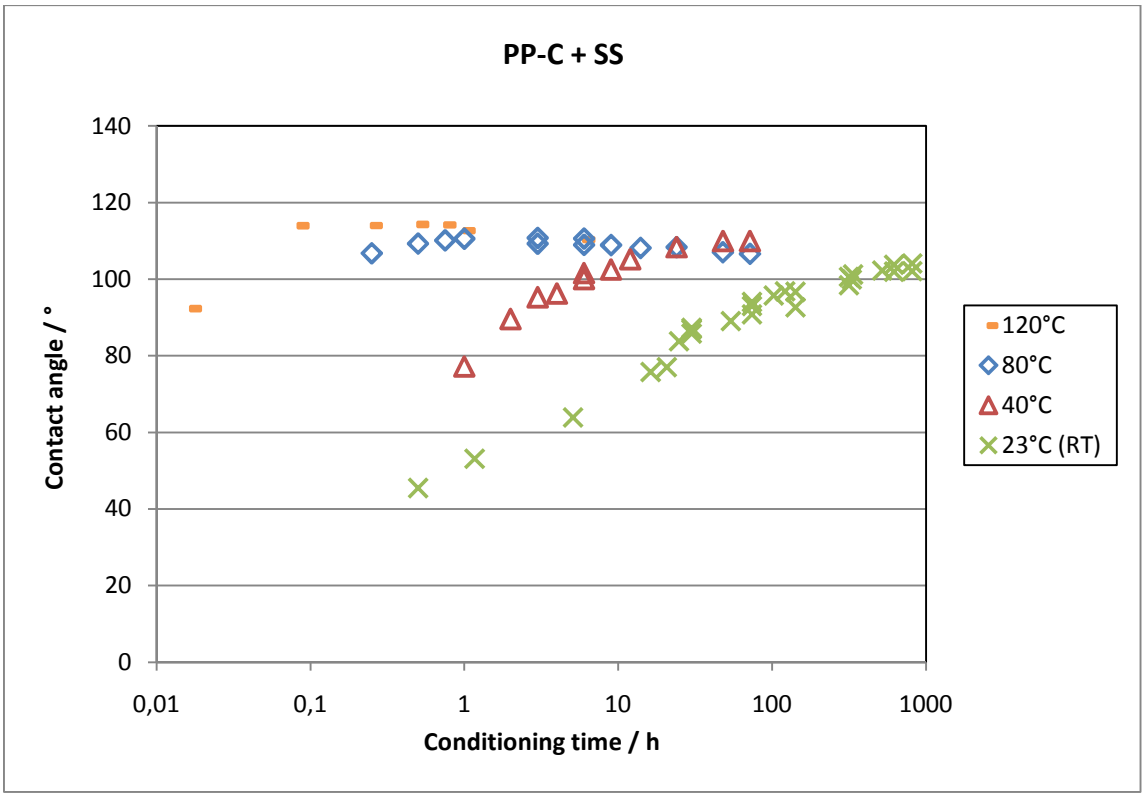

Figure 89: Contact angle of steel-coated specimens conditioned at various temperatures.

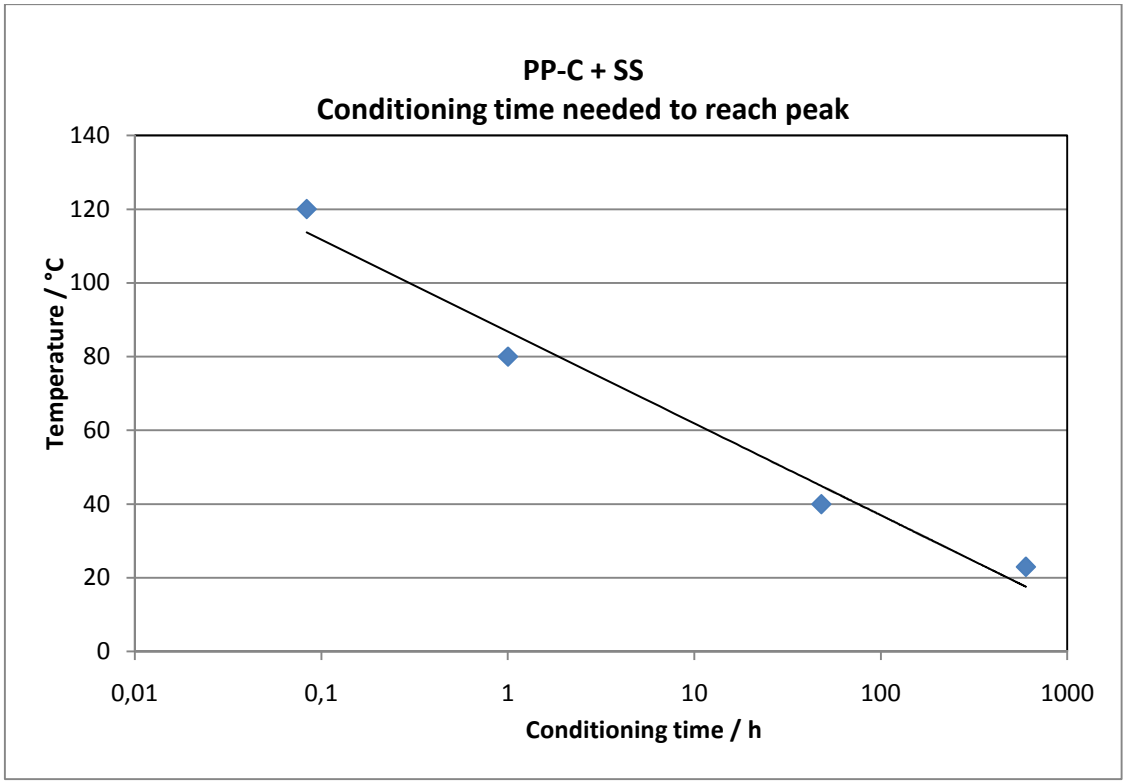

Figure 90: Time needed to reach a constant contact angle level for steel-coated targets.

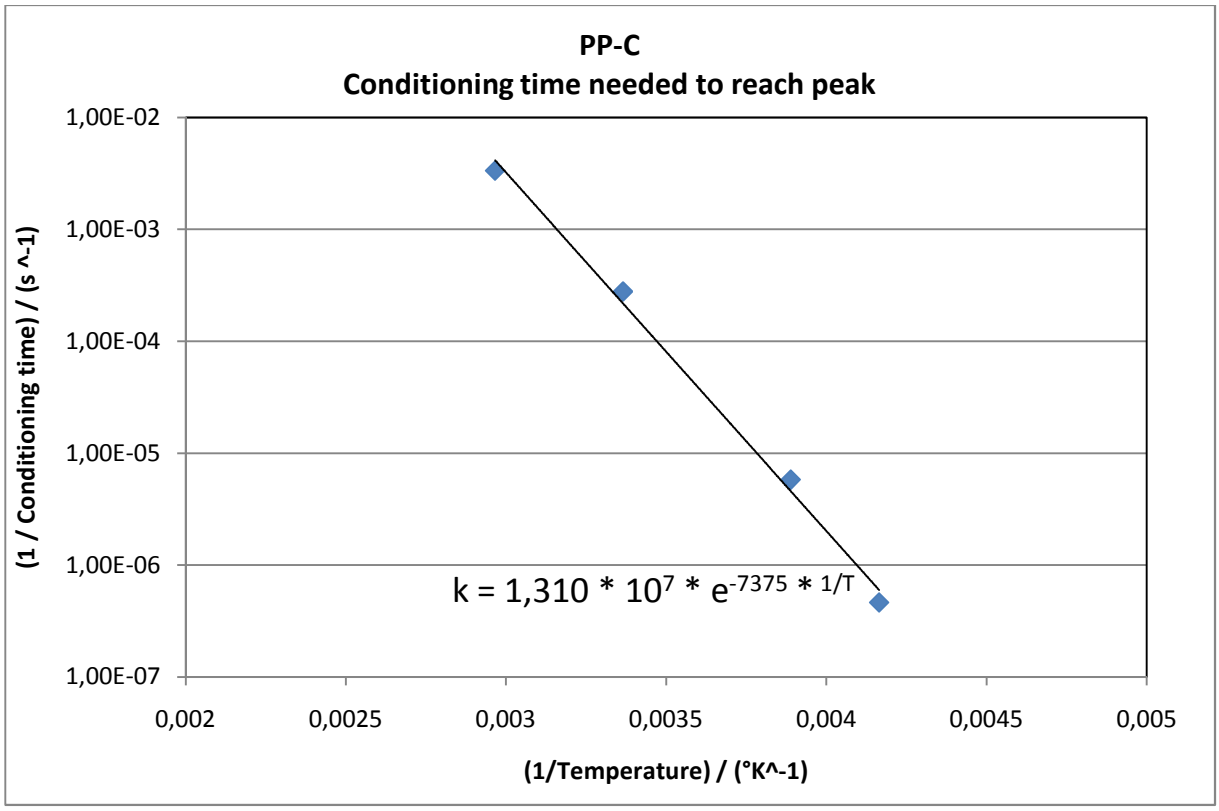

Figure 91: Time needed to reach constant contact angle level for steel-coated targets, diagram according to Arrhenius equation.

Table 18: Temperature shift factors calculated for steel-coated targets with equation (17)

Temperature / °C	Temperature shift factor a_t
120	6883
80	362
40	7.62
23	1

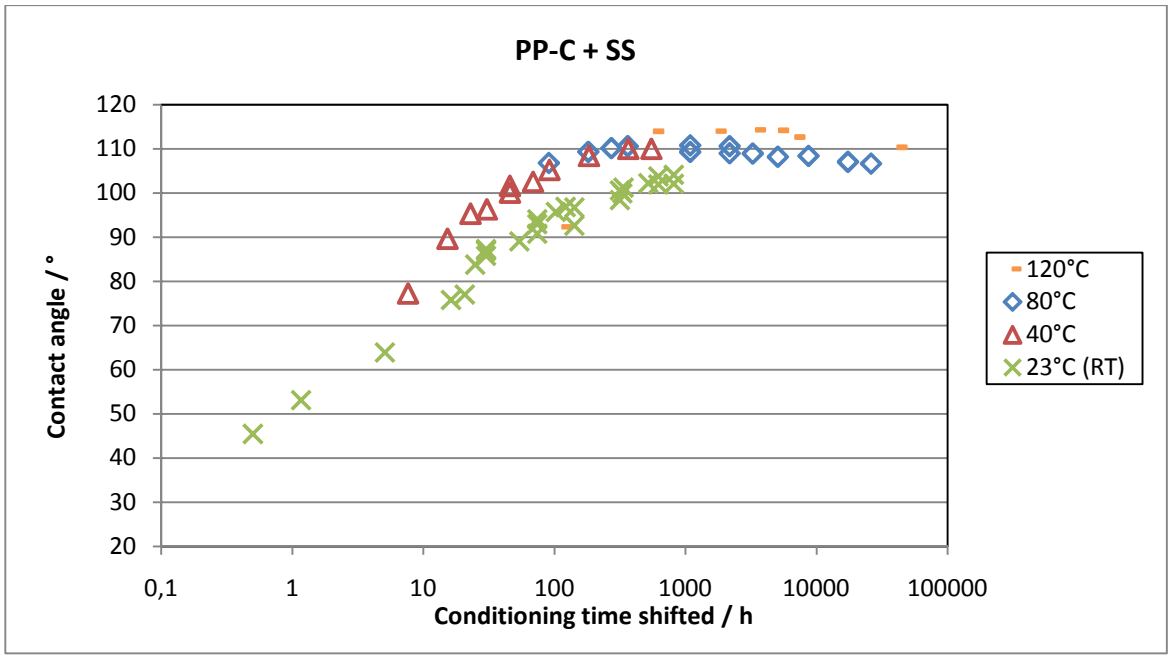

Figure 92: Contact angle of steel-coated specimens conditioned at various temperatures, conditioning time multiplied by temperature shift factor.

After reaching the constant contact angle level, regardless of the conditioning type, the contact angle values remained constant at this plateau. Aging at different temperatures and humidity levels could not change this (see Figure 93 and Figure 94). No difference between the specimens stored under cyclic and static conditions was observed either (see Figure 95).

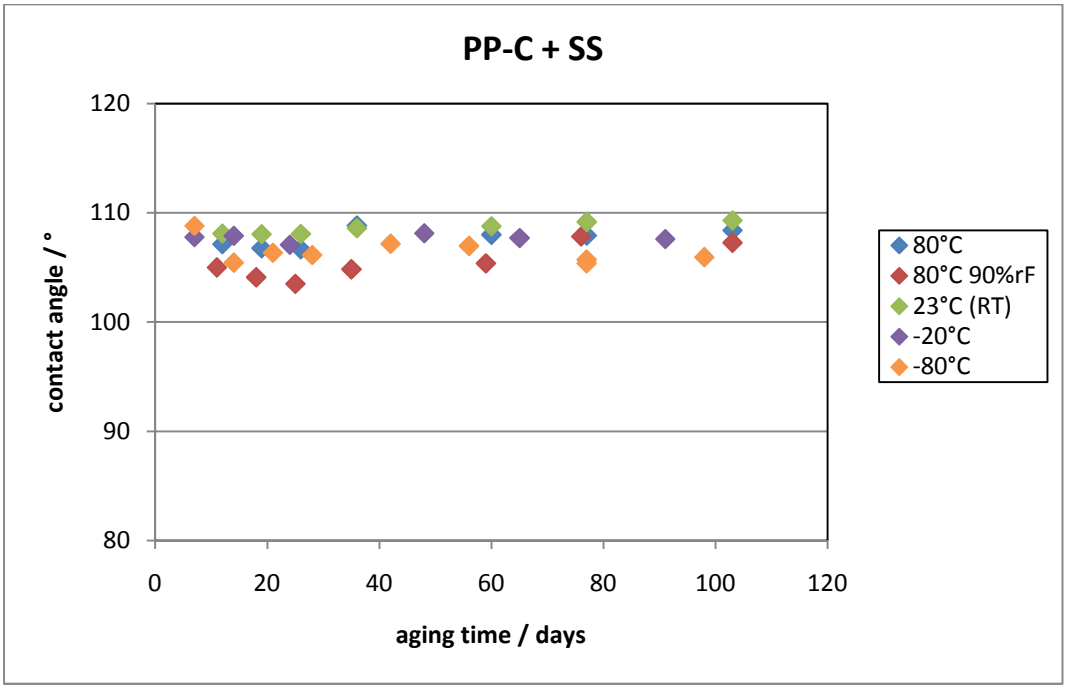

Figure 93: Contact angle of unconditioned steel-coated PP-C during aging.

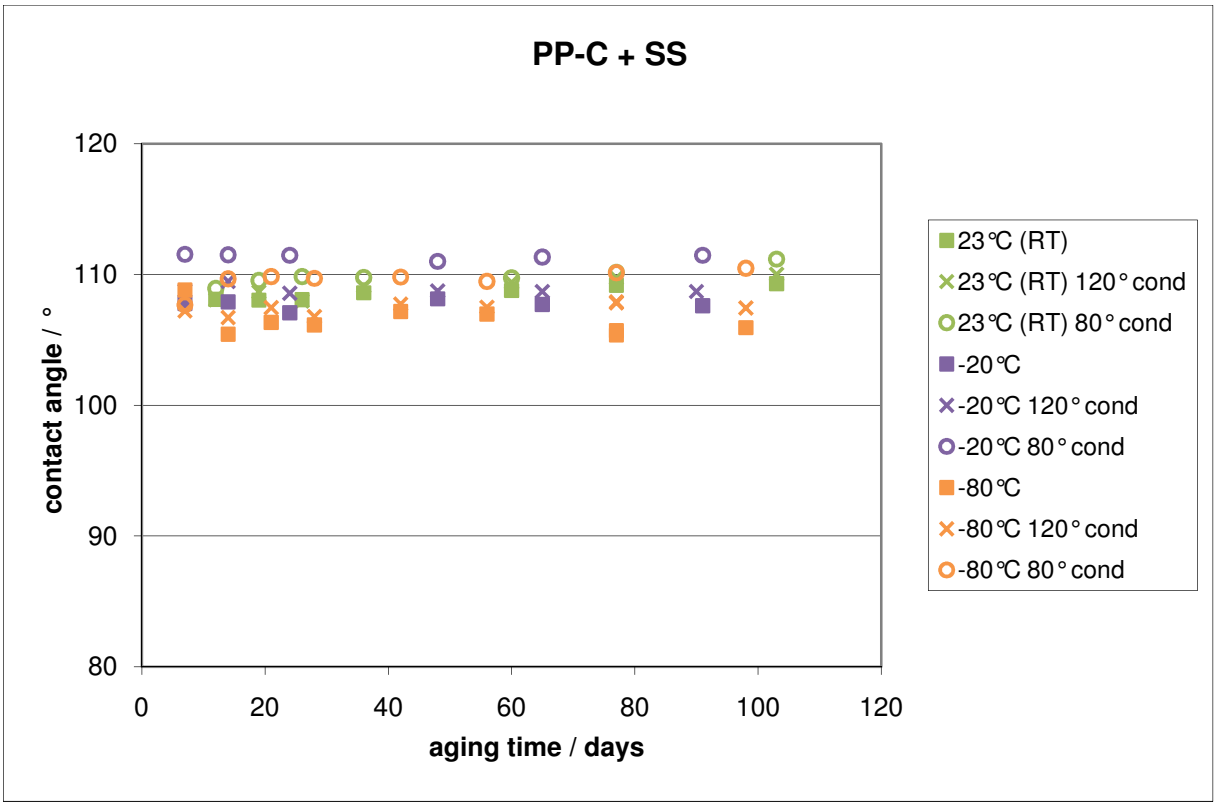

Figure 94: Contact angle during aging for steel-coated PP-C and different conditioning types.

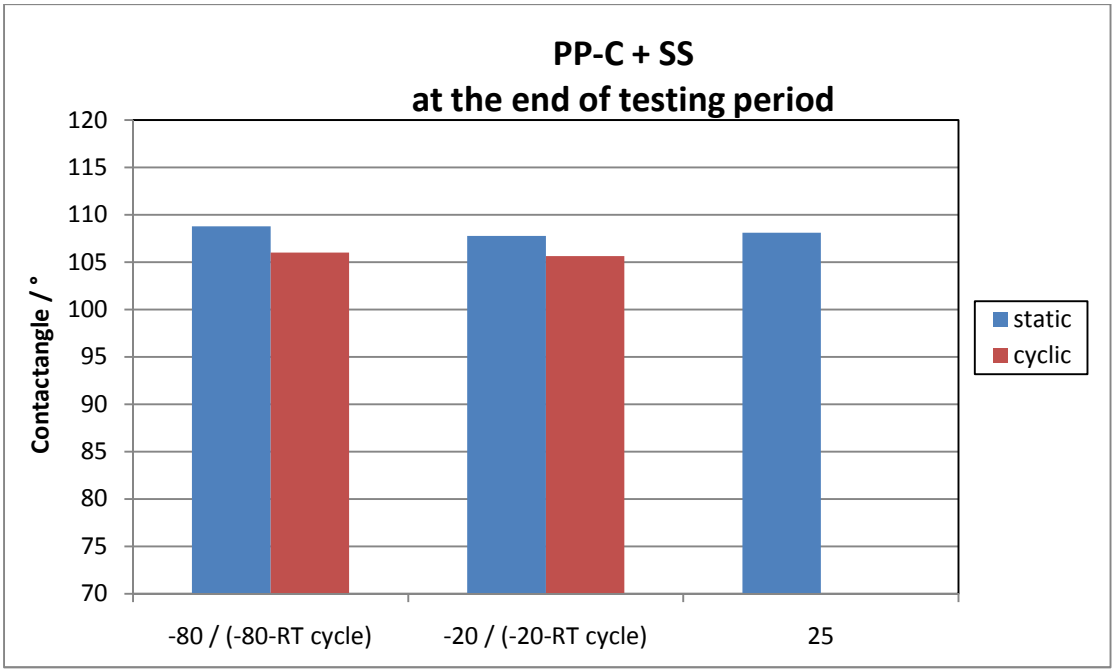

Figure 95: Contact angle comparison between short-term static and cyclic tested samples at the end of the testing period (3 days static, 7 days cylic).

4.2.2.1.7 Conclusions

This research demonstrated that the time needed to reach a constant high contact angle level can be illustrated on an Arrhenius plot and following conditioning settings could be recommended:

- 24 hours at 40 °C
- 2 hours at 60 °C
- 1 hour at 80 °C

A short treatment of 5 minutes at 120 °C is not recommended since SEM investigations showed damage on samples stored 6 hours at this temperature.

Significant after-shrinkage at high temperatures leads to great geometric changes. Since this would result in dimensions outside of the specified tolerance window, the targets should not be stored or transported at temperatures above 60 °C.

An accurate life time prediction is not possible, since no failure resulting in reduced functionality of the target was observed during the testing period of 3 month. One common technical approximation is the “rate-temperature-rule” by Van´t Hoff [48]. It predicts that the rate of chemical and physical processes leading to failure doubles every 10 °C. No damage to the target could be detected after 14 weeks of storage at 80 °C. Applied to this case the Van´t Hoff rule would predict a life time of 17 years at 20 °C. Therefore, it is safe to say that no failure is to be expected during a two year period under normal storage conditions.

Neither static nor cyclic tests at -80 °C and -20 °C had any influence on the tested targets. For this reason, storage at low temperatures, even if the target is thawed for reexamination and then frozen again, should not affect the target. Archiving can therefore be recommended.

4.2.2.2 Gold coating

A short test-series was performed with gold-coated targets. These samples showed the same results as steel-coated targets for all tests with one exception: wetting behavior.

4.2.2.2.1 Wetting behavior

Gold was chosen purposely as the second material in coating tests. Its chemical stability led to expect no changes in the molecular structure of the surface, thus eliminating this influence on contact angle behavior. The contact angle results then confirmed these expectations. After a slow increase (starting from 95 °) the gold-

coated targets reached a constant level slightly above 100 °, which they kept during the aging tests (see Figure 96 and Figure 97).

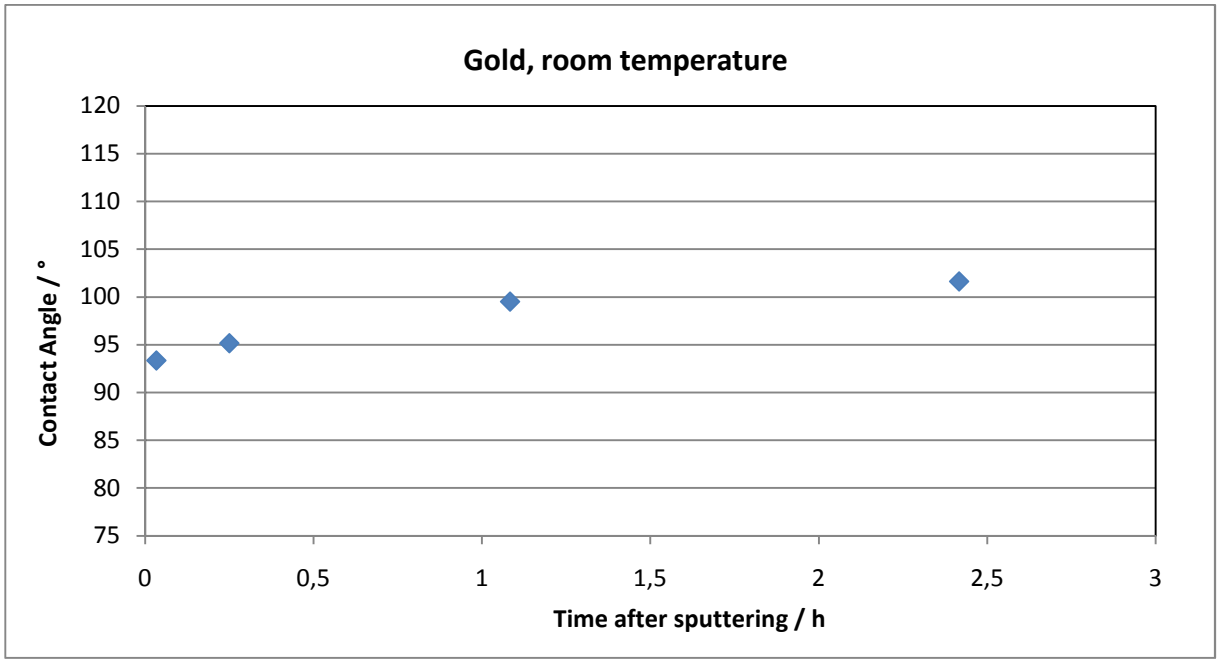

Figure 96: Contact angle measurements of gold-coated PP-C targets immediately after sputtering.

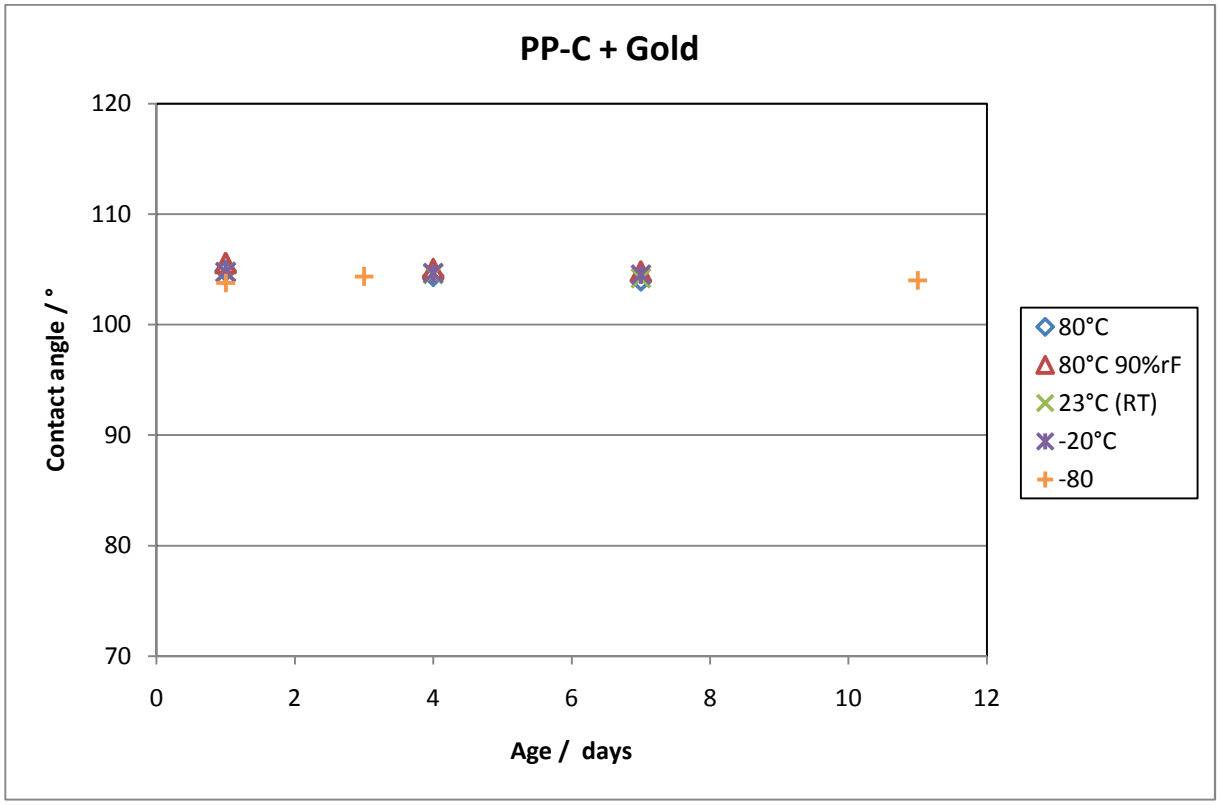

Figure 97: Aging of gold-coated PP-C targets.

4.2.2.2.2 Conclusions

Since a constant contact angle is reached nearly shortly after production, conditioning is not necessary for gold-coated targets.

All other results did not deviate from those seen for steel-coated specimens. Therefore, all conclusions drawn on storage and transport conditions, life time prediction and archiving in 4.2.2.1.7 also apply to gold-coated targets.

5 SUMMARY AND CONCLUSIONS

5.1 Shrinkage

The shrinkage of two very different materials was experimentally determined and calculated with simulation for various injection molding parameter settings. The results were compared to examine the applicability of simulation for mold design.

The first grade, a carbon-black filled semi-crystalline polypropylene grade, showed shrinkage values between 0.8 and 1.4 % during experimental measurement. The second, an amorphous cyclo-olefin-polymer shrank between 0.15 and 0.45 %. Neither of these materials finds widespread industrial use. Therefore no material data needed for simulation with MPI could be taken from the common databases. All material data was measured at the IKV-Institute of Plastics Processing at the University of Leoben.

Simulation was performed with a 2.5D model (note that no CRIMS values were available in the Moldflow database for the materials used in this research) and a 3D model. Altogether, one has to say that the predictions given by simulation were disappointing. While the mean values taken from all simulations and experimental tests were quite close for the COP especially with the 3D model, they were far off predicting the shrinkage of PP-C. A glance at the detailed results reveals the extent of the failure of simulation. At some settings and dimensions, the difference between the predicted and actual results was as big as the overall shrinkage of the material. It has to be pointed out that the spreads were lower for the 3D model than for the 2.5D model. Thus, the 3D model was chosen for the parameter study.

The trends for COP observed in the parameter study were consistent between simulation and experiment for most process parameters. The results for PP-C were less promising, since no consistency between simulation and experiment could be found for this material. Obviously, the complicated nature of this 30 % carbon-black filled semi-crystalline polymer made accurate shrinkage prediction impossible.

Still, hope remains that advances in technology, such as the implementation of crystallization processes into simulation software, will increase the accuracy of shrinkage prediction in future. With state-of-the-art software deviations between actual and predicted shrinkage are far too large especially for semi-crystalline materials to solely rely on them for mold design, especially for the investigated targets with very tight tolerances.

5.2 Aging tests

5.2.1 Conditioning

One goal of this research was to find a way to reduce the time needed to reach a contact angle above 100° on steel-coated polymeric targets used in mass spectrometry.

This thesis demonstrated that the time needed to reach a constant high contact angle level can be shown on an Arrhenius plot and following conditioning settings could be recommended:

- 24 hours at 40 °C
- 2 hours at 60 °C
- 1 hour at 80 °C

A short treatment at 120 °C is not recommended since SEM investigations showed damage on samples stored 6 hours at this temperature.

Samples pre-conditioned as above have already been tested for functionality during mass spectrometry applications. First results showed that all targets were fully functional.

5.2.2 Life time prediction

The application of any lifetime model was not possible, since no failure resulting in reduced functionality of the target could be observed during the testing period. But common technical approximations as the “rate-temperature-rule” by Van´t Hoff, indicate a life time at ambient conditions of 17 years for specimens, which survived exposure to 80 °C during 14 week [48]. For a correct life time prediction, tests would need to be done under circumstances leading to at least two failure settings.

Still one has to be cautious, if the target is stored at high temperatures for too long, since significant after-shrinkage, as seen with the targets stored at 80 °C, can lead to failure regarding the geometric specifications.

5.2.3 Archiving

Since the targets proved to not be affected by temperatures below 0 °C, nothing speaks against archiving the targets at temperatures as low as -80 °C. No damage could be detected on targets which were frozen and thawed repeatedly, either. Application tests performed on the specimens subjected to these conditions showed nothing abnormal.

6 LITERATURE

[1] *Allen, N. S.:* "Degradation and Stabilization of Polyolefins", Applied Science Publishers, submitted

[2] *Atkins, P.W.; de Paula, J.:* "Atkins' Physical Cemistry 8th Edition", Oxford University Press, Oxford, UK, 2006

[3] *Baaijens, F.P.T:* "Calculation of residual stress in injection moulded products", Rheologica Acta, Volume 30, 1991

[4] *Bikas, A.; et al.:* "Computational tools for the optimal design of the injection moulding process", Journal of Materials Processing Technology, Volume 122, 2002

[5] *Brown, R. P.; Greenwood, J. H.:* "Practical Guide to the Assessment of useful Life of Plastics", Rapra Technology Limited, Shawbury, UK, 2002

[6] *Bugovsky, S.:* "Polymer-based disposable target for MALDI mass spectrometry", Analytical Chemistry

[7] *Bushman, A.C.; McHugh, A.J.:* "A continuum model for the dynamics of flow induced crystallization", Journal of Polymer Science, Part B: Polymer Physics, Volume 34, 1996

[8] *Coppola, S.; Grizzuti, N.; Maffettone, P.L.:* "Microrheological modeling of flow-induced crystallization", Macormolecules, Volume 34, 2001

[9] *Domininghaus, H.:* "Die Kunststoffe und ihre Eigenschaften", Springer, Berlin, Germany, 2006

[10] *Doufas, A.K.; Dairanieh, I.S.; McHugh, A.J.:* "A continuum model for flow-induced crystallization of polymer melts", Journal of Rheology, Volume 43, 1999

[11] *Ehrenstein, G.W.; Pongratz, S.*: "Beständigkeit von Kunststoffen", Hanser, Munich, Germany, 2007

[12] *Fischer, J. M.:* "Handbook of Molded Part Shrinkage and Warpage", Plastics Design Library, Norwich, USA, 2003

[13] *Foster, G. N.; Wasserman, S. H.; Yacka, D. J.*: "Oxidation Behavior and Stabilization of Metallocene and other Polyolefins", Die Angewandte Makromolekulare Chemie, Volume 252, 1997

[14] *Geisbüsch, P.:* „Ansätze zur Schwindungsberechnung ungefüllter und mineralisch gefüllter Thermoplaste", Dissertation RWTH Aachen, 1980

[15] *Gröber, S.:* "Experimentelle und klinische Untersuchungen zur mikrobiellen Besiedelung weichbleibender und harter Unterfütterungskunststoffe", Dissertation, Friedrich-Schiller University, Jena, Germany, 2003

[16] *Grundke, K.*: Chapter "Characterization of Polymer Surfaces by Wetting and Electrokinetic Measurements – Contact Angle, Interfacial Tension, Zeta Potential", in "Polymer Surfaces and Interfaces", Springer Verlag, Berlin, 2008

[17] *Hepperle, J.:* „Schädigungsmechanismen bei Polymeren, Polymeraufbereitung 2002 – technischer Fortschritt zur Steigerung von Leistung und Produktqualität", VDI Verlag, Düsseldorf, 2002

[18] *Hoven-Nievelstein, W. B.:* „Die Verarbeitungsschwindung thermoplastischer Formmassen", Dissertation RWTH Aachen, 1984

[19] *Huang, W.-J.; Chang, F.-C.*: "Physical Aging of Cyclo Olefin Copolymer (COC)", Journal of Polymer Research, Vol. 10, 2003

[20] *Hutchinson, J. M.:* "Physical Aging of Polymers", Progress in Polymer Science, Volume 5, 1995

[21] *Karas, M.; Hillenkamp, F.:* "Laserdesorption ionization of proteins with molecular masses exceeding 10000 Daltons", Anal. Chem., Volume 60, 1988

[22] *Kaschta, J.; Münstedt, H.; Ehrenstein, G.W.; Pongratz, S. (Hrsg.)*: Chapter "Chemisches und physikalisches Altern", in "Thermische Einsatzgrenzen von Kunststoffen während der Verarbeitung und in der Anwedung", Springer VDI Verlag GmbH, Dusseldorf, 2000

[23] *Kennedy, P.:* "Practical and Scientific Aspects of Injection Molding Simulation", Dissertation Technische Universiteit Eindhoven, 2008

[24] *Kennedy, P, Zheng, R.:* "High accuracy shrinkage and warpage prediction for injection molding", ANTEC 2002 Annual Technical Conference, San Francisco, CA; USA, 2001

[25] *König, S.:* "Target coatings and desorption surfaces in biomolecular MALDI-MS", Proteomics, Volume 8, 2008

[26] *Koscher, E.; Fulchiron, R.:* "Influence of shear on polypropylene crystallization: Morphology development and kinetics", Polymer, Volume 32, 1999

[27] *Kumar, G.; Prabhu, K. N.*: "Review of non-reactive and reactive wetting of liquids on surfaces", Advances in Colloid and Interface Science, Vol. 133, 2007

[28] *Leezenberg, P. B.; et al.*: "Chemical modification of sputtered amorphous-carbon surfaces", Journal of Applied Physics, Vol. 89, Nr. 6, 2001

[29] *Lemmerer, S.:* "Verfahrensvergleich zur Herstellung von mikro- und nanostrukturierten Oberflächen", Diplomarbeit am Institut für Kunststoffverarbeitung, Montanuniversität Leoben, 2009

[30] *Leong, Y. W.; Bakar, M. B. Abu et al.:* "Characterization of talc/calcium carbonate filled polypropylene hybrid composites weathered in a natural environment", Polymer Degradation and Stability, Volume 83, 2004

[31] *Lucyshyn, T.:* "Messung von pvT-Daten bei prozessnahen Abkühlraten und deren Einfluss auf die Simulation von Schwindung und Verzug mit Moldflow Plastics Insight", Dissertation am Institut für Kunststoffverarbeitung, Montanuniversität Leoben, 2009

[32] *N.N.:* Delrin Moulding Manual, TRD 30 – Part 1, DuPont, Wilmington, DE 19898, USA.

[33] *N.N.:* DIN 50035: „Begriffe aus dem Gebiet der Alterung von Materialien", 1989

[34] N.N.: ISO 294-4.: "Plastics – Injection moulding of test specimens of thermoplastic materials – Part 4: Determination of moulding shrinkage, standard specification, designation", 2001

[35] *N.N.:* Product information „Certificate for Planar Magnetron Sputtering Target", Umicore Materials AG, Balzers, Principality of Liechtenstein, 2007

[36] *N.N.:* Product information „ELION Technische Daten", Netstal, Näfels. Switzerland, 2010

[37] *N.N.:* Product information „FRT CWL 3 mm", FRT GmbH, Bergisch Gladbach, Germany, 2009

[38] *N.N.:* Product information „FRT MicroSpy Topo", FRT GmbH, Bergisch Gladbach, Germany, 2009

[39] *N.N.:* Product information „Preliminary Data Sheet, Stat-Kon® MD000E, based on PP", LNP a GE Plastics company, Exton, USA

[40] *N.N.:* Product information „Zeonor – high-performance Thermoplastics from Zeon Corporation", Zeon Corporation, Tokyo, Japan, 2004

[41] *N.N.:* Program help of Moldflow Plastics Insight 6.1 Revision 2. Moldflow Cooperation Headquarters, Wayland, MA 01778, USA.

[42] *Peinhopf, W.:* "Auslegung von Spritzgießwerkzeugen mittels der Methode der Finiten Elemente", Dissertation am Institut für Kunststoffverarbeitung, Montanuniversität Leoben, 2000

[43] *Peters, G.W.M.; Swartjes, F.H.M.; Meijer, H.E.H.:* "A recoverable strain-based model for flow induced crystallization", Macromol. Symp.; Volume 185, 2002

[44] *Pongratz, S.:* "Alterung von Kunststoffen während der Verarbeitung und im Gebrauch", Dissertation, Universität Erlangen-Nürnberg, 2000

[45] *Pötsch, H. G.:* „Prozesssimulation zur Abschätzung von Schwindung und Verzug Thermoplastischer Spritzgussteile", Dissertation RWTH Aachen, 1991

[46] *Rezayat, M.; Stafford, R.O.:* "A thermoviscoelastic model for residual stress in injection moulded thermoplastics", Polymer Engineering and Science, Volume 31, 1991

[47] *Rysavy, D.; Tkadleckova, H.:* "Lebensdauer von Polypropylenerzeugnissen in heißem Wasser und Waschlaugen", Plaste und Kautschuk, Volume 38, 1991

[48] *Schreyer, G.:* "Konstruieren in Kunststoffen", Carl Hanser Verlag, München, 1972

[49] *Schwarzl, F. R.:* "Polymermechanik – Struktur und mechanisches Verhalten von Polymeren", Springer Verlag, Berlin, 1990

[50] *Shin, J. Y. et al.*: "Chemical Structure and Physical Properties of Cyclo Olefin Polymers (IUPAC Technical Report) ", Pure and Applied Chemistry, Volume 77, No. 5, 2005

[51] *Tanaka, K.; Waki, H.; Ido, Y.; Akita, S.; Yoshida, Y.; Yoshida, T.; Matsuo, T.:* "Protein and polymer analyses up to m/z 100 000 by laser ionization time-of-flightmass spectrometry", Rapid Commun.Mass Spec., Volume 2, 1988

[52] *Thomas, T. R.:* "Rough Surfaces", Imperial College Press, London, UK, 1999

[53] *Trimpin, S.; Keune, S.; Räder, H. J.; Müllen, K.:* "Solvent-Free MALDI-MS: Developmental Improvements in the Reliability and the Potential of MALDI in the Analysis of Synthetic Polymers and Giant Organic Molecules", J Am Soc Mass Spectrom, Volume 17, 2006

[54] *Valadez-Gonzalez, A.; Veleva, L.:* "Mineral filler influence on the photo-oxidation mechanism degradation of high density polyethylene. Part I: Accelerated UV chamber exposure test", Polymer Degradation and Stability, Volume 63, 1999

[55] *Valadez-Gonzalez, A.; Veleva, L.:* "Mineral filler influence on the photo-oxidation mechanism degradation of high density polyethylene. Part II: natural exposure test", Polymer Degradation and Stability, Volume 83, 2004

[56] *Wallner, G.:* Interview conducted by Alexander Pöhl, Institute of Material Science and *Testing* of Plastics, Leoben, Austria, 18th June 2009

[57] *Walsh, S.F.:* "Shrinkage and Warpage Prediction for Injection Molded Components", J. Reinforced Plas. Compos., Volume 12, 1993

[58] *Winkler, W.; Bugovsky, S.; Marchetti-Deschmann, M.; Balika, W.; Openshaw, M.; Raptakis, E.; Kraushaar, H.; Hausberger, P.; Allmaier, G.:* "Microscope Slide Format and disposable Single Use Polymer-based MALDI MS Targets for Vacuum MALDI MS of Biomolecules, Microorganisms and Polymers", 18th International Mass Spectrometry Conference, Bremen, 2009

7 ABBREVIATIONS

7.1 Latin symbols and abbreviations

a-C:H	Hydrogenated amorphous carbon
a_i	Shrinkage coefficient
a_t	Temperature shift factor
a_T	Time temperature shift factor
C	Carbon
$CaCO_3$	Calcium carbonate
c^e_{ijkl}	Tensor of elastic constants
Cl	Chlorine
COC	Cyclo-olefin-copolymer
COP	Cyclo-olefin-polymer
Cr	Chromium
CRIMS	Corrected Residual In-Mold Stress
E_a	Activation energy
Fe	Iron
H	Hydrogen
k	Reaction rate
l_1	Corresponding length of the specimen
L1	Length of the shrinkage specimen
l_2	Length of the specimen after post mold trestment
L2	Length measured between the circular positioning marks of the shrinkage specimen
L3	Length measured between the crosshair positioning marks of the shrinkage specimen
l_c	Length across the center of the cavity
MALDI-MS	Matrix-assisted laser desorption/ionization mass-spectrometry
$M_i^{//}$	Measures in the residual strain model parallel to the flow direction
$M_i^{\perp}$	Measures in the residual strain model transverse to the flow direction
Mn	Manganese

MPD	Microstructured-Polymer-Devices
MPI	Moldflow Plastics Insight
N	Nitrogen
Ni	Nickel
P	Phosphorus
PA	Polyamide
PC	Polycarbonate
PET	Polyethylene terephthalate
PMMA	Poly(methyl methacrylate)
POM	Polyoxymethylen
PP	Polypropylene
PS	Polystyrene
PU	Polyurethane
PVC	Polyvinyl chloride
R	Gas constant
r	Ratio of the actual wetted surface area to geometric or projected surface area
R_a	Roughness (arithmetic average)
rh	Relative humidity
R_q	Roughness (root mean squared)
R_{RMS}	Roughness (root mean squared)
R_z	Roughness (average distance between the 5 highest peaks and 5 lowest valleys)
S	Sulfur
$S^{//}$	In-plane shrinkage strain parallel to the flow direction
$S^{\perp}$	In-plane shrinkage strain transverse to the flow direction
SEM	Scanning electron microscope
Si	Silicon
S_{Mn}	Mold shrinkage normal to flow direction
S_{Mp}	Mold shrinkage parallel to flow direction
S_{Pn}	Post-mold shrinkage normal to flow direction
S_{Pp}	Post-mold shrinkage parallel to flow direction
SS	Stainless steel
S_{Tn}	Total shrinkage normal to flow direction

S_{Tp}	Total shrinkage parallel to flow direction
t	Time
T	Temperature
T_g	Glass-transition temperature
t_{ref}	Reference time to reach a defined identical property change
T_{ref}	Absolute reference temperature
T_t	Transition temperature
v	Specific volume
W1,l	Width away from the gate of the shrinkage specimen
W1,r	Width near the gate of the shrinkage specimen
W2, l	Width away from the gate measured between the circular positioning marks of the shrinkage specimen
W2, r	Width near the gate measured between the circular positioning marks of the shrinkage specimen
W3, l	Width away from the gate measured between the crosshair positioning marks of the shrinkage specimen
W3, r	Width near the gate measured between the crosshair positioning marks of the shrinkage specimen

7.2 Greek symbols and abbreviations

α_{kl}	Tensor of coefficients of expansion
c_{ijkl}	Viscoelastic relaxation modulus
ε_{ij}	Total strain tensor
σ_{ij}	Stress tensor
θ	Equilibrium contact angle
θ_a	Advancing contact angle
θ_r	Receding contact angle
θ_w	Apparent contact angle on the rough surface
$\xi(t)$	Pseudo time scale that accounts for the effect of temperature on material response